NASA CR-152264
ASRL TR 174-7

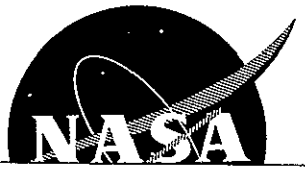

A WIND-TUNNEL INVESTIGATION OF TILT-ROTOR GUST ALLEVIATION SYSTEMS

Norman D. Ham
H. Philip Whitaker

January 1978

Prepared under Contract No. NAS2-7262 by

Aeroelastic and Structures Research Laboratory
Department of Aeronautics and Astronautics
Massachusetts Institute of Technology
Cambridge, Massachusetts 02139

for
AMES RESEARCH CENTER
NATIONAL AERONAUTICS AND SPACE ADMINISTRATION
MOFFETT FIELD, CALIFORNIA 94035

NASA CR-152264
ASRL TR 174-7

A WIND-TUNNEL INVESTIGATION OF TILT-ROTOR GUST ALLEVIATION SYSTEMS

Norman D. Ham

H. Philip Whitaker

January 1978

Prepared under Contract No. NAS2-7262 by

Aeroelastic and Structures Research Laboratory
Department of Aeronautics and Astronautics
Massachusetts Institute of Technology
Cambridge, Massachusetts 02139

for

AMES RESEARCH CENTER
NATIONAL AERONAUTICS AND SPACE ADMINISTRATION
MOFFETT FIELD, CALIFORNIA 94035

1 Report No NASA CR-152264	2 Government Accession No.	3. Recipient's Catalog No
4. Title and Subtitle A WIND-TUNNEL INVESTIGATION OF TILT-ROTOR GUST ALLEVIATION SYSTEMS		5. Report Date January 1978 6. Performing Organization Code
7. Author(s) Norman D. Ham and H. Philip Whitaker		8. Performing Organization Report No ASRL TR 174-7
9. Performing Organization Name and Address Aeroelastic and Structures Research Laboratory Department of Aeronautics and Astronautics Massachusetts Institute of Technology Cambridge, Massachusetts 02139		10. Work Unit No. 11. Contract or Grant No NAS2-7262
12. Sponsoring Agency Name and Address Ames Research Center National Aeronautics and Space Administration Moffett Field, California 94035		13 Type of Report and Period Covered Final - 1972-1978 14. Sponsoring Agency Code

15 Supplementary Notes

NASA Technical Monitors: J.P. Rabbott, Jr. and Wayne R. Johnson

16. Abstract

Tilt-rotor aircraft are sensitive to atmospheric turbulence during cruising flight due to their large, flexible, rotors mounted at the wing tips. Fatigue problems may result from wing bending, blade bending, and rotor rotational speed variations.

The purpose of the present study was to investigate the alleviation of the effects of gusts on tilt-rotor aircraft by means of active control systems. The study included the development of a novel type of gust generator, the derivation of the equations of motion of the rotor-wing combination, the correlation of these equations with the results of wind-tunnel model tests, the use of the equations to design various gust-alleviating active control systems, and the testing and evaluation of these control systems by means of wind-tunnel model tests.

17. Key Words (Suggested by Author(s))	18. Distribution Statement
Active Control Gust Alleviation System Tilt-Rotor Aircraft	Unclassified, Unlimited.

19. Security Classif. (of this report)	20. Security Classif. (of this page)	21. No. of Pages	22 Price*
Unclassified	Unclassified	138	

* For sale by the National Technical Information Service, Springfield, Virginia 22161

FOREWORD

This report has been prepared by the Aeroelastic and Structures Research Laboratory (ASRL), Department of Aeronautics and Astronautics, Massachusetts Institute of Technology, Cambridge, Massachusetts under NASA Contract No. NAS2-7262 from the Ames Research Center, National Aeronautics and Space Administration, Moffett Field, California 94035. Mr. J. P. Rabbott, Jr. and Mr. Wayne R. Johnson of Ames Research Center served as technical monitors.

The authors wish to acknowledge that the computations were carried out on an IBM 370/165 system made available at the MIT Information Processing Center.

SUMMARY

Tilt-rotor aircraft are sensitive to atmospheric turbulence during cruising flight due to their large, flexible, rotors mounted at the wing tips. Fatigue problems may result from wing bending, blade bending, and rotor rotational speed variations.

The purpose of the present study was to investigate the alleviation of the effects of gusts on tilt-rotor aircraft by means of active control systems. The study included the development of a novel type of gust generator, the derivation of the equations of motion of the rotor-wing combination, the correlation of these equations with the results of wind-tunnel model tests, the use of the equations to design various gust-alleviating active control systems, and the testing and evaluation of these control systems by means of wind-tunnel model tests.

TABLE OF CONTENTS

TABLE OF CONTENTS (Concluded)

CHAPTER 1

INTRODUCTION

1.1 General

The tilting proprotor aircraft, one of the composite aircraft family, is a very promising concept that combines into one aircraft the hover efficiency of the helicopter and the high-speed efficiency of the fixed-wing aircraft.

The typical tilting proprotor aircraft is a twin-engine aircraft with tilting rotors mounted on each wing tip. Its configuration consists of a fuselage, a high swept-forward wing, and an empennage. The empennage has a vertical stabilizer and rudder, and a horizontal stabilizer and elevator. The large diameter rotors are three bladed, hingeless or gimbal-type rotors which are mounted on the rotor shaft. The rotor shaft is connected through the gearbox to each engine in the pylon attached at the wing tip. The conversion system provides the rotation of the rotor pylon from the vertical position to the horizontal position and return, in order to obtain the helicopter mode or airplane mode corresponding to the desired flight regime.

When the aircraft takes off or lands, the rotor pylon is rotated to the vertical position to achieve vertical takeoff or landing similar to the helicopter. The flight controls apply pitch changes to the rotor to provide the longitudinal and directional control corresponding to helicopter rotor cyclic pitch, while the collective pitch controls vertical flight and roll motion.

In high-speed flight, the rotor pylon is rotated to a horizontal position similar to that of the conventional propeller type aircraft. The thrust

is produced by the rotor, and the lift by the wing. The flight controls are provided by the conventional aircraft control surfaces such as the elevator, rudder and aileron.

The tilting proprotor is exposed to a severe aerodynamic environment including gusts, the wake of preceding blades, and harmonic airloading like that of a helicopter. However, its dynamic and aeroelastic characteristics are in many ways unique; for example, the large flexible blades with a large amount of twist experience significant coupled out-of-plane (flapping) and inplane (lagging) motion.

As described later in Subsection 1.2, several years of experimental and theoretical analyses have been conducted to establish a fundamental understanding of the dynamic and aeroelastic behavior. However, it is necessary to understand the aeroelastic response of this aircraft to atmospheric turbulence more adequately and to predict it more accurately, since during the preliminary design phase, vibration level prediction is required in order: (a) to evaluate the fatigue life of the blade and wing, (b) to estimate the ride qualities of the vehicle, and, if necessary, (c) to develop suitable gust alleviation devices.

Several design compromise concepts, which make the present analysis distinct from helicopter aeroelastic analysis, are now stated briefly.

In order to obtain high hover efficiency from the rotor, it is desirable to achieve low disc loading, in other words to use large-diameter rotors whose swept discs reach nearly to the fuselage. When the aircraft is operated in high forward speed axial flight in the airplane mode, the rotor is operating at a high inflow ratio (the ratio of axial velocity to

blade tip speed). This phenomenon is very different from the helicopter rotor operation which involves low inflow. High inflow operation requires a large built-in angle of twist for efficient cruising. Therefore, significant coupled out-of-plane (flapping) and inplane (lagging) motion occurs in a large, flexible and twisted blade.

The engines and gearboxes are usually located at the wing tip to avoid transmitting high power through a long drive shaft. This leads to low wing natural frequencies and possible resonances in the low frequency range. Also, the center of gravity of the pylon and rotor does not usually coincide with the elastic axis of the wing. Hence, this results in coupled bending and torsion.

1.2 Brief Survey of Past Work

Because VTOL configurations have unconventional propeller-rotor systems, whirl flutter was a major design consideration on present proprotor aircraft.

The analysis presented in Ref. 1 is for a two-bladed rotor free to tilt on a shaft with two nacelle degrees of freedom (pitch and yaw). No lag or coning degrees of freedom are considered. The analytical method was compared with test results for an existing tilting proprotor aircraft (the Bell XV-3) and of subsequently-tested scale models. They showed good agreement.

Young and Lytwyn in Ref. 2 present a very precise analysis for the whirl stability of a multi-bladed rotor mounted on a nacelle which has pitch and yaw degrees of freedom. Each blade has one flap-wise degree of freedom. The blade mode shape is assumed to be a rigid body mode shape. It was concluded that whirl stability is poorest when the nacelle pitch

frequency equals the nacelle yaw frequency, but in this situation nacelle damping is quite effective. There is an optimum value of flap bending frequency somewhere between 1.1 and 1.35 for highly stabilized whirl motion.

This analysis neglects the effect of coning on proprotor aerodynamics, and flap bending mode shapes other than the rigid blade mode. Also, autorotation flight was not considered.

In Ref. 3, Gaffey points out that a highly coupled blade mode has substantial flap bending even if the primary mode involves in-plane motion. This occurs in the case of a highly twisted blade or a blade operating at high geometric pitch angles such as a proprotor blade. The analysis shows that a moderate amount of positive δ_3 (flapping angle at the blade root gives a pitch angle increase of $\beta \tan \delta_3$ if δ_3 is positive) has a stabilizing influence on proprotors subject to flap-lag instability at high inflows.

Preliminary design studies of prototype vehicles (Refs. 4 and 5) as a part of the current NASA/ARMY sponsored tilting proprotor research aircraft program give some results from dynamic and aeroelastic analyses done by Bell and Vertol.

Johnson, Refs. 6 and 7, derived the equations of motion for a cantilever wing with the rotor at the wing tip. He develops a nine degree-of-freedom model which involves blade flapping motion and lagging motion (each has one collective and two cyclic motions, respectively), wing vertical bending, chordwise bending, and torsion. This model is applied to two proprotor designs and compared with the results of some full-scale wind tunnel tests. It shows reasonable correlation between theory and experiment.

Yasue, Ref. 8, developed equations of motion for a rotor-propeller aircraft in cruising flight and implemented them in a computer program, Ref. 9. The formulation is based on Galerkin's method using coupled mode shapes for the blade and wing. This procedure is applied to the analysis of two types of rotors, gimballed rotor and hingeless. The results are evaluated by means of eigenvalue analysis of the stability of the system and frequency response analysis of the gust and control response.

Frick and Johnson, Ref. 10, used modern control theory to design a full state-variable feedback system to improve the dynamic characteristics of a rotor and cantilever wing representing the tilt-rotor aircraft in cruising flight. There were 17 state variables and 4 control variables in their system-dynamics mathematical model. An observer was suggested to estimate the unmeasurable state variables. To feed all 17 state variables into these 4 controllers is probably too complicated to implement, and detection of control system faults would be difficult.

Fry of Boeing Vertol Company, Ref. 11, used both low-rate and high-rate feedback systems to alleviate the gust response. In the low-rate system, pylon pitch and yaw displacements were sensed by strain gauges and fed to rotor cyclic actuators to alleviate blade loads and augment the aircraft static stability. In the high-rate system, wing tip vertical bending acceleration was fed through a phase-shifter and bandpass filter to rotor cyclic actuators to increase the damping of the wing vertical bending mode. Cyclic azimuth angle was varied experimentally to determine the optimal value which maximized the bending mode damping. The design methodology of these two control systems and the actual vertical gust alleviation capabilities were not mentioned in this report.

1.3 Objectives of the Present Study

The first objective of this investigation was to establish a verified method of predicting the dynamic and aeroelastic behavior of the tilting proprotor aircraft.

The equations of motion for a cantilever wing with a rotating rotor at the wing tip were derived as consistently as possible in Ref. 8. The great complexity of rotor blade motion was included by accounting for blade rotation (i.e., centrifugal and Coriolis forces), significant inplane motion, and the large twist and high pitch angles at high inflows.

The resulting system of equations, obtained using modal analysis, are applied to the analysis of experimental results obtained by testing two model proprotor configurations (one is a hingeless, soft-inplane type rotor and the other is a gimballed, stiff-inplane rotor: Reference 12). The tests were conducted in the MIT Wright Brothers Wind Tunnel using the gust generator described in Chapter 2. The proprotors were operated in autorotation, which is shown to be a close approximation to powered operation in Ref. 13.

The second objective of this investigation was to design a gust alleviation system for the tilt-rotor/wing combination in the presence of vertical and longitudinal gusts, either sinusoidal or as modelled by the von Karman gust spectrum. The responses of rotor cyclic flapping and wing vertical bending to vertical gust excitation, and rotor rotational speed change and wing chordwise bending to longitudinal gust excitation, were reduced by appropriate feedback control systems. Simplicity in control system design was emphasized, and physical interpretations of the control system performance were sought. A computer program was developed as a general design tool

with sufficient accuracy to accommodate high-order equations of motion, such as those describing the complicated tilt rotor aircraft dynamics. Satisfactory correlation of experimental wind tunnel data from a wing/rotor model mounted in the MIT Wright Brothers Wind Tunnel with analytical results was achieved.

CHAPTER 2

GUST GENERATOR DESIGN DETAILS AND CHARACTERISTICS

2.1 Introduction

The simulation of sinusoidal lateral and longitudinal gusts in the wind tunnel is difficult to achieve with a simple device over the range of frequencies and amplitudes of interest.

A number of investigators have developed methods of generating sinusoidal lateral gusts using various arrangements of oscillating vanes or airfoils with oscillating jet flaps in slotted, open, and closed test sections [14-18]. In some cases, the technique used is applicable to the generation of sinusoidal longitudinal gusts. The techniques of References 16 and 17 are of particular interest, since they utilize oscillating jet flaps having a minimum of vibrating mechanism and therefore a high frequency capability, do not require major modifications to the test section, and are capable of generating both lateral and longitudinal gusts. However, they both require quite large jet momentum coefficients to achieve acceptable gust amplitudes.

Since the available air supply in the Wright Brothers Wind Tunnel at MIT is of modest capacity, it was decided to apply the principle of airfoil circulation control to obtain the oscillating lift necessary for gust generation. By this means it was possible to reduce the required jet momentum coefficients by an order of magnitude.

The method of approach was taken from the work described in Reference 19, which utilized a hollow elliptical airfoil having two blowing slots at the rear, formed by truncating the elliptic section, and fitting a circular

cylinder into the resulting gap. The interior of the airfoil was divided into two plenum chambers, one supplying each slot. Tests were conducted with blowing from one or both slots. Large lift coefficients were generated at relatively small jet momentum coefficients C_μ, where

$$C_\mu = \frac{T}{qc}$$

and

T = slot thrust

q = free-stream dynamic pressure

c = airfoil chord

In the present application, oscillating lift was obtained by eccentrically mounting the trailing edge cylinder and rotating it in such a manner that the slots alternately opened and closed, as described in detail in Section 2.3.

The considerations that led to the final design configuration are described in Section 2.2.

2.2 Gust Generator Design Considerations

The following model is suggested in the literature for the power spectral density of longitudinal velocity fluctuations resulting from isotropic atmospheric turbulence [20]:

$$\phi_u(\omega_r) = \sigma_u^2 \frac{2L}{\pi} \frac{1}{[1 + (1.34\omega_r L)^2]^{5/6}}$$

where σ_u = standard deviation of longitudinal turbulence velocity

L = turbulence scale length

ω_r = spacewise circular frequency

A similar model is suggested for lateral velocity fluctuations.

The complete simulation of these models of atmospheric turbulence in the wind tunnel is obviously impossible. However, a reasonable representation at selected frequencies is possible using the technique described below.

Consider the arrangement shown in Figure 1. Twin vertical airfoils at zero incidence are mounted symmetrically to the left and right of the wint-tunnel centerline. The trailing edge portion of each airfoil consists of an oscillatory circulation control assembly driven by an electric motor (see Section 2.3). Any desired frequency of airfoil sinusoidal lift variation can be prescribed by control of motor rotational speed.

Assume in this instance that the sinusoidal lift variation of the two airfoils occurs at frequency ω and out-of-phase by 180 degrees. Then each airfoil will shed a time-varying vortex wake which will induce incremental longitudinal and vertical velocities over the region between the airfoils $u(x,h,t)$ and $w(x,h,t)$, respectively. If the lift variation is 180 degrees out-of-phase, it is seen from Figure 1 that the velocities $w(x,h,t)$ due to the wakes of both flaps cancel exactly at the tunnel centerline and tend to cancel elsewhere, while the velocities $u(x,h,t)$ are additive. The presence of the tunnel walls can be accounted for in the theoretical analysis by the method of images.*

It can be shown that the distribution of perturbation velocities generated far downstream in a rectangular wind tunnel is given by

*This portion of the analysis is due to W. Johnson, Ames Research Center.

$$\frac{u}{VC_\ell} = k \frac{\sinh k\bar{h}_1}{\sinh k\bar{h}_w} \cosh k\bar{\ell}$$

$$\frac{v}{VC_\ell} = k \frac{\sinh k\bar{h}_1}{\sinh k\bar{h}_w} \sinh k\bar{\ell}$$

in the out-of-phase case, and

$$\frac{u}{VC_\ell} = k \frac{\sinh k\bar{h}_1}{\cosh k\bar{h}_w} \sinh k\bar{\ell}$$

$$\frac{v}{VC_\ell} = k \frac{\sinh k\bar{h}_1}{\cosh k\bar{h}_w} \cosh k\bar{\ell}$$

in the in-phase case, where

u = perturbation longitudinal velocity amplitude

v = perturbation lateral velocity amplitude

V = tunnel velocity

C_ℓ = airfoil lift-coefficient amplitude

k = reduced frequency of lift variation $\omega b/V$

ω = frequency of lift variation

b = airfoil semichord

$\bar{h}_1$ = non-dimensional distance from wall to airfoil, h_1/b

$\bar{h}_w$ = non-dimensional distance from wall to tunnel centerline, h_w/b

$\bar{\ell}$ = non-dimensional distance from tunnel centerline, ℓ/b

The gust generator design was governed by the following considerations:

1. The test section of the Wright Brothers Wind Tunnel has an oval cross-section 3.05 meters (ten feet) wide and 2.13 meters (seven feet) high.
2. The model to be tested was a rotor-propeller, having a diameter of 0.914 meters (three feet) in the cruise mode.
3. The available tunnel air supply was limited in flow rate.
4. The design advance ratio of the rotor-propeller was to be unity.
5. The gust frequency range of interest was from zero to 1.5/revolution in terms of rotor rotational speed.
6. Airfoil spacing was to be two rotor diameters to avoid interference of the airfoil wakes with the rotor.
7. The maximum gust incremental velocities were to be five percent of free stream at a tunnel speed of 36.6 meters per second (120 feet per second).

At an advance ratio of unity, i.e.,

$$\frac{V}{\Omega R} = 1 \ ,$$

rotor rotational speed is given by

$$\Omega = \frac{V}{R}$$

At a frequency ratio of 1.5, i.e.,

$$\frac{\omega}{\Omega} = 1.5 \ ,$$

the gust frequency is

$$\omega = 1.5\Omega = 1.5 \frac{V}{R}$$

Then the upper limit on gust generator reduced frequency is

$$k_{max} = \frac{\omega b}{V} = 1.5 \frac{V}{R} \frac{b}{V} = 1.5 \frac{b}{R}$$

It is desirable to keep the reduced frequency low to minimize flow distortion over the rotor disk. On the other hand, the incremental gust velocities are proportional to kC_ℓ, and since from Reference 19

$$C_\ell \sim C_\mu^{1/2}$$

then

$$kC_\ell \sim (\text{chord})^{1/2}$$

Since the tunnel air supply was limited, the airfoil chord was sized by the requirement to achieve maximum gust incremental velocities of five percent of free stream at the design tunnel speed of 36.6 meters per second (120 feet per second).

The above considerations led to the following gust generator parameters:

$$b = 0.305 \text{ meters (1 ft)}$$

$$h_1 = 0.610 \text{ meters (2 ft)}$$

$$h_w = 1.525 \text{ meters (5 ft)}$$

The design details of the gust generator are described in the following section.

2.3 Gust Generator Design Details

The gust generator described in this study uses two identical airfoils. A method for producing high-frequency, sinusoidal variations of the lift of each airfoil is required. The high frequencies precluded oscillating the airfoils or a flap mounted on the airfoils. The available air supply also

placed restrictions on the possible alternatives. It was determined that the requirements could be met by a special form of circulation-controlled airfoil (CCA).

A typical CCA has a thick section and a blunt trailing edge having an upper slot (see Figure 2a). Pressurized air ejected from the slot delays upper surface boundary-layer separation, while moving the rear stagnation point to the underside of the trailing edge and creating lift. The amount of lift generated is governed by the jet-momentum coefficient, C_μ. Such an airfoil can produce lift at zero angle of attack, and is also capable of generating a lift coefficient near the theoretical maximum.

R.J. Kind has experimented with a somewhat different form of CCA [19]. (See Figure 2b). It has an elliptical section and both an upper and a lower blowing slot. The position of the stagnation point is then governed by ΔC_μ, the difference between the upper and lower values of C_μ. For the present application, the primary advantage of such a symmetrical CCA is that it produces positive or negative lift equally well. A method of rapidly varying ΔC_μ would then produce a lift variation suitable for present purposes. Such a method, using a rotating cylinder to act as an air valve, is described below.

The basic design of the CCA used is shown in Figure 3. It is an elliptical section airfoil, modified by the addition of a rotatable cylinder recessed into the trailing edge. The cylinder is smaller in diameter than the width of the channel containing it, and the resulting gaps form the upper and the lower blowing slots. Most importantly, the cylinder is eccentrically mounted to act as a cam. The channel width, cylinder diameter

and eccentricity are chosen so that the cylinder completely closes each slot once per revolution. The channel also forms a secondary plenum forward of the cylinder, and it, in turn, is connected by air passages to the primary plenum inside the airfoil.

The airfoil configuration chosen has several advantages:

(1) The ability to operate at high frequency

(2) Mechanical simplicity since the only moving part is the rotating cylinder

(3) The capability of generating a high lift coefficient at low jet momentum coefficients.

The two CCA that comprise the gust generator are identical, elliptical section, constant chord wings of 168-centimeter (66-inch) span and 65.7-centimeter (25.9-inch) chord. The section has zero camber, 20% thickness/chord ratio, and 7.7% cylinder diameter/chord ratio. The cylinder center is mounted at the 96% chord position. The thickness ratio, cylinder size, and cylinder position were chosen to match those of Reference 19, while the span was dictated by the size of the test section of the Wright Brothers Wind Tunnel.

The primary structure of the wing consists of a forward spar at 50% chord, an aft channel (spar) at 90% chord and two tip ribs. (See Figure 4). The portion ahead of the spar consists of simple mahogany fairing, while the space between the spar and the channel forms the primary plenum.

The slot width was determined by an initial measurement that showed the air supply capable of providing a flow velocity of 214 meters per second (700 feet per second). Since that was the desired slot velocity, the total

gap (upper plus lower) was set at a convenient .0508 centimeters (0.020 inches), for a total slot area (both airfoils) 12.9 square centimeters (2.5 square inches).

The cylinder itself is made from thick wall 4130 steel tubing, centerless ground to an outside diameter of 5.03 centimeters (1.980 inches). It is divided into four equal spanwise segments, supported by three intermediate and two tip bearings. In order to provide for eccentric mounting, the ends of the cylinder segments were bored out and fitted with aluminum bushings having 2.23-centimeter (7/8-inch) holes offset 0.0254 centimeter (0.010 inch) from the center.

The trailing-edge channel was divided into four equal segments, with intermediate bearing supports between the segments. The channels were machined from aluminum. The cavity width in conjunction with the cylinder outside diameter and eccentricity provides for the desired slot width and closure. The cavity is deeper than necessary and acts as a secondary plenum. Holes of diameter 1.27 centimeters (0.5 inches) and 1.91-centimeter three-quarter-inch) spacing are drilled through the channel to connect primary and secondary plenums.

The channels and intermediate bearing supports are tied together by bolted-in splicing plates. These allow the channels to be centered over the cylinder during assembly so that equal upper and lower slot widths can be adjusted. The adjustment guarantees that alignment will be maintained after assembly of the wing is completed.

The forward spar is a simple rectangular section aluminum bar. Holes are drilled through for the attachment of the mahogany fairing, while the ends are inset into the tip ribs for added rigidity.

The tip ribs are cut out of 2.54-centimeter (one-inch) aluminum plate. Two 6.35-centimeter (2.5-inch) air inlets are cut in the aft portion. The trailing edge of the rib carries a ball bearing mounted in a holder adjustable for preload. On one end of the wing, the ball bearing rides on a stub shaft coming out of the end cylinder, while on the other, an extended shaft is used to connect the cylinder to the drive mechanism.

The wing skin over the aft portion must hold the primary plenum pressure. It is, therefore, made from 0.635-centimeter (1/4-inch) aluminum plate, bent to the elliptical contour. Because of the skin thickness, no internal ribs are used, but equally-spaced tie-bolts hold the skins together at 70% chord.

Figures 5 and 10 show the gust-generator airfoils mounted in the Wright Brothers Wind Tunnel. They are mounted vertically and have a separation of 1.83 meters (six feet). Air is supplied to a large manifold of 15.25-centimeter (six-inch) PVC pipe and then to the upper and lower tip ribs of each wind by 10.2-centimeter (four-inch) PVC pipe runners. A D.C. motor, mounted on top of the tunnel, drives the cylinders by means of timing belts and pulleys.

Perturbation velocity measurements were made by an "x" configuration hot-wire anemometer probe. The wind tunnel is run at a series of speeds. At each speed, the flow velocity and perturbation are measured for a series of cylinder rotational speeds. This is done for the cylinders synchronized in-phase to produce lateral gusts, and then for the cylinders 180 degrees out-of-phase to produce longitudinal gusts.

2.4 Gust Generator Characteristics

Since testing was conducted at constant air supply mass flow and pressure, the jet momentum coefficient C_μ of the airfoils varied inversely as the square of tunnel velocity. Then from the results of Reference 19, the airfoil lift coefficient, C_ℓ varies approximately with C_μ as

$$C_\ell \sim C_\mu^{1/2}$$

Therefore, $$C_\ell \sim \frac{1}{V}$$

From the theory of Section 2.2 for this case

$$\frac{u}{V} \text{ or } \frac{v}{V} \sim C_\ell \sim \frac{1}{V}$$

Therefore, the ratio of perturbation velocity to tunnel velocity should vary inversely with tunnel velocity for constant air flow and pressure.

The experimental results indicated such an inverse variation with tunnel velocity. Typical experimental results at tunnel center are shown in Figures 6 and 7. Shown for comparison in each figure is a theoretical curve for the case V = 132 kph (82.5 mph). Since the airfoil lift coefficient C_ℓ was unknown, the theoretical curve in each figure was arbitrarily matched to the experimental point at reduced frequency k of 0.6. It is seen that the theoretical curves predict the experimental trends fairly well.

The experimental distributions of longitudinal and lateral gust perturbation velocities over a 1.22-meter (four-foot) square centered on

the tunnel center line are shown in Figures 8 and 9 for a reduced frequency of 0.5. The theoretical curves shown were arbitrarily matched to an experimental point on the line $x = 0$. The theoretical prediction of the lateral distributions is seen to be reasonable. The scatter in the data is presumably due to tunnel flow peculiarities.

Further details of the gust generator are contained in Reference 21.

CHAPTER 3

THEORETICAL AND EXPERIMENTAL GUST RESPONSE

3.1 Model Description

The model is a semi-span, Froude-scaled, unpowered tilt-rotor with a diameter of 85.8 centimeters (33.75 inches). (See Figure 10.) It provides a dynamic simulation of either a 7.93-meter (26-foot) diameter three-bladed hingeless rotor system (scale factor = 1/9.244) or a 7.62-meter (25-foot), three-bladed, gimballed rotor system (scale factor = 1/8.888). A high performance closed-loop proportional control system is provided for collective pitch and two orthogonal components of cyclic pitch. A fully mass-balanced aerodynamic forcing vane driven by a constant velocity servo loop is included for model forcing. Both the rotor blades and wing are fully strain-gage instrumented.

A separate, special purpose electronic controller is used to drive the collective and cyclic servos and forcing vane. In addition, the controller contains a patchable analog computer which allows signals originating in any part of the model to be used in a closed-loop manner to control swash plate tilt.

Precise Froude scaling could not be rigidly adhered to, but similarity of natural frequencies has been maintained in order to preserve dynamic similarity.

The model parameters are listed in Reference 22. The wing is composed of a solid aluminum spar covered by a two-piece molded fiberglas fairing. The bottom of the spar fits with a 5.5-degree forward sweep into a mounting

pedestal, while the top carries the nacelle attachments. Since the two rotor systems require different wing natural frequencies, tip weights are added to the top of the spar in the hingeless rotor configuration. The spar carries beamwise, chordwise, and torsional bending gages at the 5% and 79% semi-span positions.

The nacelle exterior consists of upper and lower molded fiberglas fairings. Carried inside the nacelle are: rotor shaft, swash plates, cyclic and collective servo actuators, slip rings, one-per-rev pulser, rotor shaft tachometer, forcing vane motor, forcing vane tachometer, and gimbal position potentiometers (used only with the gimballed rotor).

The cyclic actuators are 90-degrees apart and each drives a lead screw to control swash-plate tilt. The entire cyclic control assembly rides on a pair of lead screws driven by the collective actuator.

Rotating system instrumentation wires run inside the hollow rotor shaft to a 38-channel slip ring mounted at the rear of the nacelle.

The forcing vane has an area of 56.4 square centimeters (8.75 square inches) and is a symmetric 0012 section. It can oscillate through either $\pm$ 5 or $\pm$ 10 degrees. The vane is driven by a D.C. motor and balanced crank.

The hingeless rotor blades are constructed of epoxy resin impregnated glass fiber over a foam core. The spar is rectangular inboard, transitioning to a 'D' spar at $r/R = 0.45$. The inboard section is solid epoxy-impregnated glass fiber, with instrumentation leads imbedded inside. The skin inboard of $r/R = 0.45$ is not load-bearing and can be removed for access to blade instrumentation. Aluminum pitch horns are secured to steel root fittings. A cylindrical cavity is provided at each blade tip for small tuning weights used to match blade frequencies.

The hub is a single piece of machined aluminum, incorporating 2.5 degrees of precone.

Each blade has flapwise and chordwise bending strain gages at r/R = 0.08 and a torsional bending gage at r/R = 0.10. Additionally, No. 3 blade has outboard instrumentation consisting of flapwise and chordwise gages at r/R = 0.42 and a torsional gage at r/R = 0.44.

The gimballed rotor blades are constructed similarly to those of the hingeless rotor, except that the spar is a hollow box section of preimpregnated glass cloth and the aft skin is stabilized with balsa sheet. In this case, the entire blade skin is load carrying. Aluminum pitch horns are bonded integrally into the spar.

The same molds were used for both types of blades, resulting in small out-of-scale effects in chord and twist distribution for the gimballed rotor.

The gimballed rotor hub consists of a free-swivelling hub carrying the blades and a rotating gimbal, an outer fixed gimbal, three flap-restraining springs and a spring retainer. Two links, 90 degrees apart, connect the outer gimbal with the gimbal position potentiometers in the nacelle. The hub incorporates 1.5 degrees of precone.

All three blades are instrumented inboard and outboard, with flapwise and chordwise gages at r/R = 0.11 and 9.30, and torsional gages at r/R = 0.12 and 0.29. A spare chordwise gage is provided at r/R = 0.30 because of the inaccessibility of the outboard gage.

The model controller contains three servo-amplifiers to drive the cyclic and collective actuators, the forcing vane controller, and the patchable analog computer (see Figure 11).

The servo-amplifiers are fully solid state, providing D.C. control signals and receiving feedback potentiometer position voltages. Thus, each actuator is provided with an independent closed-loop positioning servo-mechanism. Command signals can be generated manually through digital potentiometers or automatically through the analog computer. The analog computer contains summing amplifiers, inverters, buffers, switches, and a phase shifter, all accessible through patching bays. Various control laws can be easily implemented. In this way, strain-gage signals from any part of the model can be mixed and phased to drive the servo-actuators.

3.2 Test Instrumentation

The primary purpose of these tests was to determine the model response to vertical and longitudinal gusts. Gust response was measured by an RMS voltmeter switched to the appropriate strain gage.

Since the model was being operated in a harsh environment, oscilloscopes were used to monitor blade and wing stresses. Flapwise and chordwise signals from the Number 3 blade inboard gages were fed into the vertical and horizontal axes of an oscilloscope to form a Lissajou's figure. This display was monitored to ensure that the imposed stresses did not exceed the allowable values. The wing stresses were monitored in a similar manner.

For gimballed rotor tests, the blade display monitored the outboard gages (30% radius) at the critical station, while the second display monitored gimbal position instead of wing stresses.

A 12-channel oscillograph was also used. During the gust response tests, the following inputs were recorded: wing flapwise, chordwise, and torsion; blade flapwise, chordwise, and torsion; pitch and yaw gimbal position; one-per-rev pulses from the rotor shaft and from the generator.

3.3 Test Procedures

For the gust tests, the model was run at constant tunnel speed and rotor rpm while excitation was provided by sinusoidal gusts of increasing frequency. At each frequency, RMS voltage measurements were made of all three wing signals and blade flapwise and chordwise signals. During tests on the gimballed rotor, blade torsion and gimbal position signals were also measured.

Tests were conducted in autorotation at 132 kph (82.5 mph) and 1200 rpm (advance ratio 0.7) for the hingeless rotor. Vertical and longitudinal gusts of RMS amplitude 1.5% of free stream were varied from 200 to 900 cpm in 100 cpm increments, with finer increments near resonances.

Tests were conducted in autorotation at 152 kph (95 mph) and 1360 rpm (advance ratio 0.7) for the gimballed rotor. Vertical and longitudinal gusts of RMS amplitude 2.0% and 2.5% of free stream, respectively, were varied from 300 to 1400 cpm in 100 and 200 cpm increments. In both cases, finer increments were taken near resonances. Oscillograph records were taken along with RMS voltmeter signal readings.

3.4 Hingeless Rotor Gust Response

The hingeless rotor model described in Section 3.1 and in Reference 12 was subjected to sinusoidal longitudinal and vertical gusts at various frequencies (Figure 12), at a wind tunnel velocity of 132 kph (82.5 mph), and with a rotor rotational speed of 1200 revolutions per minute. This test case corresponded to full-scale operation at an advance ratio of 0.7. Model response was measured in terms of blade inplane and out-of-plane bending motion, wing vertical and chordwise bending, and wing torsion.

Test results are presented in Figures 13 and 14. Also shown are theoretical predictions of the model response using the method of Refs. 8 and 9. In comparing theory with experiment, it was necessary to add "tare" RMS values of model motion due to tunnel turbulence, measured with the gust generator shut down, to the theoretical values. The RMS magnitude of the tare value used in each case is indicated by an arrow at the left axis of each figure.

For the longitudinal gust case, Figure 13, agreement is seen to be fairly good except in the vicinity of the resonance peaks, where structural damping not accounted for in the theory reduced the experimental values.

For the vertical gust case, Figure 14, the theory underpredicts the blade bending responses. The discrepancy between theory and experiment is believed to be due to difficulties in representing the blade root boundary conditions in the theoretical calculation of the coupled blade bending mode shapes.

Wing vertical bending response to longitudinal gusts, wing chordwise bending response to vertical gusts, and wing torsional response to both types of gust are not shown since these responses were negligible, both experimentally and theoretically.

Wing chordwise bending response to longitudinal gusts and wing vertical bending response to vertical gusts are not shown since these responses are similar to those for the gimballed rotor described in Section 3.5.

3.5 Gimballed Rotor Gust Response

The gimballed rotor model described in Section 3.1 and in Ref. 12 was subjected to sinusoidal longitudinal and vertical gusts at various

frequencies (Figure 12) at a wind tunnel velocity of 152 kph (95 mph), and with a rotor rotational speed of 1360 revolutions per minute. This test case corresponded to full-scale operation at an advance ratio of 0.7. Model response was measured in terms of blade inplane and out-of-plane bending motion, longitudinal and lateral gimbal motion, wing vertical and chordwise bending, and blade and wing torsion.

Test results are presented in Figures 15 and 16. Also shown are theoretical predictions of the model response using the method of Refs. 8 and 9. In comparing theory with experiment, it was necessary to add "tare" RMS values of model motion due to tunnel turbulence, measured with the gust generator shut down, to the theoretical values. The RMS magnitude of the tare value used in each case is indicated by an arrow at the left axis of each figure.

For both gust cases, the theory underpredicts the blade bending responses, Figures 15(a), 15(b) and 16(a) and 16(b), while the wing bending responses are reduced by structural damping not accounted for in the theory, Figures 15(e) and 16(e).

In Fig. 15(e), the wing chordwise bending response to the longitudinal gust has a small peak at 0.29 pre revolution. It was observed from the oscillograph trace that this chordwise response had a frequency which was the same as the wing chordwise natural frequency. It was also confirmed that the peak was largest when the gust frequency was one-half the wing chordwise bending natural frequency. Therefore, it is believed that this second harmonic vibration is due to a second harmonic component of the gust waveform.

The discrepancy between theory and experiment for the blade bending responses is believed to be due to difficulties in representing the blade root boundary conditions in the theoretical calculation of the coupled blade bending mode shapes, and to difficulties in blade bending strain-gage calibration.

The theory overpredicts the gimbal motion response to wing chordwise bending motion excited by longitudinal gusts, Figs. 15(c) and 15(d), presumably due to the reduction of wing bending response by structural damping not accounted for in the theory, and the further reduction of blade flapping response by high friction in the gimbal potentiometers. The increase in the experimental gimbal response at the higher frequencies is believed to be due to blade imbalance (1/rev. in the rotating system) exciting the rotor precession mode (about 2/rev. in the non-rotating system); an increasing 2/rev. signal was seen in the gimbal oscillograph record as gust frequency approached 1/rev.

The theory predicts the gimbal motion response to vertical gusts fairly well, as seen in Figs. 16(c) and 16(d). The apparent increase in the experimental lateral gimbal response at the higher frequencies is due to an increase in the noise level of the RMS voltage signal from the gimbal potentiometer due to a loose wire.

Wing vertical bending response to longitudinal gusts, wing chordwise bending response to vertical gusts, and blade and wing torsional responses to both types of gust are not shown since these responses are negligible, both experimentally and theoretically.

3.6 Conclusions

The investigation described in this chapter had two primary objectives. The first objective was the acquisition of gust response test data for use in the design of a gust alleviation system for proprotor aircraft. The second objective was the correlation of this test data with a previously developed ten degree-of-freedom theory (Refs. 8 and 9).

It was found that, in general, the theory adequately predicted the test data. As would be expected, structural damping present in the model greatly reduced the magnitudes of resonant responses from those predicted by the theory. The difficulty of correctly representing the coupled blade bending mode root boundary conditions led to discrepancies between theory and test in the blade bending response. Finally, the random turbulence present in the wind tunnel produced a "tare" RMS response of the model which could be accounted for only approximately in the comparison between theory and test, leading to some small degree of error.

It is believed that the theory in its present form gives a reasonable representation of proprotor gust and control response at an advance ratio of 0.7.

Further details of the model tests described above are given in Reference 22.

CHAPTER 4

GUST ALLEVIATION SYSTEM DESIGN

4.1 Introduction

The objective of this design investigation is to ascertain whether improvement in wing bending and rotor flapping responses could be obtained through the use of feedback control loops. Such improvement could lead to load alleviation and better ride qualities during operation in atmospheric turbulence. The concept involves using sensors to indicate response characteristics and feeding appropriately processed signals to force-generators on the wing and/or rotor systems. Such systems which use automatic control techniques to modify response characteristics are known as active control systems to differentiate their action from the "passive" characteristics of the wing/rotor combination due to its inherent structural and mass properties.

In order for the active control concept to be successful, it must be possible to make the required sensor measurements and to exert the required forces using equipment that will be reliable and reasonably low in both acquisition cost and lifetime costs. It is anticipated that these systems would be operated whenever the airplane flies. Since failures could imperil the aircraft, fail operational redundancy would have to be provided. These factors lead to serious constraints upon the system design, and it is not clear that even a substantial improvement in bending and flapping responses warrants the cost of such systems.

One can use optimal control design techniques for such a system (Ref. 10), and they in general lead to the feedback of many state variables using

estimators to approximate those variables not easily measured. One is then faced with the task of simplifying the configuration to one that is practically realizable. An alternative approach was taken here. The simplest realizable system configuration was specified, and parameter optimization was employed to specify the design values which would give the best performance achievable with that configuration. Complexity was added only if there was reasonable assurance that significant improvement could thereby be realized.

In any optimization procedure one has to define what performance measures are to be used in the optimization. In this case the performance was summarized as either the root-mean-square value of the wing bending displacement or the root-mean-square value of the rotor flapping coordinate resulting during flight in turbulence. The capability of the active control system was then expressed as the percentage reduction in response achieved using the system over that resulting with no system.

The work described in this report involved wind tunnel testing of active control systems added to a model of the tilt-rotor, rotor-wing combination. One of the most serious constraints in such a system was that the only force-producer available was the rotor, with control inputs fed to cause either collective or cyclic blade angle changes. To achieve effective control of wing bending displacements, a more powerful generator of vertical forces would be desirable, such as a direct lift device of some type. Atmospheric turbulence is primarily a low frequency input relative to the rotor and wing modal frequencies, and hence higher order states contribute little to the improvement of the response to turbulence. Hence only relative simple system configurations were investigated.

The design procedure thus consisted of the following steps: (1) specification of a single sensor feedback configuration; (2) use of a parameter optimization digital computer program to select an open-loop gain value that would minimize the selected performance measure; (3) correlation of the results with root locus and frequency response analysis; (4) addition of other feedback paths where a significant improvement was to be expected; (5) reoptimization of the multi-loop configuration; (6) iteration as needed. The computer program computed the root-mean-square of the selected output for the specified gust spectrum. The program then used a gradient search algorithm to determine the parameter set that minimized the (RMS) value.

An analytical study of control systems for full scale gimballed tilt rotor aircraft was summarized in Reference 23. The dynamics of the wing tunnel model were a little different from those of the full scale aircraft. Although the model was scaled to have wing and rotor natural frequencies close to those of the full scale airplane the structural mode shapes were not reproduced properly. Thus, new analyses and syntheses of the feedback control systems had to be made.

The following four types of feedback configurations were investigated:

System 1: Alleviation of wing vertical bending and rotor flapping due to vertical gust, v_g, by using rotor longitudinal cyclic pitch, θ_{1s}:

System 1-1: Wing vertical bending displacement fed to rotor longitudinal cyclic.

System 1-2: Wing vertical bending velocity fed to rotor longitudinal cyclic.

System 2: Alleviation of wing vertical bending due to vertical gust, v_g, by by using the wing tip mounted vane, δ_s:

System 2-1: Wing vertical bending displacement fed to wing tip mounted vane.

System 2-2: Wing vertical bending velocity fed to wing tip mounted vane.

System 3: Alleviation of wing chordwise bending due to longitudinal gust, u_g, by using collective pitch, θ_o:

System 3-1: Wing chordwise bending displacement fed to collective pitch.

System 3-2: Wing chordwise bending velocity fed to collective pitch.

System 4: Alleviation of rotor rotational speed change, due to longitudinal gust by using collective pitch.

System 4-1: Rotor rotational speed change fed to collective pitch.

Each of the systems is seen to be a single sensor feedback control system which can be represented by the general block diagram of Figure 17. For these preliminary design studies, the dynamic effects of sensors and servos were neglected.

System 1 was investigated for the full scale airplane in Reference 2. It was also shown there that use of multiple feedback loops could achieve only marginal improvement in performance, and therefore such configurations have not been investigated with the wind tunnel model. Reference 2 also investigated the use of a trailing edge flap as a control effector. Since the model had no flaps, the tip mounted vane was used to simulate the wing trailing edge flap.

In the following sections the design of control systems for the gimballed rotor/wing combination is discussed. The process is similar for the hingeless rotor/wing combination.

Figure 18 presents the power spectral density for the vertical gust used in the design optimization process. This is an approximation to the von Karman model of atmospheric turbulence. A characteristic gust length of 14.4 m (46.4 ft) was used. With a model scale factor of $(8.88)^{-1}$, this corresponds to a full scale gust length of 126 m (412 ft).

4.2 System 1-1: Wing Vertical Bending, Fed to the Rotor Longitudinal Cyclic Pitch

Figure 19 presents a summary of the predicted reduction in the RMS levels of both q_1 and β_{1c} that resulted with this feedback configuration. Plotted is the ratio of the (RMS) value with the active control system to that without the control system versus the loop feedback gain. The latter is the change in rotor longitudinal cyclic angle per unit change in (non-dimensional) bending deflection. The value of the feedback gain which minimized RMS (β_{1c}) is -4.85 rad/rad, instead of the -4.05 rad/rad obtained for the full scale airplane (Ref. 23). This feedback gain value also achieved the major fraction of the possible reduction in wing bending of which this configuration is capable. Increasing the gain resulted in some improvement in bending, but at the cost of increased flapping. Thus, this value was considered to be the optimum design value.

The corresponding closed-loop power spectral densities for wing bending and for rotor flapping are presented in Figures 20 and 21. For comparison purposes, the open loop spectra (no control system) are also shown. The

area under the curve is proportional to the mean square value. It is seen that the improvement in flapping was achieved through a reduction in magnitude over the low frequency range, and that feeding wing bending to the rotor increased the high frequency portion of the spectrum. The improvement in bending response was achieved both by a reduced spectrum at low frequency and by improved damping of the wing bending mode at high frequency. The gust spectrum itself attenuated the response spectra by more than 2 orders of magnitude for normalized gust frequencies greater than 0.2. Consequently it was the very low damping ratio assumed for the wing bending mode that resulted in a significant contribution of that mode to the bending spectrum of Figure 20.

4.3 System 1-2: Wing Vertical Bending Velocity Fed to Rotor Longitudinal Cyclic Pitch

Although it would appear from the results of System 1-1 that by adding more damping to the wing bending mode one could have further improved the bending response and correspondingly used higher feedback gains without causing flapping to deteriorate, the analysis indicated that one was constrained by the wing torsion characteristics. Using wing bending rate feedback would add damping to the wing bending mode, but it would also decrease the stability margin as determined by the wing torsion mode. The response characteristics of this system are shown in Figure 22.

In addition to increasing the damping, the bending rate feedback decreased the natural frequency of the wing vertical bending mode. Increasing q_1 mode damping resulted in a lower resonant peak in the wing bending gust response, and hence RMS(q_1) was reduced. At the same time the

reduction in q_1 natural frequency moved the resonant peak to a lower frequency where the gust magnitude was stronger. If the peak magnitude had remained the same, the RMS level of the wing bending would have increased due to this effect. Actually, the reduction in the resonant peak of the q_1 response was a larger effect than the reduction in q_1 natural frequency, as the feedback static sensitivity was increased. Further increases in the feedback gain would both reduce the resonant peak of the q_1 mode and move this peak to a lower frequency. At the higher gain values these two effects tended to cancel each other, and RMS(q_1) remained relatively flat until the feedback gain was -0.4 second at which point the wing torsion mode became unstable. The normalized frequency of the torsion mode was 1.6, and therefore it contributed a negligible amount to the response power spectra until the feedback gain was very close to the value resulting in instability. Thus, the plot of (RMS) response versus feedback gain shown in Figure 22 gives little indication of the approaching instability.

In considering flapping response it is seen that by feeding the high frequency bending motion to the longitudinal cyclic motion, the bending rate feedback increased the flapping power spectrum at the bending mode frequency. Since the bending velocity was 90 degrees out of phase with the rotor flapping at low frequency, the use of $\dot{q}_1$ fed to θ_{1s} also increased the flapping at low frequency. System 1-2 therefore reduced wing bending at the price of amplification of rotor cyclic flapping and tended to destabilize the wing torsion mode. Accordingly, the use of bending velocity feedback to the rotor longitudinal cyclic pitch was not attractive.

4.4 System 2-1: Wing Vertical Bending Fed to a Wing Tip Mounted Vane

The wind tunnel model that was available for the experimental tests had a tip mounted vane to be used as an excitation device. Since it was not feasible to redesign the wing with trailing edge flaps on this program, the vane was considered for simulating a direct lift control device. The vane was mounted at the half chord location and was driven by a position servo. Due to its size and location, the vane provided a vertical force coefficient about 1/40 of that of the wing trailing edge flap in the full size airplane, and only one third that of the rotor longitudinal cyclic pitch control.

Analysis of this system showed that even with a feedback gain, $S_{cs}[q_1, \delta_s]$, of -9.0 rad/rad, the (RMS) of wing vertical bending was reduced only 5% with a negligible change in flapping. Open-loop tests in which the vane was oscillated sinusoidally verified the ineffectiveness of the vane as a vertical force producer. It was concluded that bending fed to the vane would not be effective in alleviating vertical gust effects, even if the vane size were increased by a factor of 10. The limited power of the vane servo set a further limit on the maximum feedback gain and thus the achievable performance. As a result System 2-1 was not tested experimentally.

4.5 System 2-2: Wing Vertical Bending Velocity Fed to the Wing Tip Mounted Vane

In spite of its relative ineffectiveness the wing tip mounted vane was capable of supplying sufficient force to make a significant change in the damping ratio of the wing vertical bending mode (of the order of a factor of 3). This is because the damping ratio of the unaugmented wing mode was

approximately 0.03, so that the inherent damping forces in the structure are also very small. Since the bending mode was a significant contributor to the power spectral density of the bending response, increased damping of the wing bending mode made possible approximately 30% improvement in the (RMS) bending response as shown in Figure 23. The bending response was comparable to that achieved feeding wing bending velocity to the longitudinal cyclic (see Figure 22). However, using the vane had a negligible effect upon the rotor flapping, and it did not destabilize the wing torsion mode. In these respects one would prefer System 2-2 over System 1-2. Similarly, the combination of System 1-1 and System 2-2 would be an optimum choice for reducing both rotor flapping and wing bending response. This is similar to the conclusion reached in Reference 2 utilizing the trailing edge flaps.

4.6 System 3-1: Wing Chordwise Bending Displacement Fed to Collective Pitch

The collective blade pitch control was the only available control effector on the model capable of exerting forces to oppose the effects of longitudinal gusts. A longitudinal gust in the aft direction produced a blade angle of attack change which in turn resulted in an aft force on the wing and an accelerating force on the rotor. If wing chordwise bending displacement were measured and fed back to the rotor collective pitch control, only small changes in the low frequency portion of the closed loop chordwise bending response resulted with practical levels of feedback gains. Hence, the primary potential for reducing the (RMS) bending response was through increasing the damping ratio of the chordwise bending mode. The effect of bending feedback upon the bending mode was to increase the undamped natural frequency and the damping ratio. Since increasing the natural frequency

shifted the peak amplitude into a region where the gust spectrum was lower, both effects acted to reduce the (RMS) response. Figure 24 presents the performance achieved. Since the blade collective changes introduced rotor accelerating force changes as well as lift changes, the (RMS) level of the change in rotor speed increased.

4.7 System 3-2: Wing Chordwise Bending Velocity Fed to the Collective Pitch Control

Wing chordwise bending velocity feedback was effective in adding damping to the wing chordwise bending mode as would be expected. There was also a decrease in undamped natural frequency which shifted the peak amplitude ratio to a region of increased gust spectrum. The increased damping was the more important effect, and Figure 25 which summarizes the expected performance shows that the (RMS) response improvement can be of the order of 50%. This improvement in chordwise bending response was accompanied by little deterioration in the rotor rotational speed response and hence System 3-2 is to be preferred over System 3-1.

4.8 System 4-1: Rotor Rotational Speed Change Fed to the Collective Pitch Control

Longitudinal gust induced changes in rotor angle of attack produce force components tending to accelerate or decelerate the rotor. Unsymmetric forces on the two rotors would also increase the stresses in the interconnect shafting between the rotors. Hence, it was of interest to investigate the use of a feedback controller to reduce the (RMS) change in rotor speed.

The transfer function relating rotor speed change to collective pitch is dominantly a first order lag. The most important effect of the feedback

loop was the reduction of the static sensitivity of the closed-loop transfer function relating rotor speed change to the longitudinal gust input by the factor $(1 + S_{OL})^{-1}$, where S_{OL} is the open-loop static sensitivity. Figure 26 shows that this feedback loop was very effective in reducing the (RMS) level of rotor speed change induced by longitudinal gusts. The fore and aft forces accompanying the collective changes resulted in increased excitation and decreased damping of the chordwise bending mode so that the (RMS) level of chordwise bending increased as shown in Figure 26.

The motivation for alleviation of rotor rotational speed change due to longitudinal gust is that $\Delta\Omega$ has a large low frequency response. Furthermore, unsymmetric rotor rotational speed change would put torsional stress on the interconnect shaft, which allows one engine to power both rotors in the event of one engine failure.

4.9 Effects of Servo System Dynamics

In Sections 4.2 to 4.8, the servos needed to actuate the controls were assumed to be ideal in that dynamic lags and saturation effects were assumed to be negligible. The actual rotor cyclic pitch and collective pitch controllers of the wind tunnel model were electrical servos which could be modelled as second order lag elements. The servo damping and natural frequencies are listed in Table 4.1.

TABLE 4.1

NATURAL FREQUENCIES AND DAMPING RATIOS

OF MODEL SERVOS

Servo	Damping Ratio ζ	Natural Frequency ω_n (Hz)
Longitudinal Cyclic	.225	40
Collective Pitch	.25	13.5
Wing Tip Mounted Vane	.22	14.5

The gust alleviation system performance is deteriorated by servo lags. Hence, the previous results establish limits on the best performance of the gust alleviation systems to be expected.

A sensitivity analysis of (RMS)β_{1c} at the optimal gain of System 1-1 as a function of the longitudinal cyclic servo natural frequency and damping ratio was summarized in Figure 27. The q_1 mode became unstable when the θ_{1s} servo natural frequency was less than 27 Hz ($\frac{\omega_n}{\Omega} = 1.19$) regardless of the servo damping. Also, (RMS)β_{1c} showed little variation with servo damping when the servo had a natural frequency higher than 100 Hz ($\frac{\omega_n}{\Omega} = 4.4$). In other words, a second order servo with a natural frequency higher than 100 Hz could be considered to be an ideal servo with negligible dynamic lag for this particular airplane model. In between these two frequencies, (RMS)β_{1c} increased as natural frequency decreased, and for a given natural frequency, low damping ratio was the best. This was because the primary improvement in (RMS) response was the result of low frequency effects.

4.10 Effects of Accelerometer Dynamics and Location

It was proposed that the wing vertical bending displacement could be sensed using an accelerometer whose output signal could be integrated twice. The effect of the accelerometer dynamics in System 1-1 can be investigated by adding a cascaded second order system in the feedback path, and Figure 27 can thus be used to specify desirable accelerometer characteristics. Figure 27 shows that an accelerometer whose natural frequency is higher than 100 Hz has almost no effect upon the gust alleviation system performance.

Depending upon the chordwise and spanwise locations of the accelerometer on the wing, its output will contain various combinations of wing vertical bending and torsional mode accelerations. The wing elastic axis is assumed to be straight, and along the wing span in the analytical dynamical analysis of the wing/rotor assembly in Reference 8. Two accelerometers on the wing tip which are mounted 1.5 inches fore and aft of the wing elastic axis were analyzed. The former tends to destabilize, and the latter to stabilize, the wing torsion mode. With the present model the torsion component of the accelerometer input was less than 10%, and the chordwise location of the accelerometer had negligible effect upon the system.

The chordwise location of the accelerometers has no effect on the longitudinal gust alleviation systems.

4.11 Integrating Circuits

Integrating circuits were used to obtain signals approximately proportional to the bending velocity and displacement from the output signal of an accelerometer. The dynamics of the integrating circuits can be modelled as first order lags. The mathematical block diagram is shown

in Figure 28 . In order to provide a guide in choosing time constants in the wind tunnel experiment, a sensitivity analysis of the RMS value of the rotor longitudinal cyclic flapping as a function of the time constant in the pseudo integrator of System 1-1 was performed with the results shown in Figure 29. The first integrator was assumed to be ideal, and the feedback static sensitivity, $S_{cs}(q_1, \theta_{1s})$, is at its optimum value for minimizing rotor flapping. A first order lag with time constant greater than 3 seconds could be considered to have negligible effect upon system performance.

If both integrators are modelled by first order lags, the deterioration in the feedback system was greater than that shown. Higher time constants would then be desirable, or a re-optimization of the system gains should be carried out.

4.12 Filtering Circuits

Comparing the open loop power spectral density of rotor longitudinal cyclic flapping to vertical gust with the closed loop (PSD) of System 1-1 in Figure 21, one can see that the reduction in RMS(β_{1c}) was due primarily to the attenuation of the low frequency response. The oscillatory component of the rotor cyclic flapping response at the wing vertical bending mode frequency was amplified, but the high frequency components contributed relatively little to the RMS level of the rotor cyclic flapping. If the high frequency oscillations are objectionable from the standpoints of wear or structural loads, however, one would need to provide filtering of the bending signal.

The parameter optimization of a second order filter resulted in the

choice of the filter shown in Figure 30. The minimal RMS level of the rotor longitudinal cyclic flapping could be reduced as shown at the cost of a slight increase in the RMS level of wing vertical bending. Alternatively, the filter would permit increased feedback gain to reduce bending while maintaining the same level of flapping response.

Further details of the model gust alleviation system design are given in Reference 24.

CHAPTER 5

GUST ALLEVIATION SYSTEM TESTING - GIMBALLED ROTOR

5.1 Introduction

Several of the gust alleviation system configurations described in Chapter 4 were tested in the MIT Wright Brothers Wind Tunnel. The wing/rotor assembly is shown in Figure 10. The gust generator described in Chapter 2 was used to generate sinusoidal gusts. A wind tunnel speed of 95 mph and a rotor rotational speed of 1360 rpm were used for all tests. Three single feedback configurations of the vertical gust alleviation system and one single feedback configuration of the longitudinal gust alleviation were tested.

A Honeywell Visicorder 12-channel oscillograph was used to record signals indicating wing bending, pitch gimbal motion, blade inboard flapping, gust input as measured by a hot-wire anemometer, one-per-rev pulses from the rotor shaft and from the gust generator cylinders, the servo follow-up potentiometer, the integrator outputs, and the rotor tachometer. An HP-3960 4-channel tape recorder was also used. A Federal Scientific Spectrum Analyzer was used to obtain the power spectral density from the experimental data recorded on the magnetic tape. Two minutes of data were recorded for each test for which a spectrum was desired. For a spectrum width of 100 Hz, 4 seconds of data were required, so that a two minute run provided approximately 16 segments for obtaining an overall average spectrum.

5.2 Model Frequency Response to Control Inputs

In order to obtain the static sensitivities and low frequency response

to control inputs, sinusoidal inputs with frequency up to 7 Hz or three tenths of rotor rotational speed were fed to the rotor cyclic pitch, the wing tip mounted vane, and the rotor collective pitch.

For the sinusoidal longitudinal cyclic tests, wing vertical bending displacement and rotor lateral cyclic flapping were analyzed from the data recorded on the oscillograph. Because of an instrumentation failure of a gimbal potentiometer, the longitudinal cyclic flapping was not measured experimentally.

The comparisons of the experimental data with analytical results for the open loop responses of the wing vertical bending displacement and rotor lateral cyclic flapping are summarized in Figures 31 and 32. The experimental data for wing bending displacement on the oscillograph record contained both the controlled response and the response at the wing bending natural frequency as excited by the wind tunnel turbulence. The resulting difficulty in reading oscillograph traces resulted in the scatter in the experimental data. The analytical results predicted higher values for wing vertical bending and rotor lateral cyclic flapping than the experimental values. (See further discussion of this below.)

Since the wing tip mounted vane had little effect upon the rotor flapping, the primary effect of this control input was upon the wing vertical bending response. The experimental values of wing vertical bending to a sinusoidal wing tip mounted vane input are summarized in Figure 33. The correlation between experimental and analytical data was good.

For the sinusoidal rotor collective pitch test, wing chordwise bending displacement and rotor rotational speed change were measured. The

experimental values of wing chordwise bending displacements to sinusoidal collective pitch are summarized in Figure 34. The experimental values were larger than the analytical values. The experimental values of the rotor rotational speed change are summarized in Figure 35 .

5.3 Closed Loop Response Tests

In the vertical gust alleviation system, three single feedback configurations were tested: wing vertical bending displacement fed to the rotor longitudinal cyclic pitch; wing vertical bending velocity fed to the rotor longitudinal cyclic pitch; and wing vertical bending velocity fed to the wing tip mounted vane. The use of wing vertical bending displacement fed to the wing tip mounted vane was not tested because of its predicted ineffectiveness.

Because the available collective servo had about the same natural frequency as that of the wing chordwise bending mode, the use of wing chordwise bending displacement or velocity fed to rotor collective pitch would have resulted in an unstable system. It was not feasible to redesign the servo in this research program. Thus, rotor rotational speed change fed to rotor collective pitch was the only longitudinal gust alleviation system actually tested.

The first feedback configuration tested, System 1-1, is shown in Figure 36. The wing vertical bending acceleration signal as measured by an accelerometer mounted at the wing tip aft of the wing elastic axis was fed through two first order lags with time constants of 1 and 1.25 seconds to obtain an approximation to the wing vertical bending displacement. Due to rotor unbalance, a one-per-rev signal was present in the wing vertical

bending signal. The electrical servomotor could not follow this one-per-rev signal, due to an excessive current in the motor armature which caused the motor protective fuse to burn out. Four values of the feedback static sensitivity relating wing vertical bending displacement to rotor longitudinal cyclic pitch, $S_{cs}(q_1, \theta_{1s})$, were tested in the wind tunnel. They were 0, 2, 4, and 6 rad/rad, which were values below, near, and above the optimal theoretical feedback gain which minimized the RMS rotor cyclic flapping. In the analysis, dynamics of the servo, filter and integrators were included for correlation with the experimental data.

The gust generator, which could generate a sinusoidal gust at a specified frequency in the wind tunnel, was used in the closed loop response tests to generate a low magnitude sinusoidal gust near the wing vertical bending mode natural frequency at 8.2 Hz and a larger magnitude sinusoidal gust at 1.67 Hz. Figure 37 summarizes the analytical and experimental values of the wing vertical bending response to sinusoidal gust inputs. Figure 38 presents the analytical and experimental ratios of closed loop to open loop responses versus loop gain. At 1.67 Hz, the control system had no measurable effect on the wing vertical bending response. The analytical study predicted approximately 15% reduction over the range of open loop gain. At 8.2 Hz, the experimental showed less percentage reduction than the analytical results.

Figure 39 summarizes the analytical and experimental values of the rotor longitudinal cyclic flapping response to sinusoidal gust inputs. Figure 40 presents the ratio of closed loop to open loop response of rotor flapping at 1.67 Hz versus loop gain. There was greater inaccuracy in the

xperimental data for rotor cyclic flapping, because flapping was measured y a gimbal potentiometer whose output contained a large one-per-rev response nd a small response at the gust excitation frequency. Rotor longitudinal yclic flapping was reduced, but the percentage reduction was smaller than predicted analytically. Figure 41 presents the ratio of closed loop to open loop response of rotor flapping at 8.2 Hz. The experimental data showed amplification with loop gain, but the percentage amplification was smaller than predicted analytically.

The RMS level of the wing and rotor responses to atmospheric turbulence modelled by an approximation to the von Karman gust power spectral density were used as performance criteria in designing the gust alleviation system (see Chapter 4). The effectiveness of the control systems in reducing the RMS levels of flapping and bending to random gust inputs was assessed in the tunnel turbulence environment. Tunnel turbulence was measured experimentally using a hot wire anemometer whose output was recorded on magnetic tape, and the power spectral density is plotted in Figure 42. A von Karman gust PSD with a gust characteristic length of seven feet was used to approximate the tunnel turbulence. Experimental data of tunnel turbulence (PSD) were close to the von Karman PSD at frequencies less than 10 Hz.

Figure 43 summarizes the RMS levels of the wing vertical bending and rotor longitudinal cyclic flapping responses to wind tunnel turbulence. The RMS level of wing vertical bending showed nearly the same percentage reduction as the analytical results. For all three experimental measurements, there was an apparent amplification, rather than a reduction, in the RMS level of the rotor longitudinal cyclic flapping. The low energy content

in the tunnel turbulence resulted in a very small magnitude of rotor flapping response. Thus, RMS(β_{1c}) measurements were subject to considerable inaccuracy. The RMS magnitude of flapping was approximately 0.2 degrees if the one-per-rev component due to rotor unbalance was removed from the data. the one-per-rev component, however, was approximately five times that level. Hence, the RMS(β_{1c}) estimate was inaccurate and the deviations indicated by the experimental points on Figure 43 may be considered questionable.

The second feedback configuration tested, System 1-2, is shown in Figure 44. The accelerometer, integrator with high-pass filter, amplifier and rotor longitudinal cyclic-pitch servo were the same as those of System 1-1. In addition to the one-per-rev signal, the integrated wing vertical bending velocity signal contained two- and three-per-rev signals and other higher frequency components, which overloaded the servo armature current. Thus, two-per-rev and three-per-rev notch filters and a low-pass filter with cutoff frequency at 80 Hz were included in the feedback path.

Figure 45 presents the analytical and experimental values of the wing vertical bending response to sinusoidal gust inputs. Figure 46 summarizes the analytical and experimental values of ratios of closed loop to open loop response of wing vertical bending to 1.67 Hz and 8.2 Hz gusts versus loop gain. At 1.67 Hz, the control system made little change in the wing vertical bending response. The analytical study predicted a 5% amplification over this range of open loop gain. At 8.2 Hz, the percentage reduction in the experimental values of the wing vertical bending was smaller than the analytical prediction.

Figure 47 summarizes the analytical and experimental values of the

rotor longitudinal cyclic flapping response to sinusoidal gust inputs. Because rotor longitudinal cyclic flapping had a very small magnitude response to a 8.2 Hz gust, no data were analyzed at this frequency. At 1.67 Hz, rotor longitudinal cyclic flapping had a smaller percentage amplification than analytical predicted, Figure 48.

Figure 49 summarizes the ratio of closed loop to open loop RMS level of wing vertical bending due to the wind tunnel turbulence shown in Figure 42. The percentage reduction in RMS(q_1) was smaller than analytical predictions. The analytical study predicted amplification in the RMS level of rotor longitudinal cyclic flapping. However, the small magnitude of rotor flapping resulted in inaccurate data. Hence, rotor flapping data were not included here.

The third feedback configuration, System 2-2, shown in Figure 50 was similar to System 1-2, except different amplifier gains and the wing tip mounted vane were used. The values of the closed loop frequency responses are summarized in Figure 51. The ratio of the closed loop responses of wing vertical bending to the open loop response versus loop gain for both analytical and experimental studies are summarized in Figure 52. In the wing bending resonance test, the reductions in the ratio of the closed loop values of wing vertical bending to open loop value were 30% less than analytical calculations at the highest gain. For the 1.67 Hz data, both analytical and experimental data showed almost no change in the closed loop values of wing vertical bending, but the response was 35% lower than predicted. In the wind tunnel turbulence, the RMS level of the closed loop response of wing vertical bending decreased, Figure 53. The

reduction in RMS(q_1) was approximately 10% less than predicted analytically. The wing tip mounted vane had little effect on rotor cyclic flapping in the wind tunnel tests.

The fourth feedback configuration tested, System 4-1, is shown in Figure 54. The rotor rotational speed signal as measured by a tachometer was passed through a high-pass filter with a time constant of one second to obtain the rotor rotational speed change, amplified, and fed to the collective pitch servo.

Feedback static sensitivity relating percentage change in the rotor rotational speed to the rotor collective pitch of 0.05, 0.10, and 0.15 rad/rad were tested. Higher feedback gains would reduce the RMS level of the rotor rotational speed change even more, but were not tested because of slow response and limited power in the rotor collective pitch servo.

The natural frequency of the rotor collective pitch servo was close to that of the wing chordwise bending mode. The excitation of the wing-rotor assembly by a longitudinal gust at the wing chordwise bending natural frequency was not tested because of the analytically predicted large response of both the rotor rotational speed change and wing chordwise bending. The analytical results showed that the reduction in the rotational speed change was primarily a low frequency effect. Thus, three low frequency sinusoidal gusts at 1.67, 3.33, and 5.0 Hz were used for these tests.

Figure 55 summarizes the analytical and experimental values of the rotor rotational speed change response to sinusoidal gust inputs. The measured magnitudes were in considerable error. Figure 56 presents the analytical and experimental values of ratios of closed loop to open loop

responses at 1.67, 3.33, and 5.00 Hz versus loop gain. The percentage reduction in rotor rotational speed change showed excellent agreement with analytical predictions, so that the variation with loop gain was more accurate than the actual amplitude ratio estimate. Part of the error is attributable to the uncertainty in the magnitude of the gust input.

Figure 57 summarizes the analytical and experimental values of chordwise bending response to sinusoidal gust inputs. Figure 58 presents the analytical and experimental values of ratios of closed loop to open loop responses. Due to the small magnitude of the wing chordwise bending response, the accuracy in these experimental data were judged to be poor.

Figure 59 summarizes the analytical and experimental RMS levels of the rotor rotational speed change and wing chordwise bending response due to the wind tunnel turbulence shown in Figure 42. The correlation with analytical predictions is good.

Since there were differences between analytical and experimental results, one could modify the open loop equations of motion to see whether a different set of design parameters would give closer analytical agreement with the experimental data.

In the open loop control frequency response tests, the experimental data of the wing vertical bending displacement and the rotor lateral cyclic flapping responses to the rotor longitudinal cyclic pitch were smaller than the analytical results, as shown in Figures 31 and 32. In the closed loop gust test using rotor longitudinal cyclic pitch, Figures 38 and 40 showed that the percentage reductions in both wing vertical bending and rotor longitudinal cyclic flapping were also smaller than the analytical

predictions. Thus, one could conclude that the rotor longitudinal cyclic pitch control effectiveness was less than that used in the analytical predictions.

If the static sensitivities of both wing vertical bending and rotor longitudinal cyclic flapping response to the rotor longitudinal cyclic pitch were reduced by 25%, the experimental values of the open loop control frequency responses would have excellent correlation with analytical results. This has the effect of reducing the open loop static sensitivity by 25%. Referring to Figures 43 and 38 for System 1-1, in which the wing vertical bending signal is fed back to rotor longitudinal cyclic pitch, this change in open loop gain values for the test conditions would shift the experimental data to the left by 25%. These data would then almost coincide with the analytical curves. However, little improvement in correlation would result in the rotor longitudinal cyclic flapping. In System 1-2, in which the wing vertical bending velocity signal was fed back to rotor longitudinal cyclic pitch, a 25% reduction in the effectiveness of the rotor longitudinal cyclic pitch makes the analytical predictions correlate well with analytical results.

In the open loop frequency response tests, the wing vertical bending displacement response to the wing tip mounted vane showed good agreement with the analytical results as shown by Figure 33. In System 2-2, in which the wing vertical bending velocity signal was fed to the vane, the percentage reduction of the wing vertical bending response to an 8.2 Hz gust was larger than for the analytical results, but the percentage reduction of RMS(q_1) in the wind tunnel turbulence was smaller than for the

analytical results, Figure 53. Therefore a change in control effectiveness of the vane would not explain the difference. However, the overall trend of the effect of the control system was verified by the experimental tests.

In the open loop control frequency response tests, the rotor rotational speed change response to the rotor collective pitch showed good correlation with analytical predictions, Figure 35, but the wing chordwise bending responses were larger than the analytical results, Figure 34. In System 4-1, in which the rotor rotational speed change signal was fed to rotor collective pitch, the rotor rotational speed again correlated well with the analytical predictions at three low frequencies and in wind tunnel turbulence, Figures 56 and 59. The experimental percentage reduction in the wing chordwise bending responses to 3.33 and 5.00 Hz gusts were greater than analytical results, Figure 58, but these data are very doubtful because of the small magnitude of the wing chordwise response. The experimental levels of RMS(q_2) in wind tunnel turbulence, Figure 59, were close to the analytical results. However, because the wing chordwise bending resonant response accounted for most of the RMS(q_2), these data offered little information about the low frequency characteristics.

Further details of the model gust alleviation system tests are given in Reference 24.

CHAPTER 6

CONCLUSIONS

For a given spectrum of atmospheric turbulence, the minimization of the root mean square value of response is the process of shaping the magnitude of the closed-loop frequency response such as to minimize the area under the curve of the output power spectral density. Since it was not possible to generate turbulence in the wind tunnel that would model the expected full scale turbulence, the objective of the experimental tests was to measure the closed-loop frequency response to sinusoidal gust inputs. If the measured frequency response data correlated well with analytical predictions, an indirect measurement of the achievable performance would be obtained. The present analytical and experimental investigation of a gust alleviation system for tilt-rotor aircraft has led to the following conclusions:

1. The open-loop wing vertical bending response to rotor longitudinal cyclic inputs and the closed-loop wing vertical bending response to sinusoidal gust inputs indicate that the rotor longitudinal cyclic control was approximately 25% less effective in producing wing vertical bending response per unit of cyclic control input than was predicted theoretically. Hence, a 25% higher feedback loop gain was required to achieve a given reduction in the RMS level of wing vertical bending.
2. The rotor flapping response data obtained from the tests were inconclusive. The accelerometer sensed a one-per-revolution component due to rotor unbalance which resulted in corresponding cyclic control and flapping response. The one-per-revolution

component of the flapping response was large relative to the gust-induced component, and the data reduction inaccuracies were large.

3. The experimental tests generally confirmed the analytical predictions of the effects of the active control system in reducing the wing vertical bending response to atmospheric turbulence. For the model, reductions of approximately 30% are achievable with simple feedback systems feeding wing vertical bending motion to the rotor longitudinal cyclic control. An accelerometer can serve as the sensor of bending motions. The reduction in bending is achieved by reducing the amplitude ratio of the closed-loop frequency response over both the low and the high frequency ranges. The high-frequency improvement is due to an increase in the damping ratio of the wing vertical bending mode. Only moderate increases in damping ratio are effective since the bending mode frequency is high relative to the bandwidth of the gust spectrum. Hence, a moderate reduction in the peak response is sufficient to cause the contribution of this mode to become an insignificant contributor to the RMS level of response. The low-frequency improvement can be considered to result from an effective increase in wing bending stiffness due to the presence of the control system. The improvement here is constrained by the limited capability of the rotor to produce vertical force without excessive levels of control input.

4. Feeding the wing bending signal to the rotor cyclic introduced wing bending mode oscillations into the rotor cyclic and rotor

flapping response. Thus, increasing the loop gain to high values causes increased flapping response which further limits the improvement in wing vertical bending that can be achieved.

5. The wing-tip-mounted flap was not as effective as a wing trailing edge flap in that it was too small to provide a large change in wing stiffness. The reduction in wing bending achieved by feeding bending velocity to the flap resulted from the fact that small increases in the bending mode damping ratio caused large changes in the peak magnitude in the bending frequency response.
6. The (RMS) level of rotor rotational speed change was reduced 20% by feeding rotor speed change to the collective pitch control. Greater reduction would have been possible if a collective pitch servo with a wider bandwidth had been available.
7. The predicted destabilizing effect upon the wing torsion mode of feeding back wing vertical bending velocity to the rotor longitudinal cyclic pitch was not observed in the experimental tests. The damping ratio of the torsion mode of the model can thus be considered to be larger than that predicted.
8. The experiments verified that accelerometers whose signals are doubly integrated can be used to provide estimates of wing vertical bending and bending velocity which can be used in active control systems. The integrating networks should have time constants greater than 5 seconds for their effects to be negligible. Notch filters may be required to eliminate rotor frequency harmonics, and this may add complication if narrow notches are needed.

REFERENCES

1. Hall, E.W. Jr., "Prop-Rotor Stability at High Advance Ratios". Journal of American Helicopter Society, Vol. 11, No. 2, 1966, pp. 11-26.
2. Young, M.I. and Lytwyn, R.I., "The Influence of Blade Flapping Restraint on the Dynamic Stability of Low Disk Loading Propeller-Rotors", Journal of American Helicopter Society, Vol. 2, No. 4, 1968, pp. 38-54.
3. Gaffey, T.M., "The Effect of Positive Pitch-Flap Coupling on Rotor Blade Motion Stability and Flapping". Journal of American Helicopter Society, Vol. 14, No. 2, 1969, pp. 49-67.
4. Bell Helicopter Company, "V/STOL Tilt-Rotor Study Task II -- Research Aircraft Design". NASA CR 114442, March 1972.
5. Boeing Vertol Company, "V/STOL Tilt-Rotor Aircraft Study Volume II -- Preliminary Design of Research Aircraft". NASA CR 114438, March 1972.
6. Johnson, W., "Dynamics of Tilting Proprotor Aircraft in Cruise Flight". NASA TN D-7677, May 1974.
7. Johnson, W., "Theory and Comparison with Tests of Two Full-Scale Proprotors". Proceeding of the AHS/NASA-Ames Specialists' Meeting on Rotorcraft Dynamics, Feb. 1974.
8. Yasue, M., "A Study of Gust Response for a Rotor-Propeller in Cruising Flight", NASA CR-137537, August 1974.
9. Yasue, M., "User's Manual for Computer Program ROTOR", NASA CR-137553, August 1974.

10. Frick, J. and Johnson, W., "Optimal Control Theory Investigation of Proprotor/Wing Response to Vertical Gust", NASA TXM-62, 384, Sept. 1974.

11. Fry, Bernard, "Feedback Control Tests on a Windmilling 2.81 foot Diameter Soft-in-plane Hingeless Tilt Rotor in the Cruise Mode", Vertol Division, The Boeing Company, 1972.

12. Nicely, J. and Walsh, G., "Technology Data, Operations and Maintenance Manual for a Wind Tunnel Model of a Proprotor and Cantilever Wing", Boeing Document D210-10961-1, June 1975.

13. Johnson, W., "The Influence of Engine/Transmission/Governor on Tilting Proprotor Aircraft Dynamics", NASA TM X-62455, June 1975.

14. Abbott, F.T., "Brief Description of the Characteristics of the Langley Transonic Dynamic Tunnel Airstream Oscillator", Paper 6, September 1968, NASA.

15. Buell, D.A., "An Experimental Investigation of the Velocity Fluctuations Behind Oscillating Vanes", NASA TN D-5543, November 1969.

16. Simmons, J.M. and Platzer, M.F., "Experimental Investigations of Incompressible Flow Past Airfoils with Oscillating Jet Flaps", Journal of Aircraft, 8, 8, August 1971.

17. Poisson-Quinton, P., "Note on a New V/STOL Rig in the S1 Modane Sonic Tunnel", ONERA presentation at the Third AGARD Meeting on V/STOL Tunnels, Amsterdam, February 1972.

18. Bicknell, J. and Parker, A.G., "A Wind-Tunnel Stream Oscillation Apparatus", Journal of Aircraft, 9, 6, June 1972.

19. Kind, R.J. and Maull, D.J., "An Experimental Investigation of a Low-Speed Circulation-Controlled Aerofoil", The Aeronautical Quarterly, May 1968.

20. Houbolt, J.C., Steiner, R. and Pratt, K.G., "Dynamic Response of Airplanes to Atmospheric Turbulence Including Flight Data on Input and Response", NASA R-199, 1964.

21. Ham, N.D., Bauer, P.H. and Lawrence, T.H., "Wind Tunnel Generation of Sinusoidal Lateral and Longitudinal Gusts by Circulation Control of Twin Parallel Airfoils", NASA CR-137547, August 1974.

22. Ham, Norman D., Bauer, Paul H., Lawrence, Thomas, H. and Yasue, Masahiro, "A Study of Gust and Control Response of Model Rotor-Propellers in a Wind Tunnel Airstream", NASA CR-137756, ASRL, MIT, August 1975.

23. Whitaker, H.P. and Cheng, Y., "Use of Active Control Systems to Improve Bending and Rotor Flapping Responses of a Tilt Rotor VTOL Airplane", ASRL TR 183-1, Oct. 1975.

24. Cheng, Yi, "Application of Active Control Technology to Gust Alleviation System for Tilt Rotor Aircraft", NASA CR-137958, November 1976.

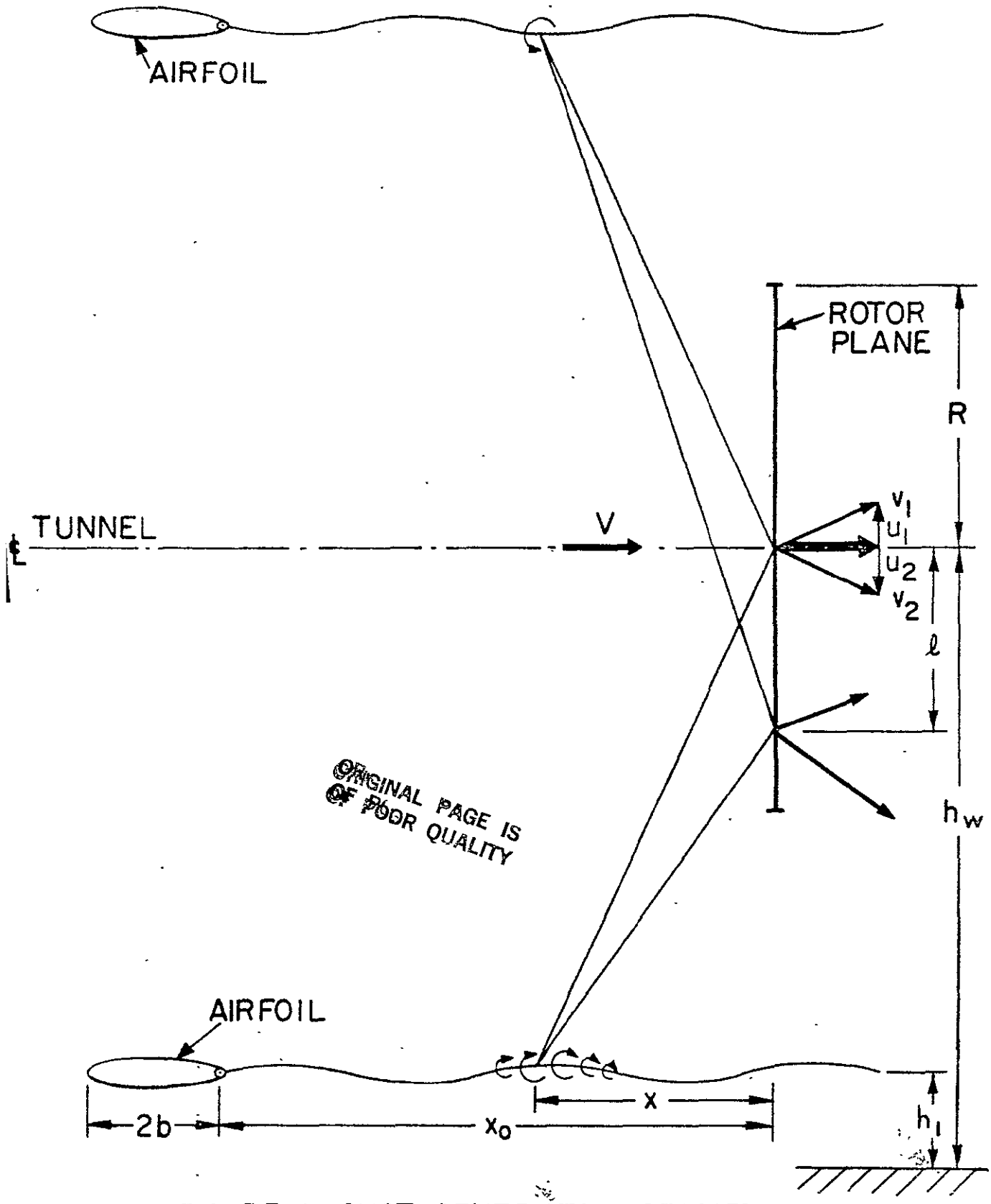

FIGURE I. GUST GENERATOR GEOMETRY

CONVENTIONAL CCA

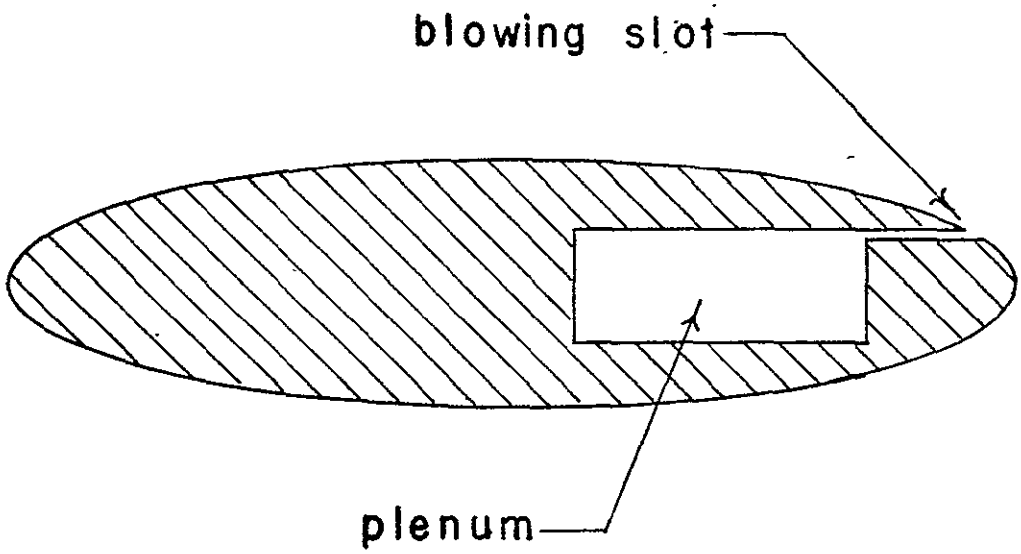

FIGURE 2a

KIND'S CCA

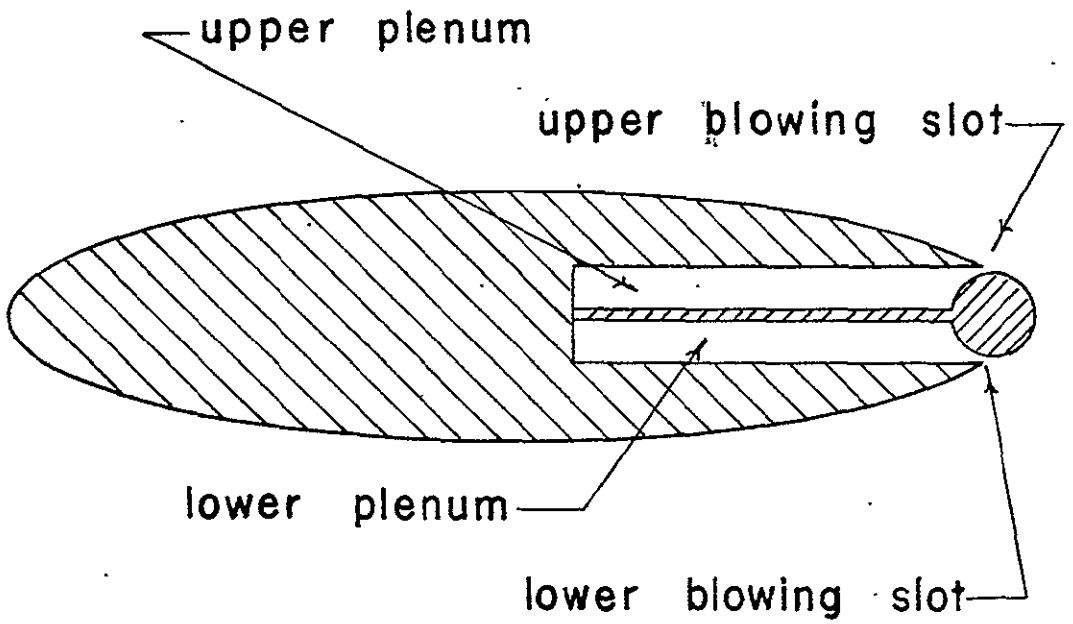

FIGURE 2b

GUST GENERATOR AIRFOIL CROSS-SECTION

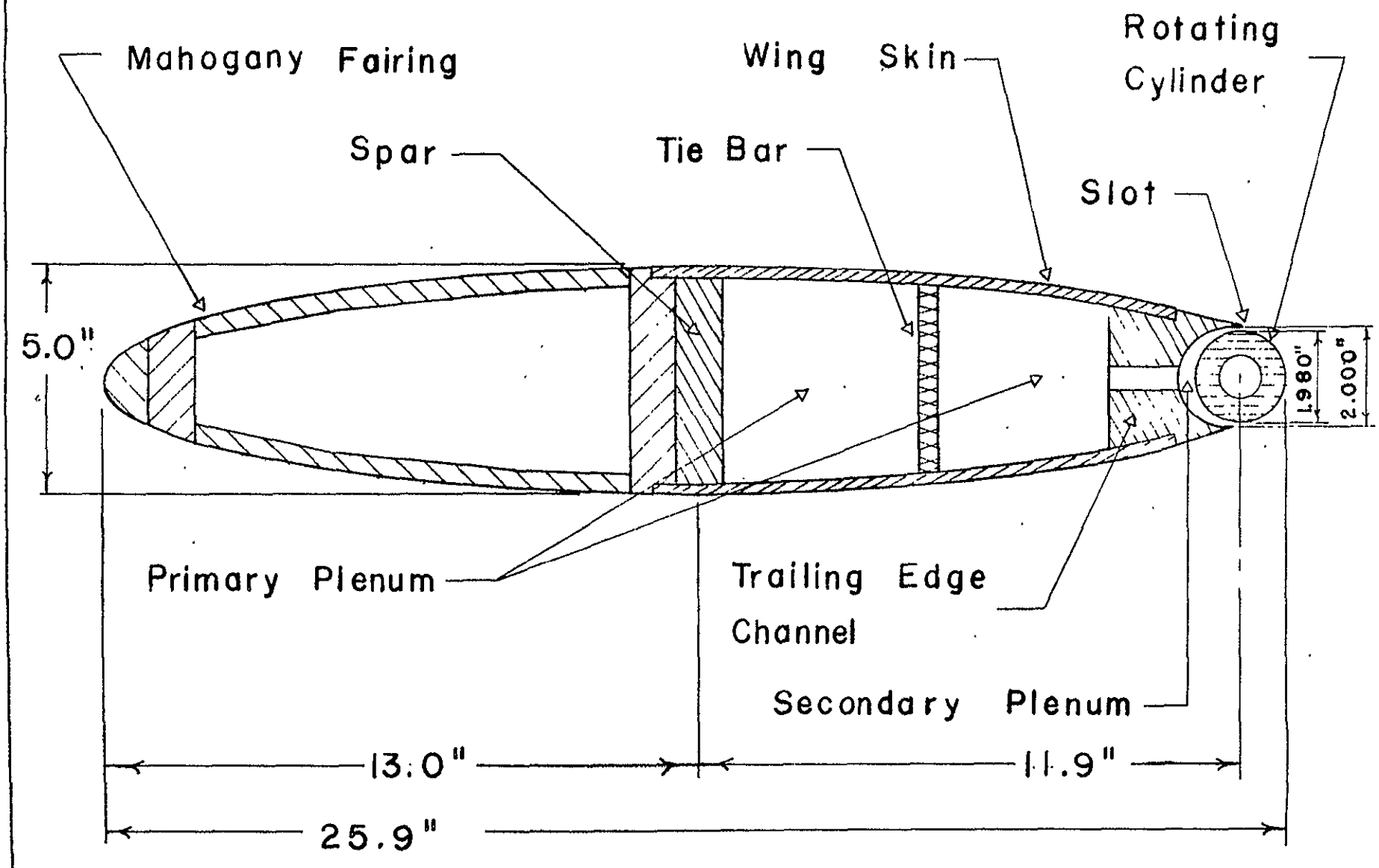

FIGURE 3

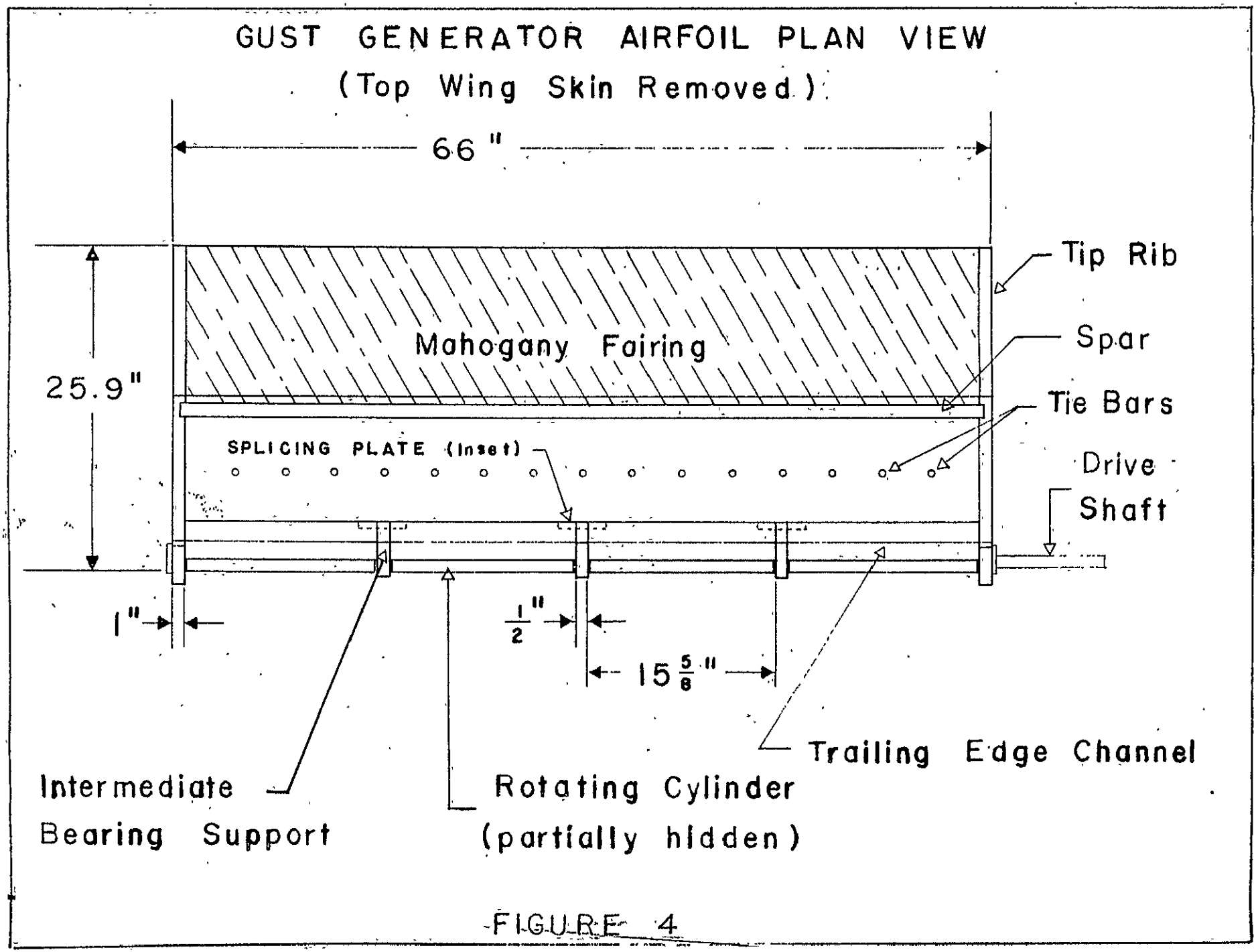
GUST GENERATOR AIRFOIL PLAN VIEW
(Top Wing Skin Removed)
66"
25.9"
Tip Rib
Mahogany Fairing
Spar
Tie Bars
SPLICING PLATE (Inset)
Drive
Shaft
1"
1/2"
15 5/8"
Trailing Edge Channel
Intermediate
Bearing Support
Rotating Cylinder
(partially hidden)

FIGURE 4

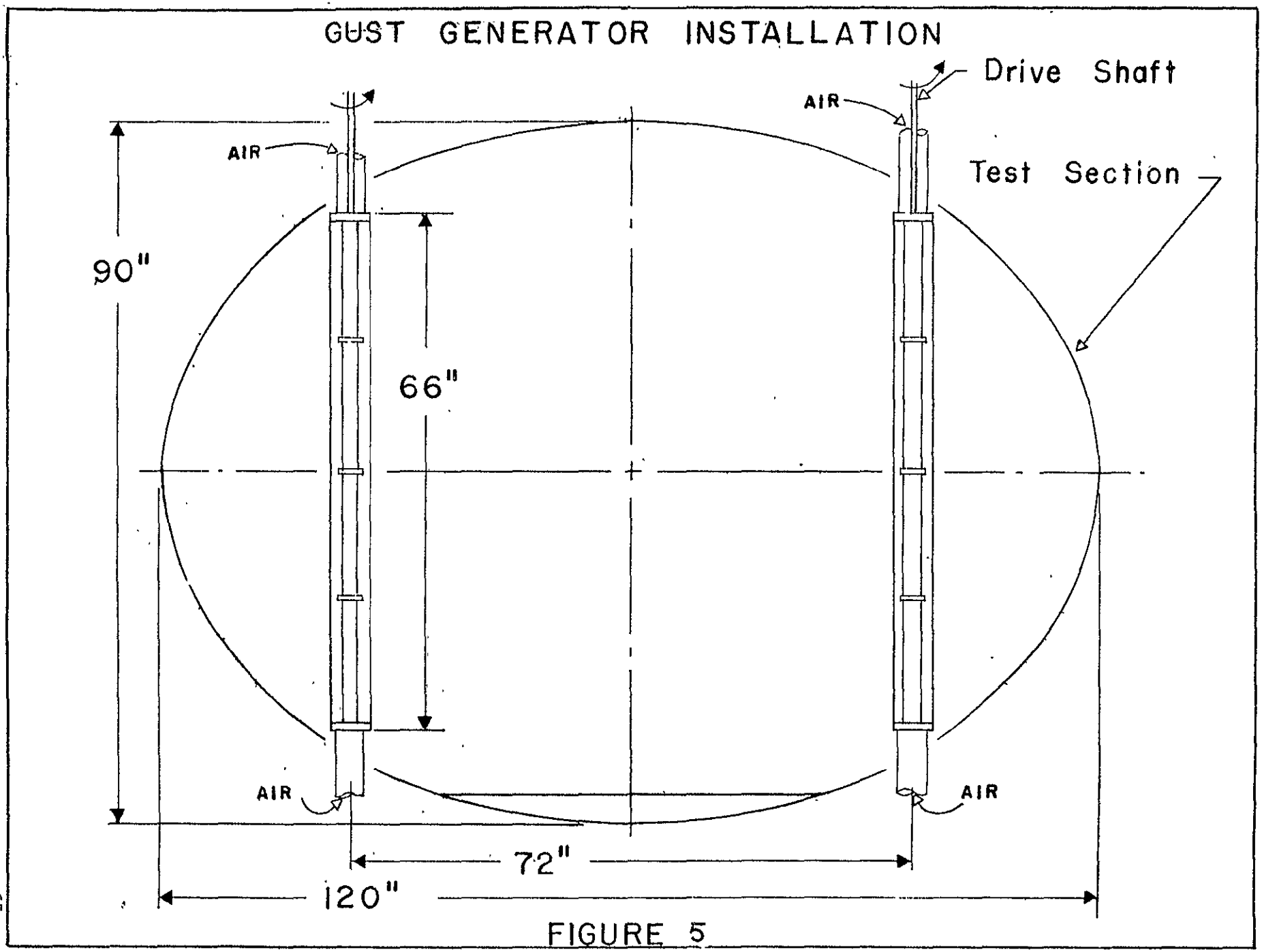
GUST GENERATOR INSTALLATION
Drive Shaft
AIR
AIR
Test Section
90"
66"
AIR
AIR
72"
120"

FIGURE 5

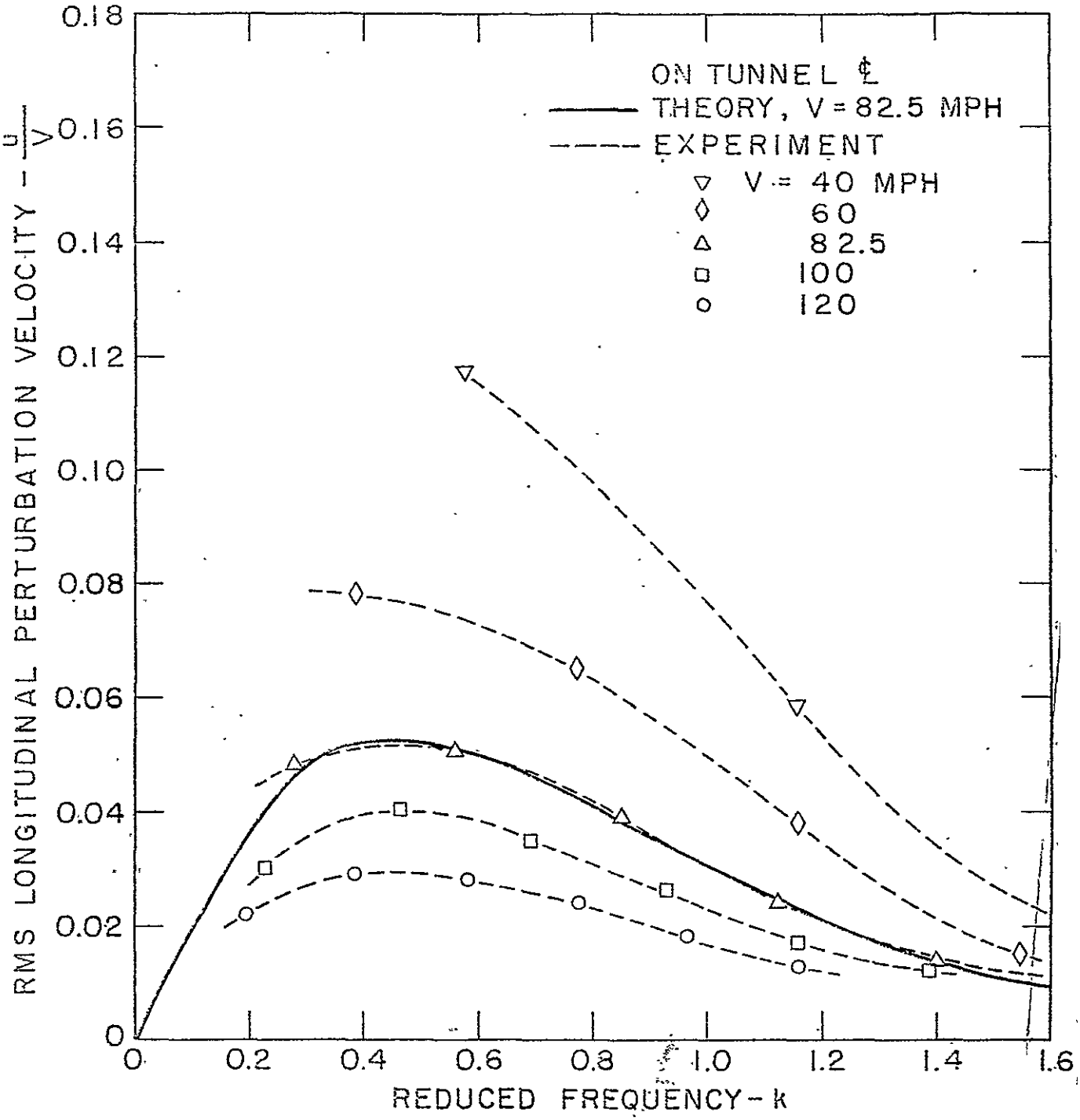

FIGURE 6 LONGITUDINAL GUST VELOCITY VERSUS REDUCED FREQUENCY

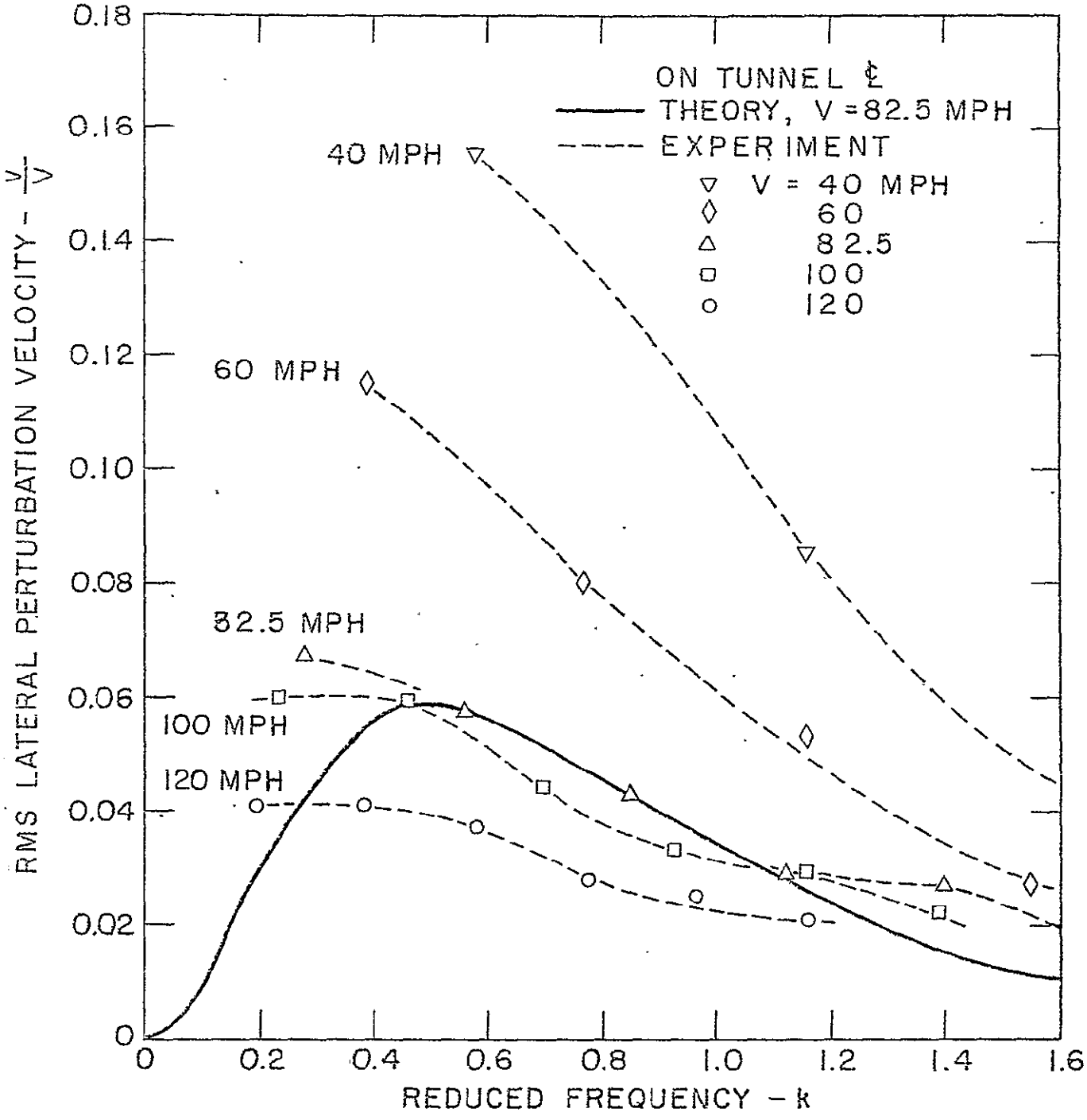

FIGURE 7 LATERAL GUST VELOCITY VERSUS REDUCED FREQUENCY

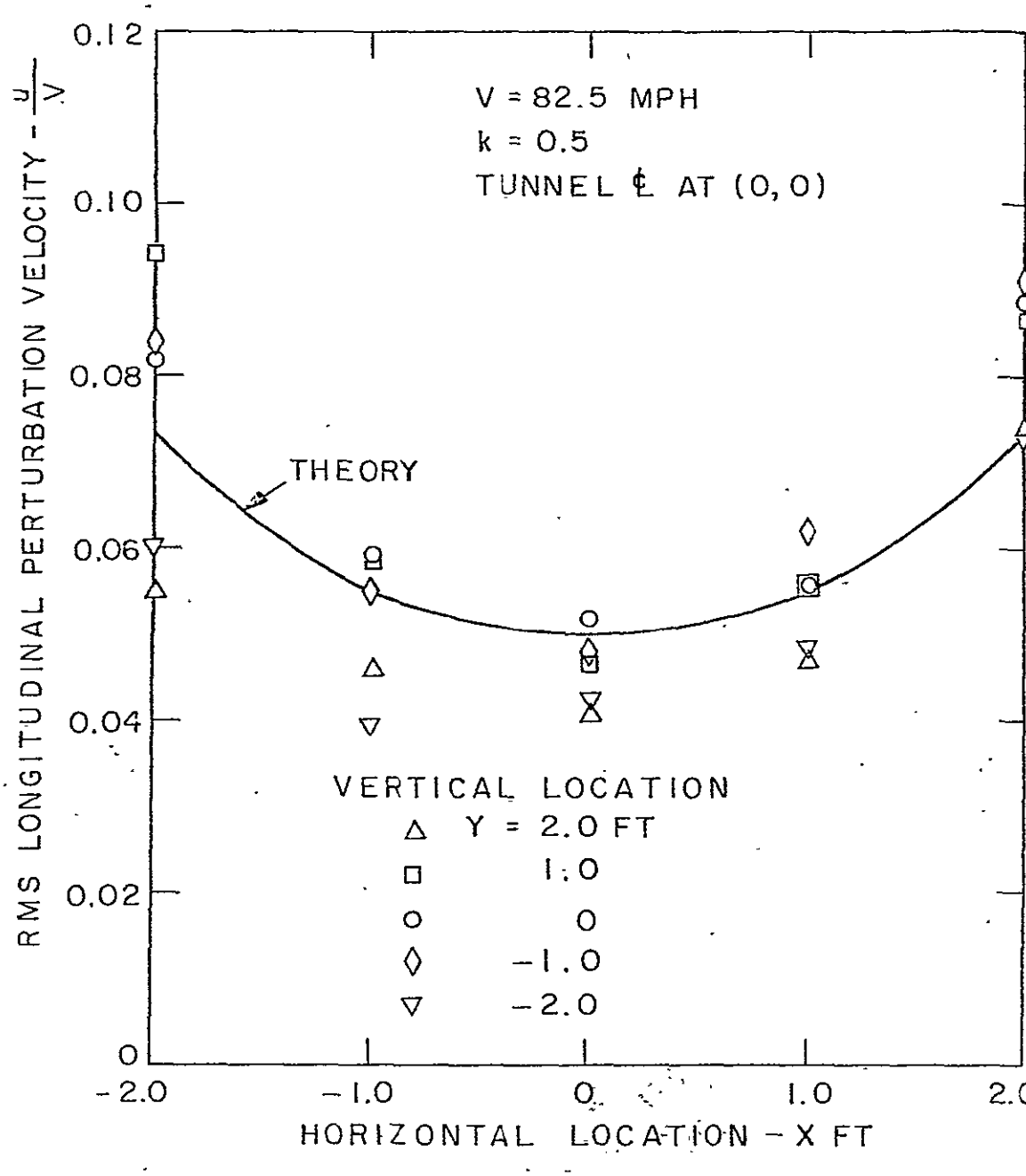

FIGURE 8 LONGITUDINAL GUST VELOCITY DISTRIBUTI
k = 0.5

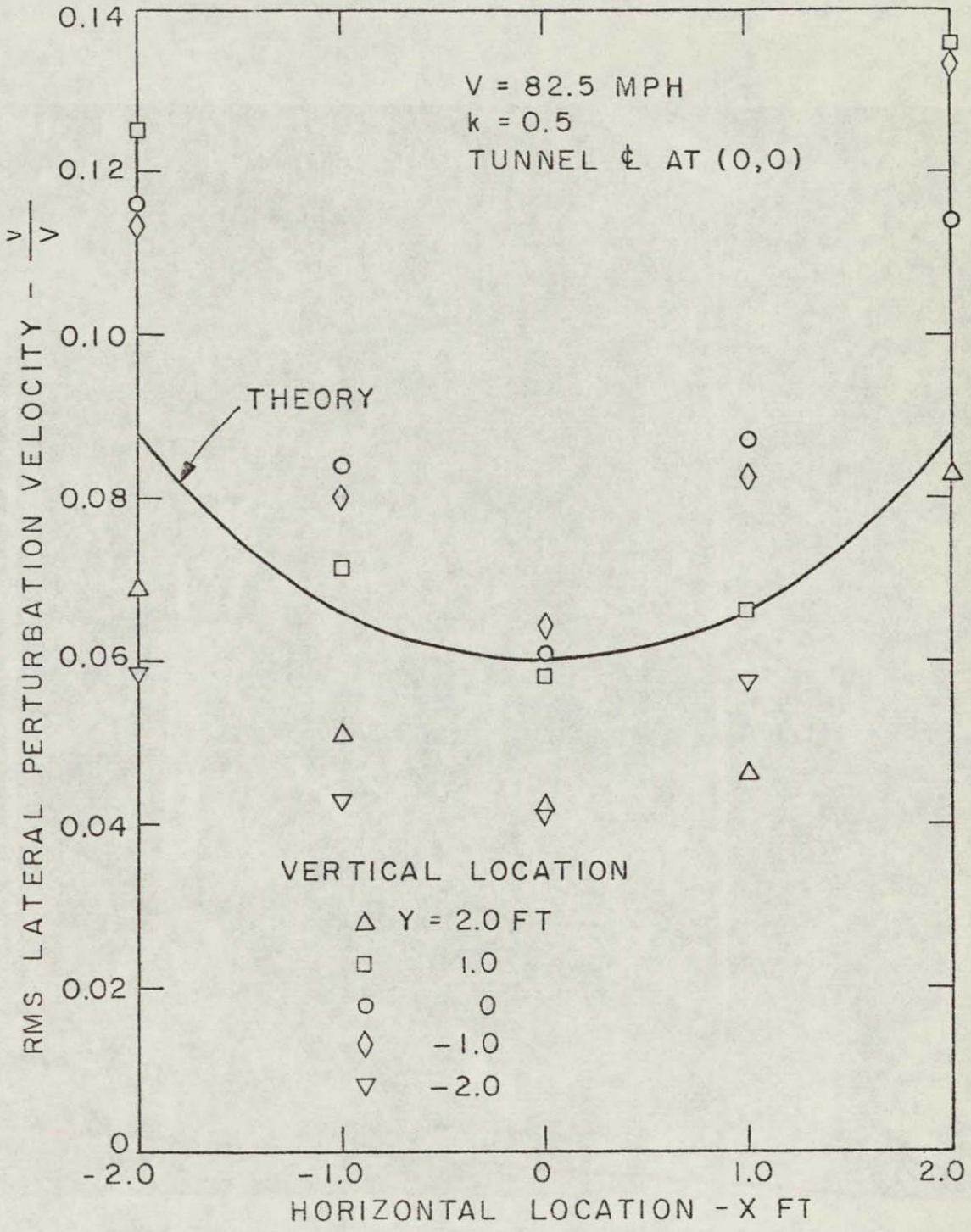

FIGURE 9 LATERAL GUST VELOCITY DISTRIBUTION, k =0.5

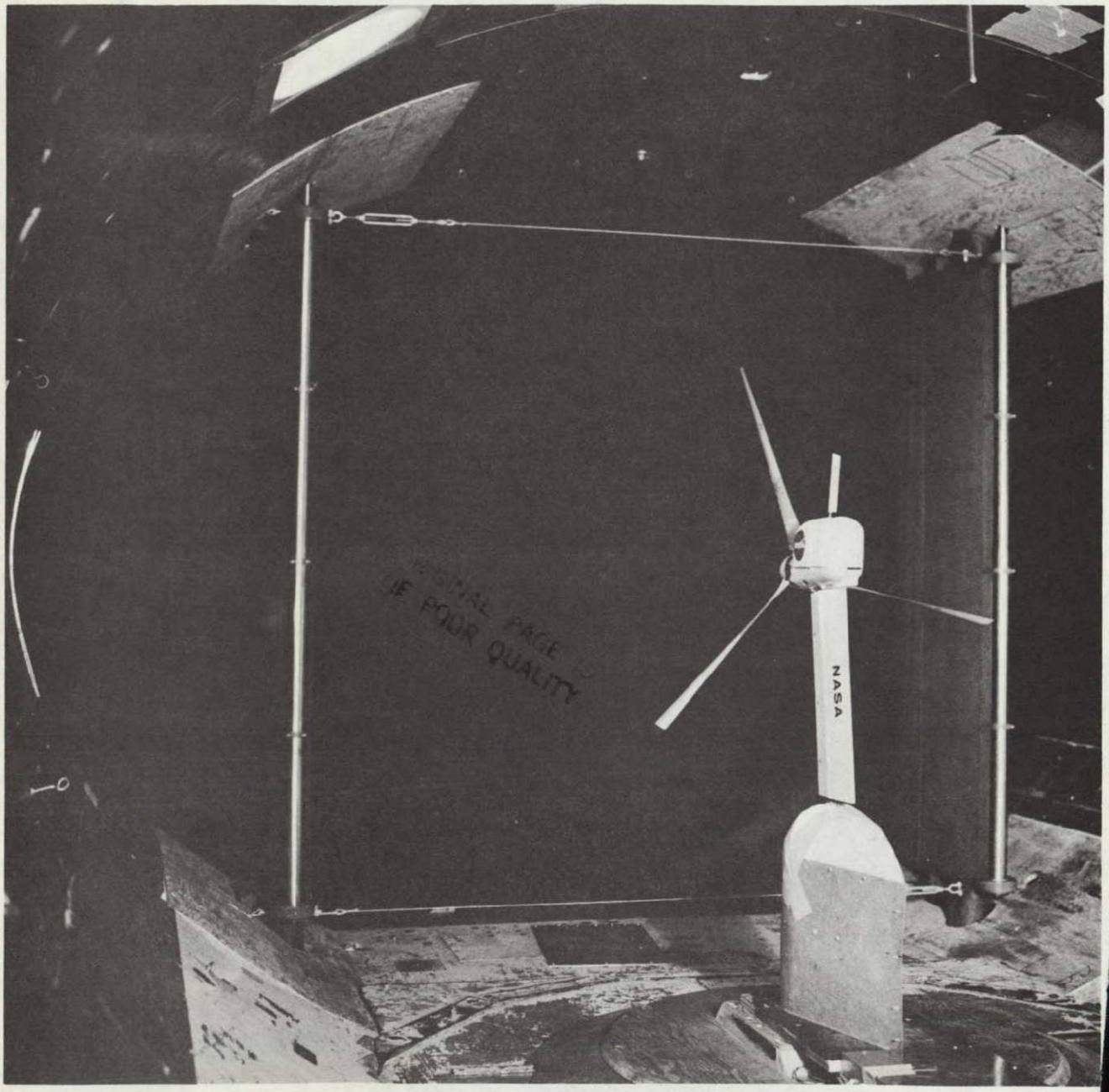

FIG. 10 MODEL SHOWN MOUNTED IN WIND TUNNEL WITH GUST GENERATOR IN BACKGROUND

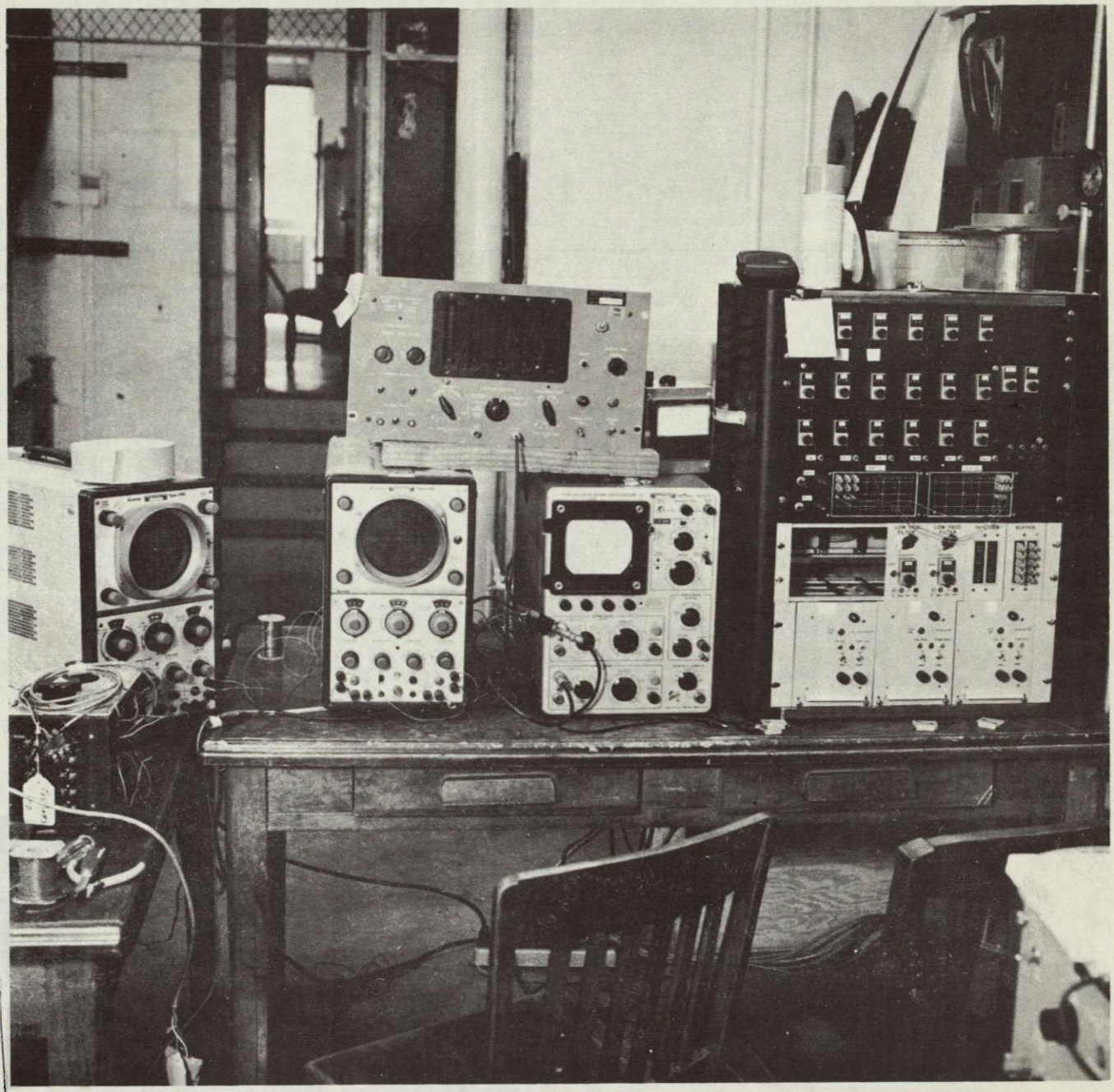

FIG. 11 MODEL OPERATOR'S STATION SHOWING CONTROL PANEL AND INSTRUMENTATION

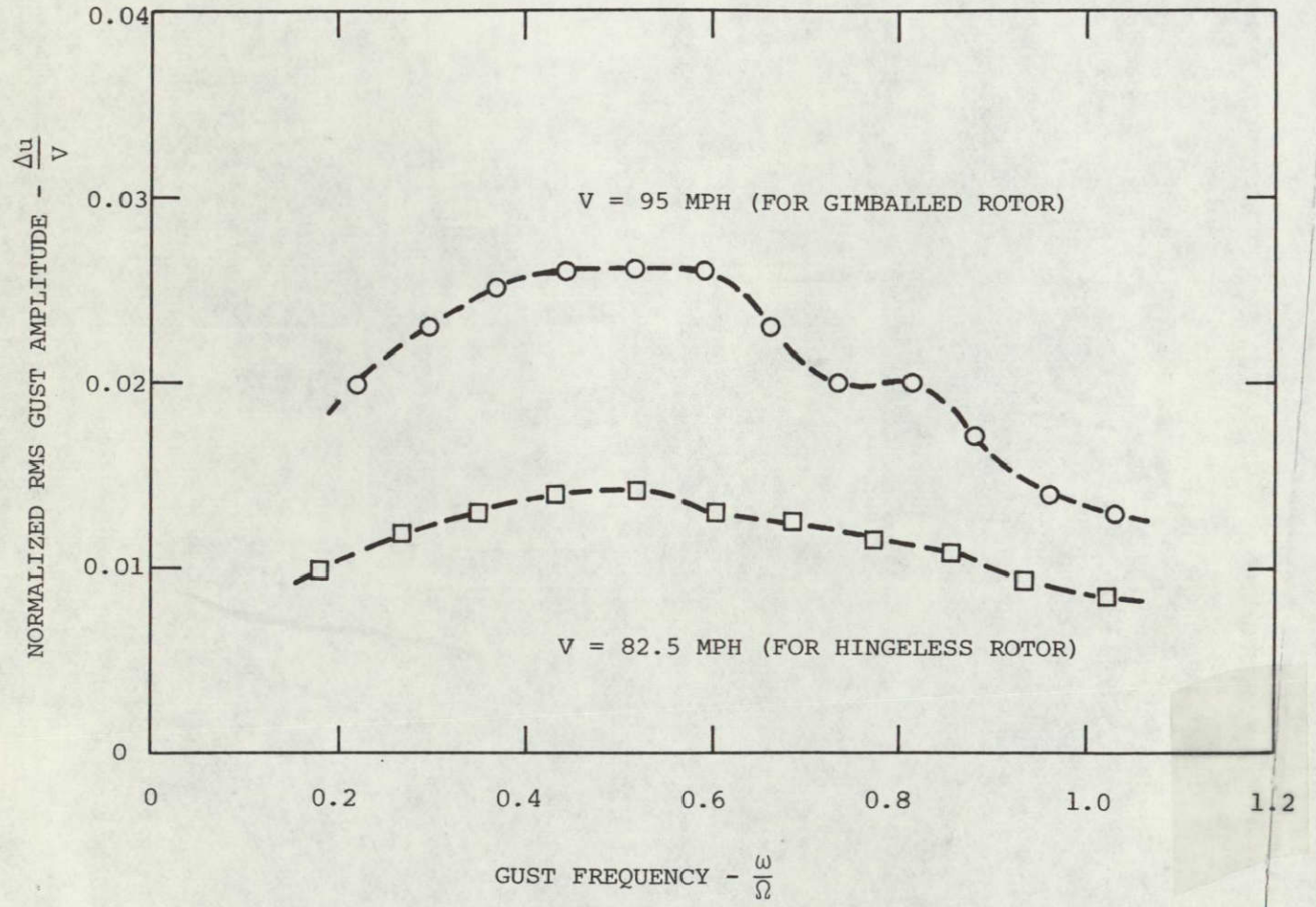

FIG. 12(a) LONGITUDINAL GUST AMPLITUDE

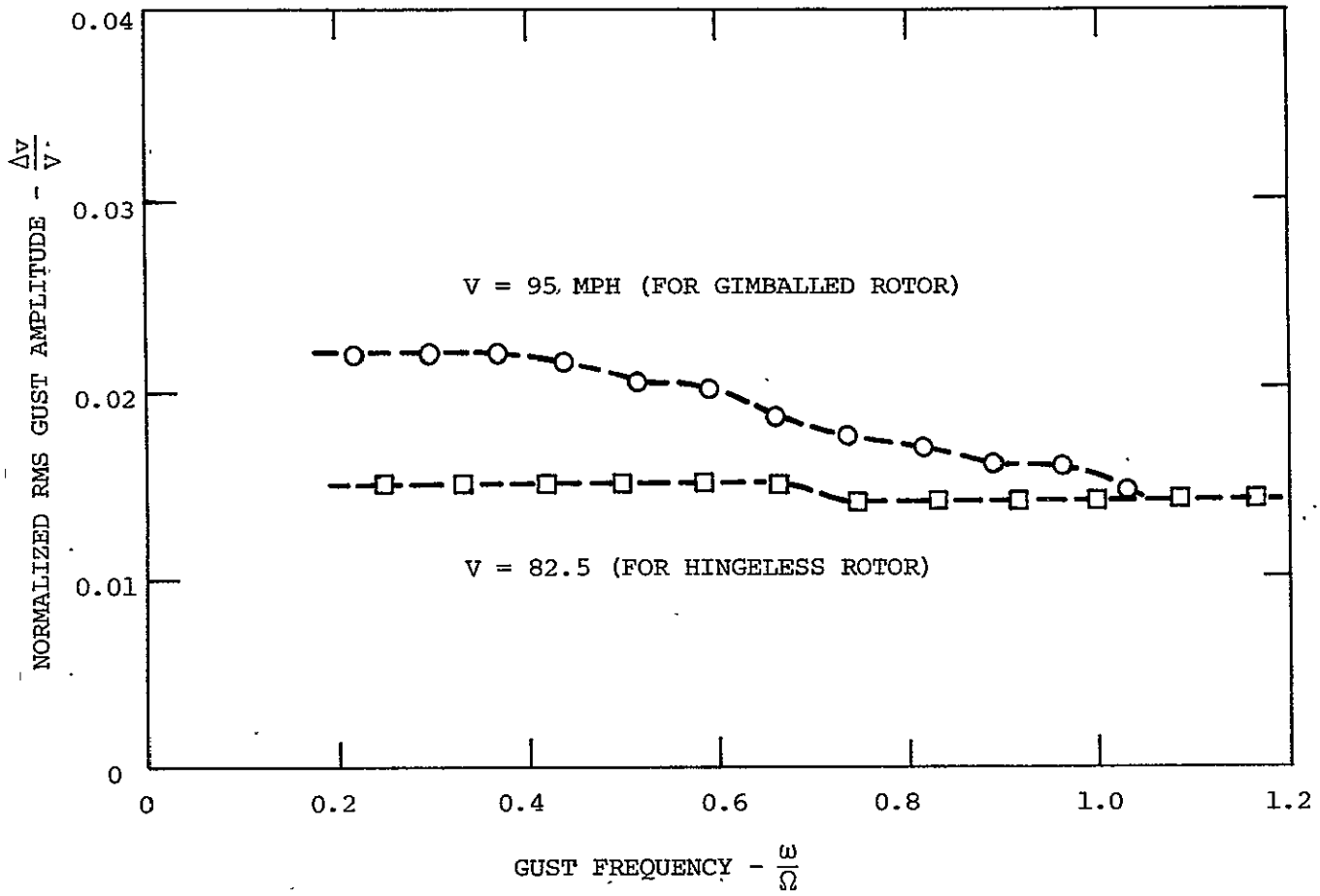

FIG. 12(b) VERTICAL GUST AMPLITUDE

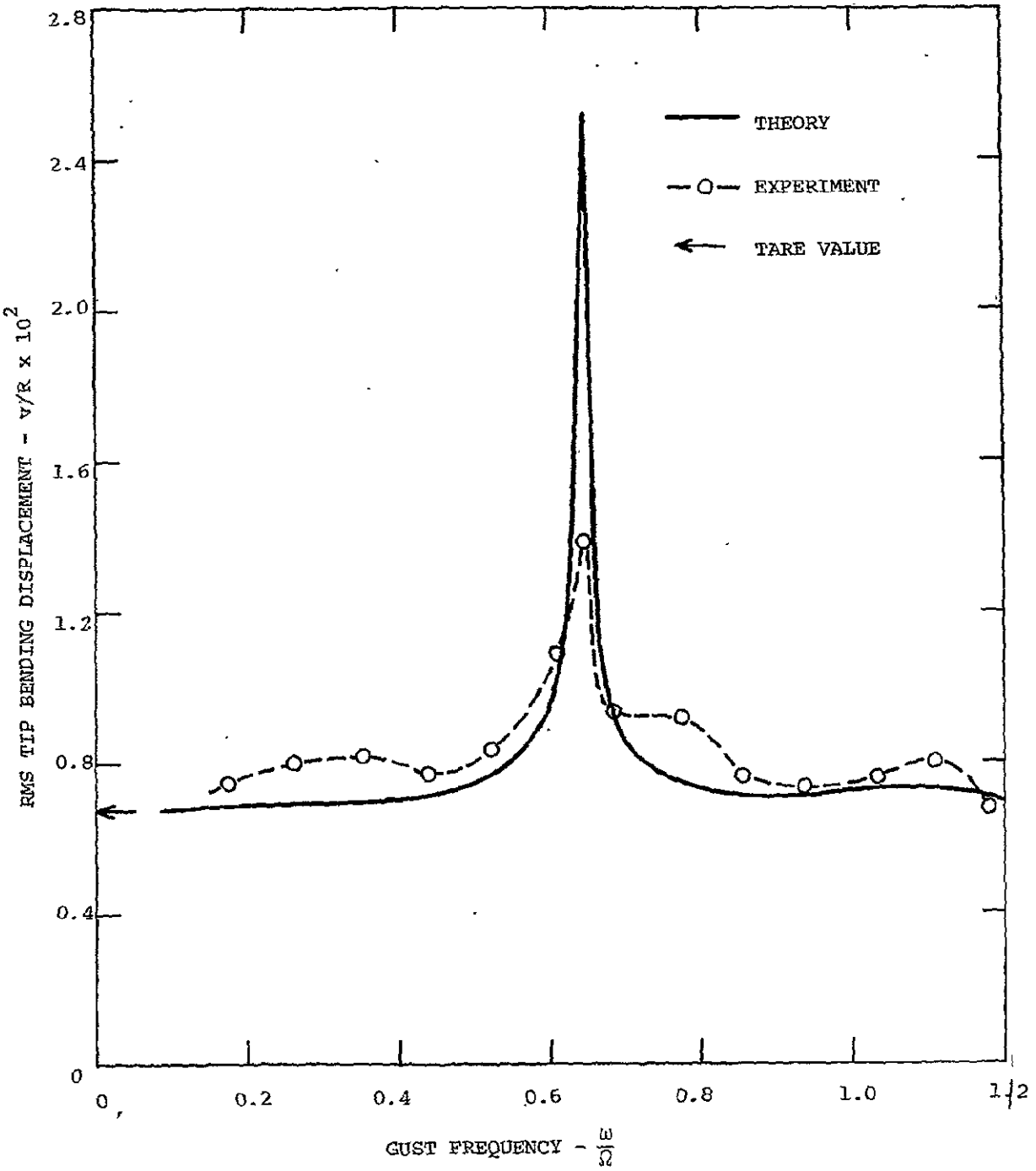

FIG. 13(a) LONGITUDINAL GUST RESPONSE OF HINGELESS ROTOR BLADE INPLANE BENDING

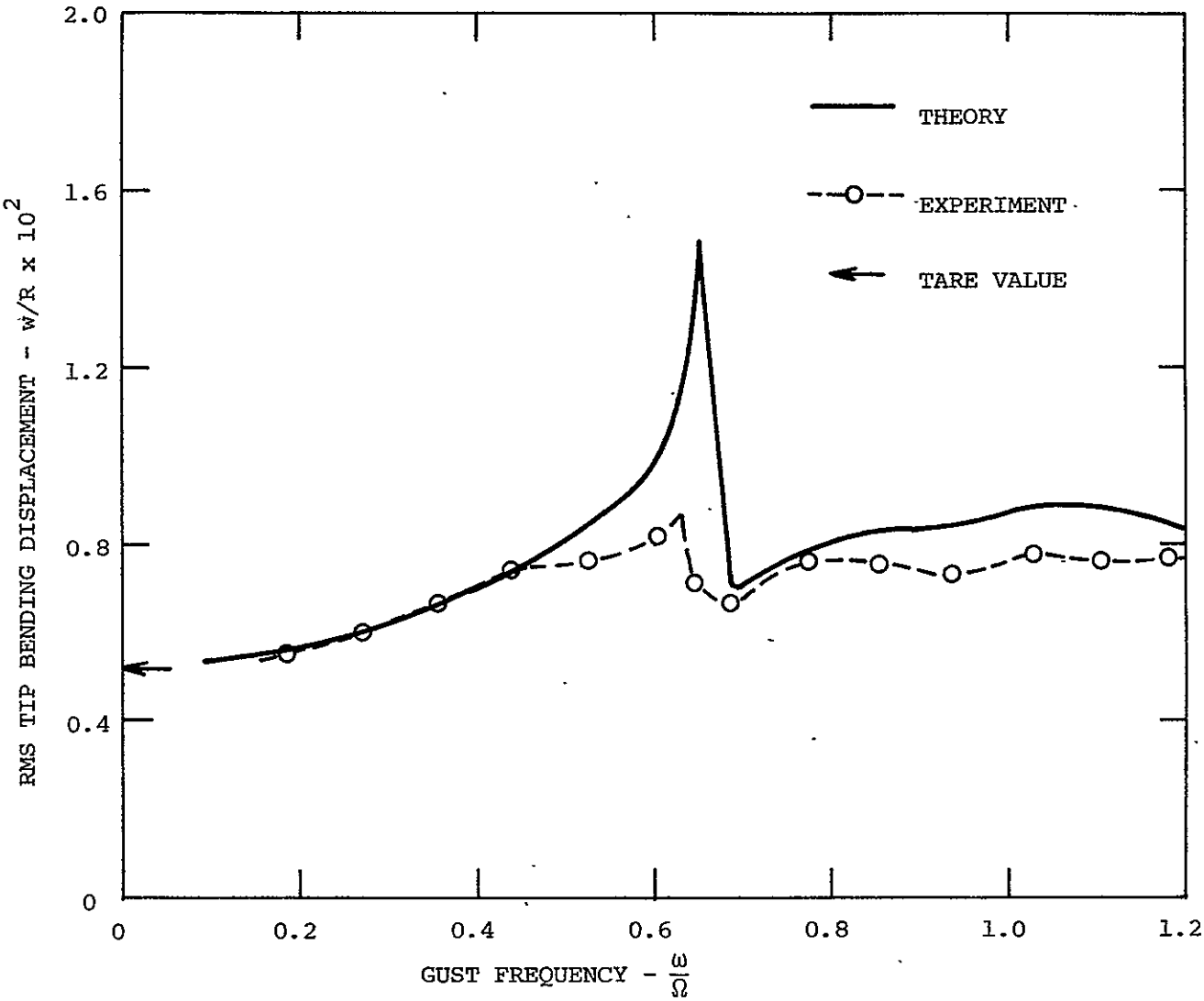

FIG. 13(b) LONGITUDINAL GUST RESPONSE OF HINGELESS ROTOR BLADE OUT-OF-PLANE BENDING

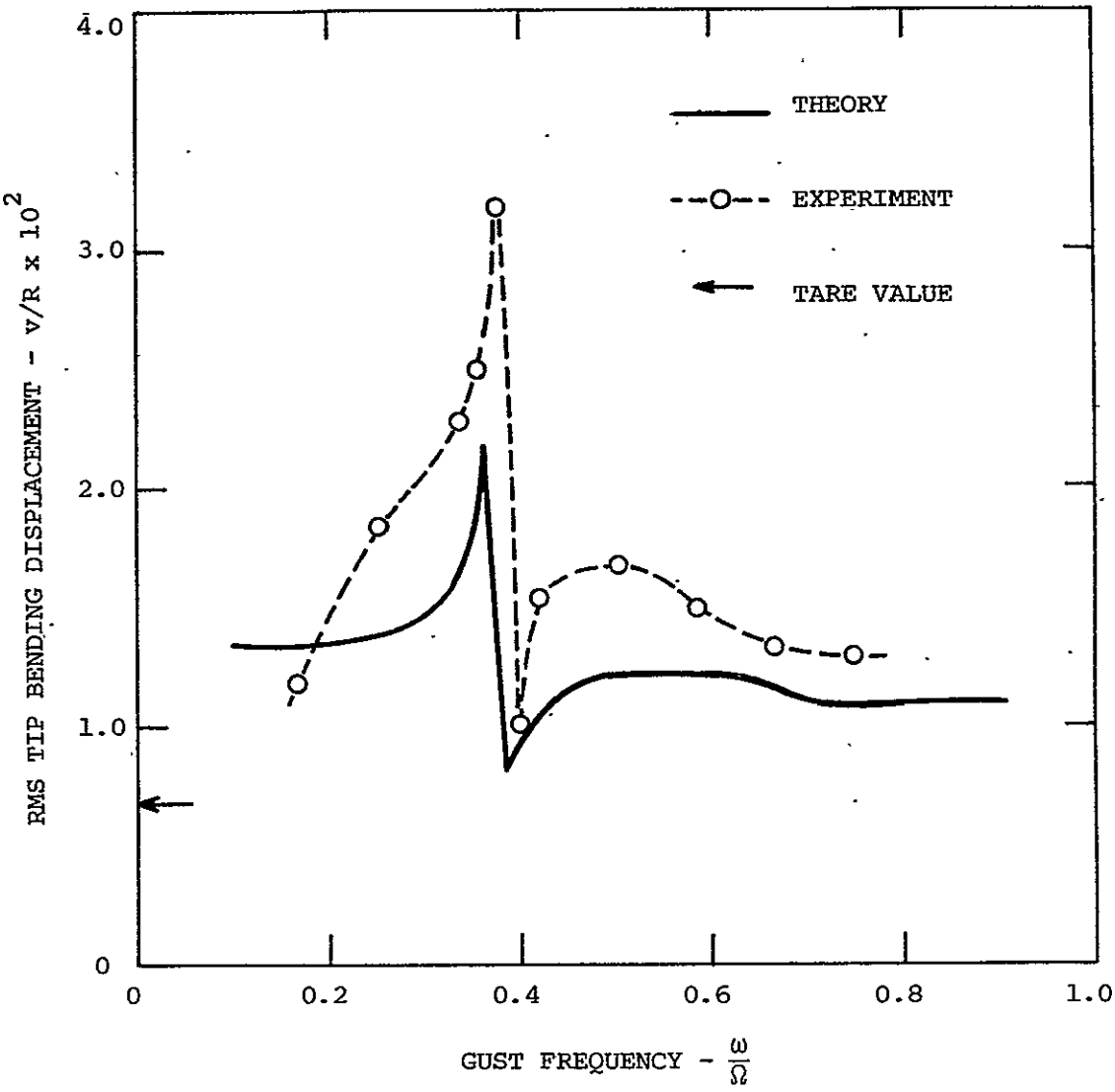

FIG. 14(a) VERTICAL GUST RESPONSE OF HINGELESS ROTOR BLADE INPLANE BENDING

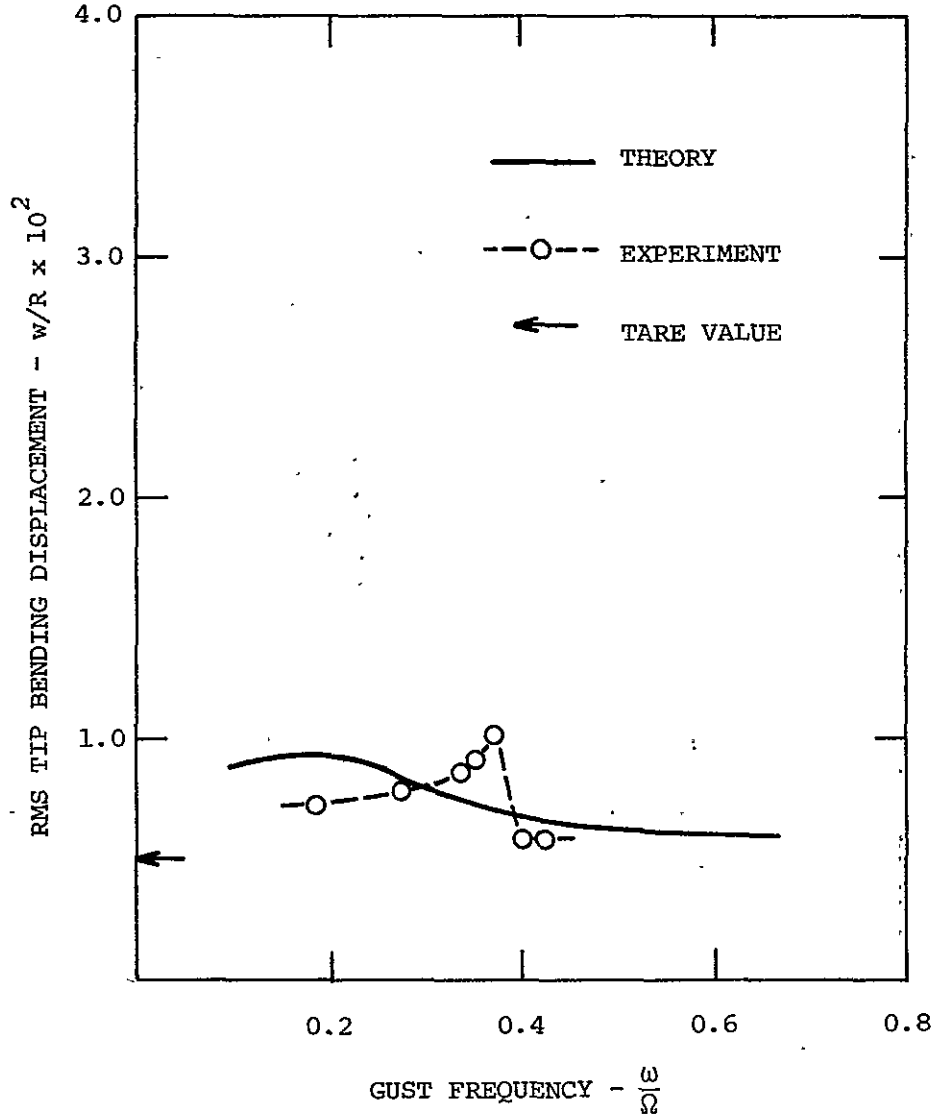

FIG. 14(b) VERTICAL GUST RESPONSE OF HINGELESS ROTOR BLADE OUT-OF-PLANE BENDING

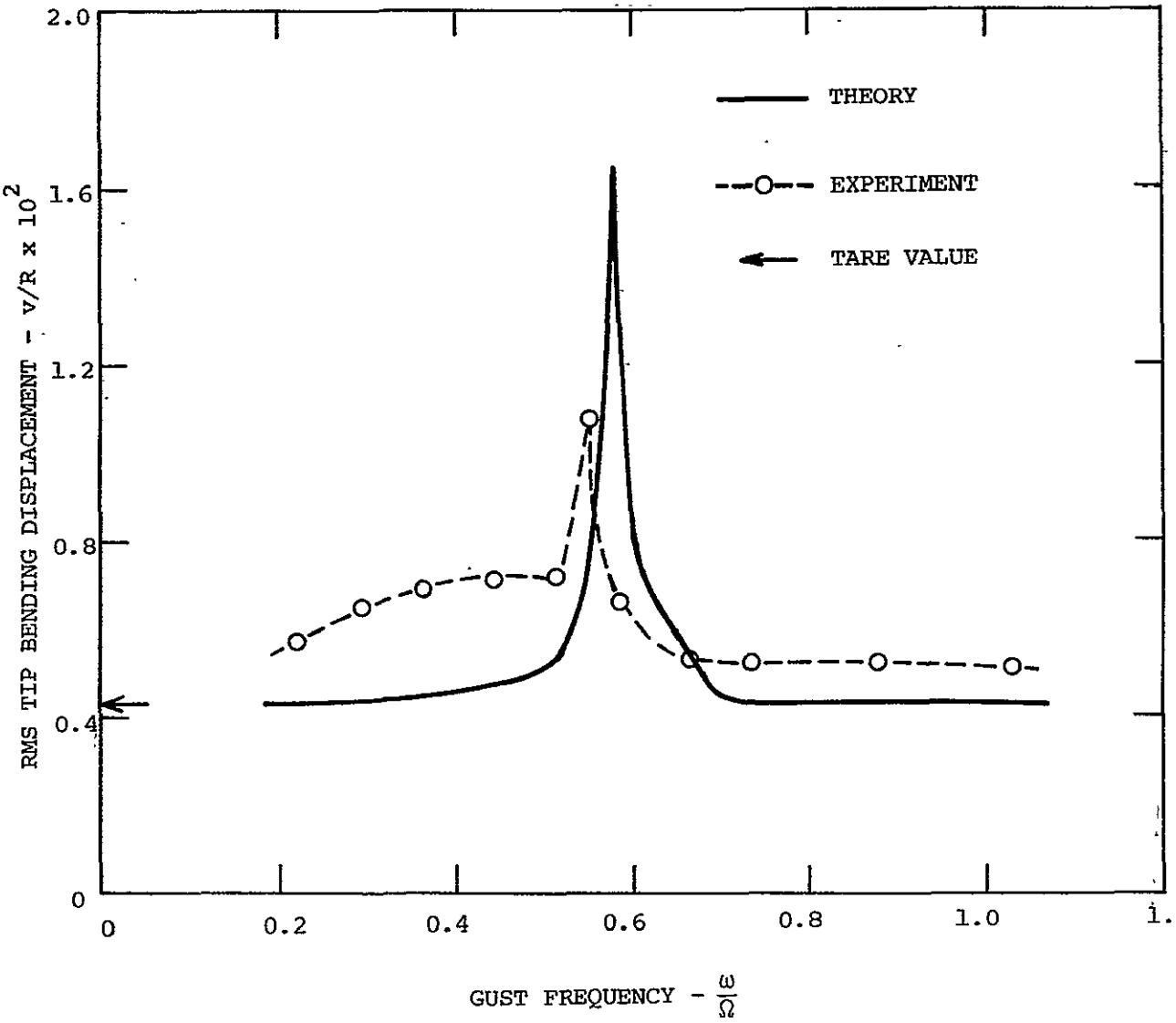

FIG. 15(a) LONGITUDINAL GUST RESPONSE OF GIMBALLED ROTOR BLADE INPLANE BENDING

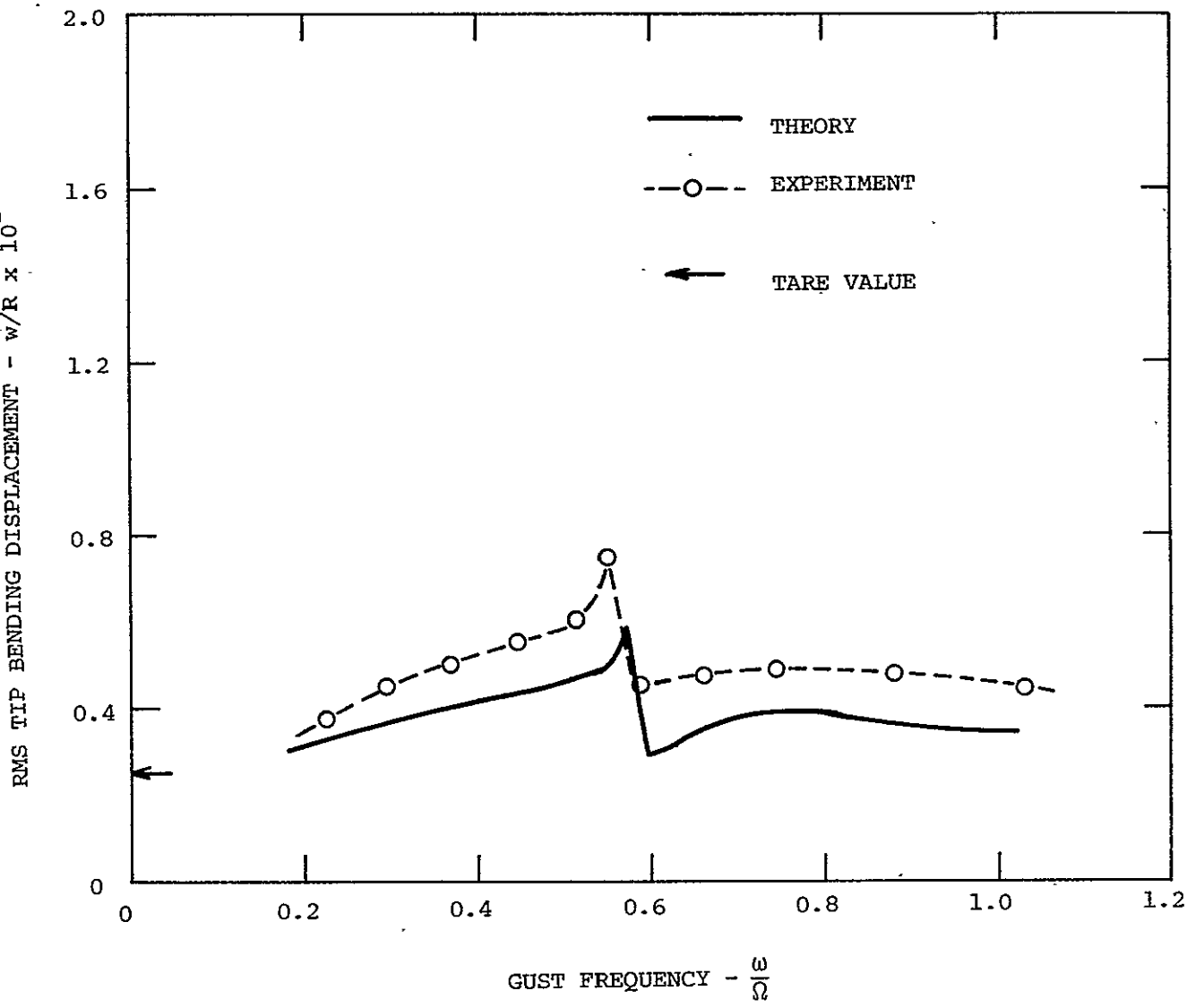

FIG. 15(b) LONGITUDINAL GUST RESPONSE OF GIMBALLED ROTOR BLADE OUT-OF-PLANE BENDING

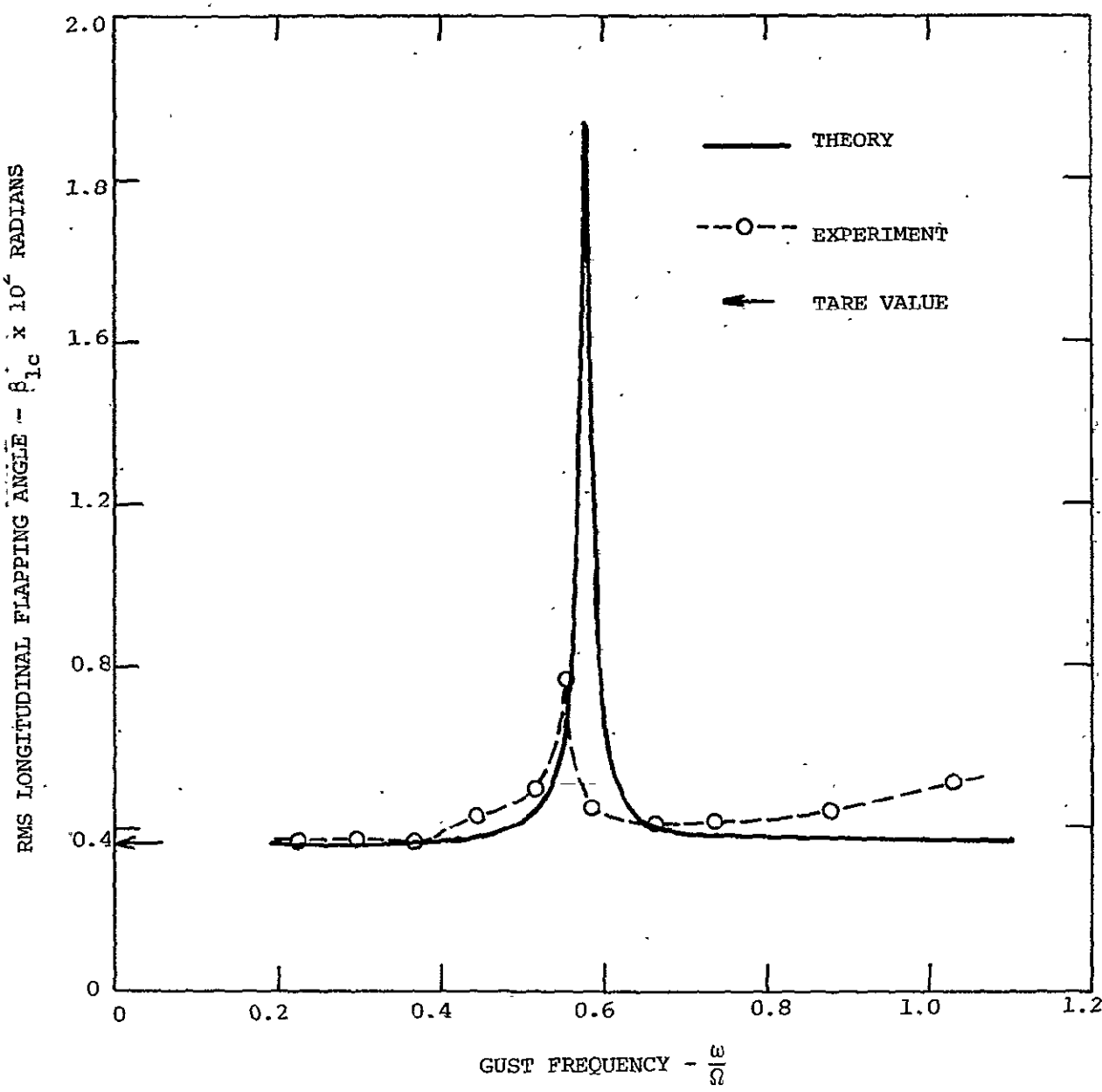

FIG. 15(c) LONGITUDINAL GUST RESPONSE OF GIMBALLED ROTOR LONGITUDINAL FLAPPING

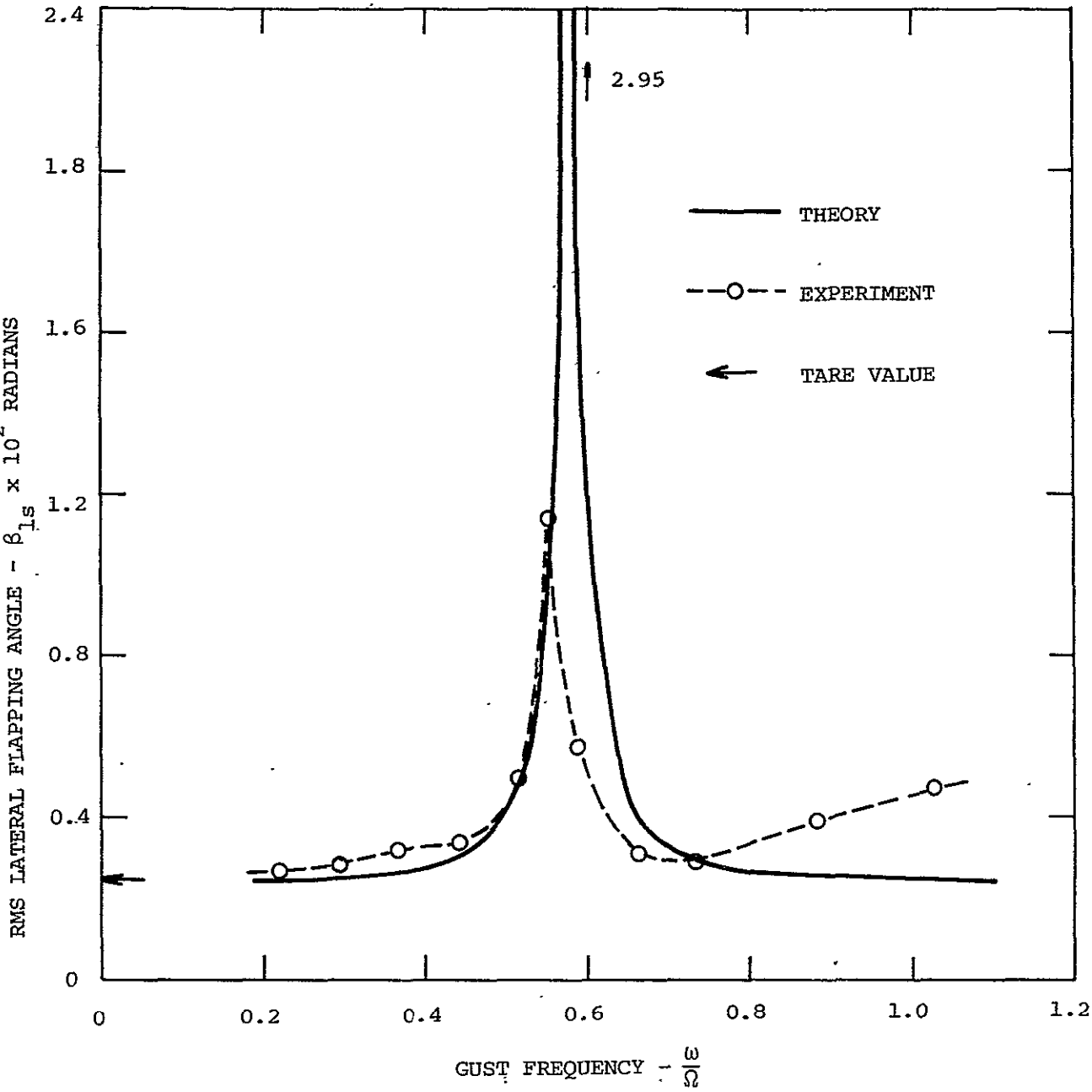

FIG. 15(d) LONGITUDINAL GUST RESPONSE OF GIMBALLED ROTOR LATERAL FLAPPING

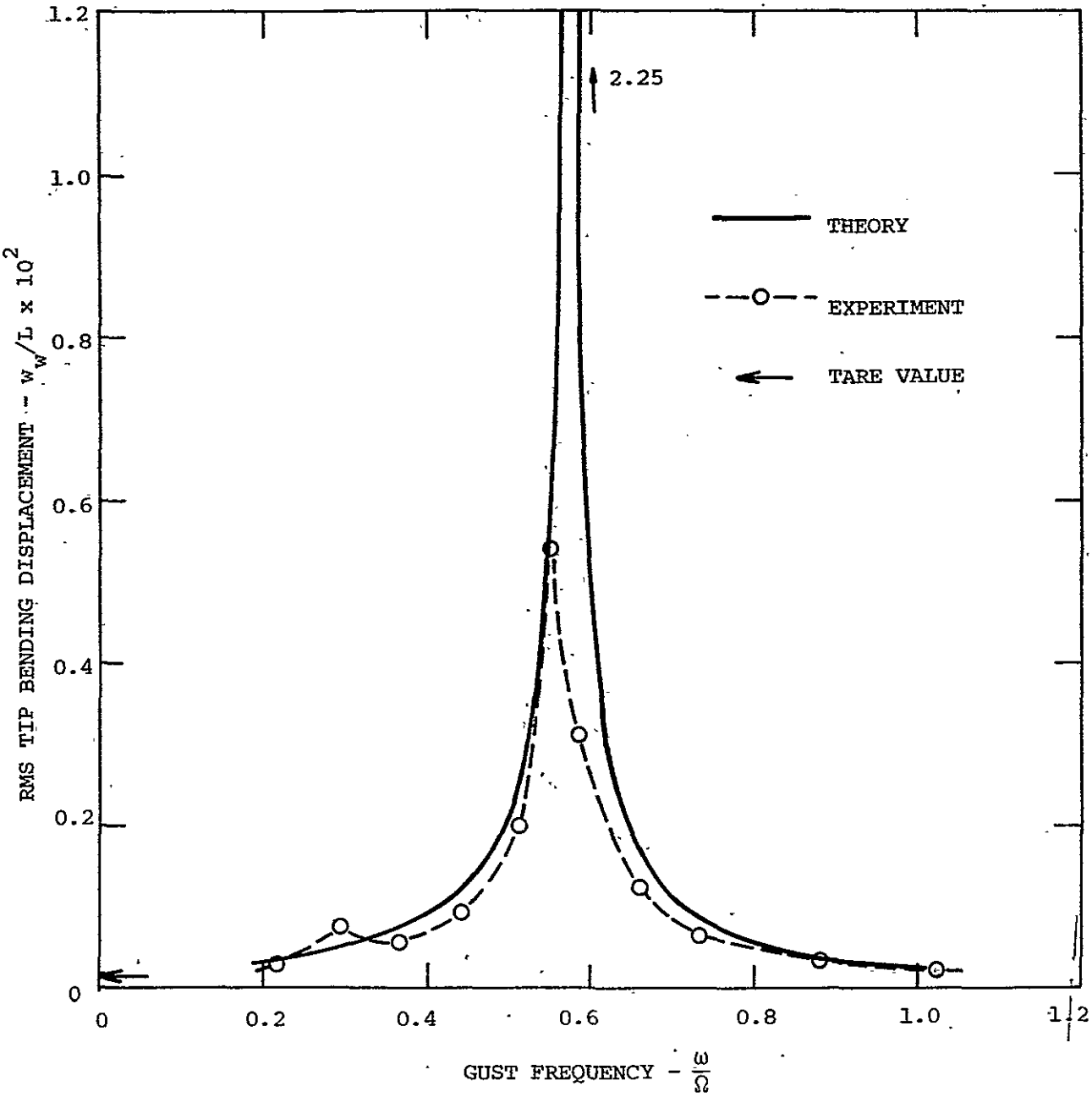

FIG. 15(e) LONGITUDINAL GUST RESPONSE OF GIMBALLED ROTOR WING CHORDWISE BENDING

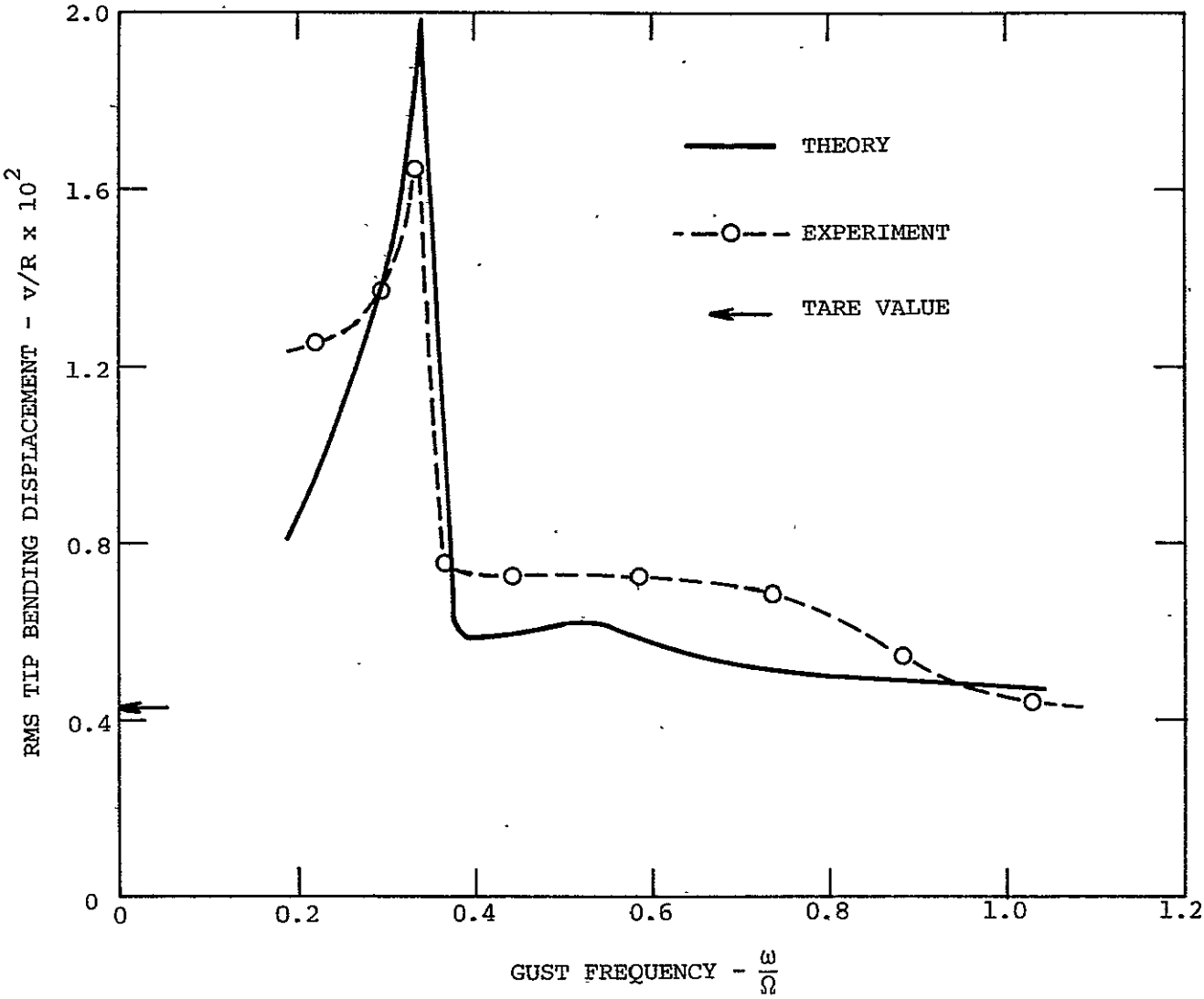

FIG. 16(a) VERTICAL GUST RESPONSE OF GIMBALLED ROTOR BLADE INPLANE BENDING

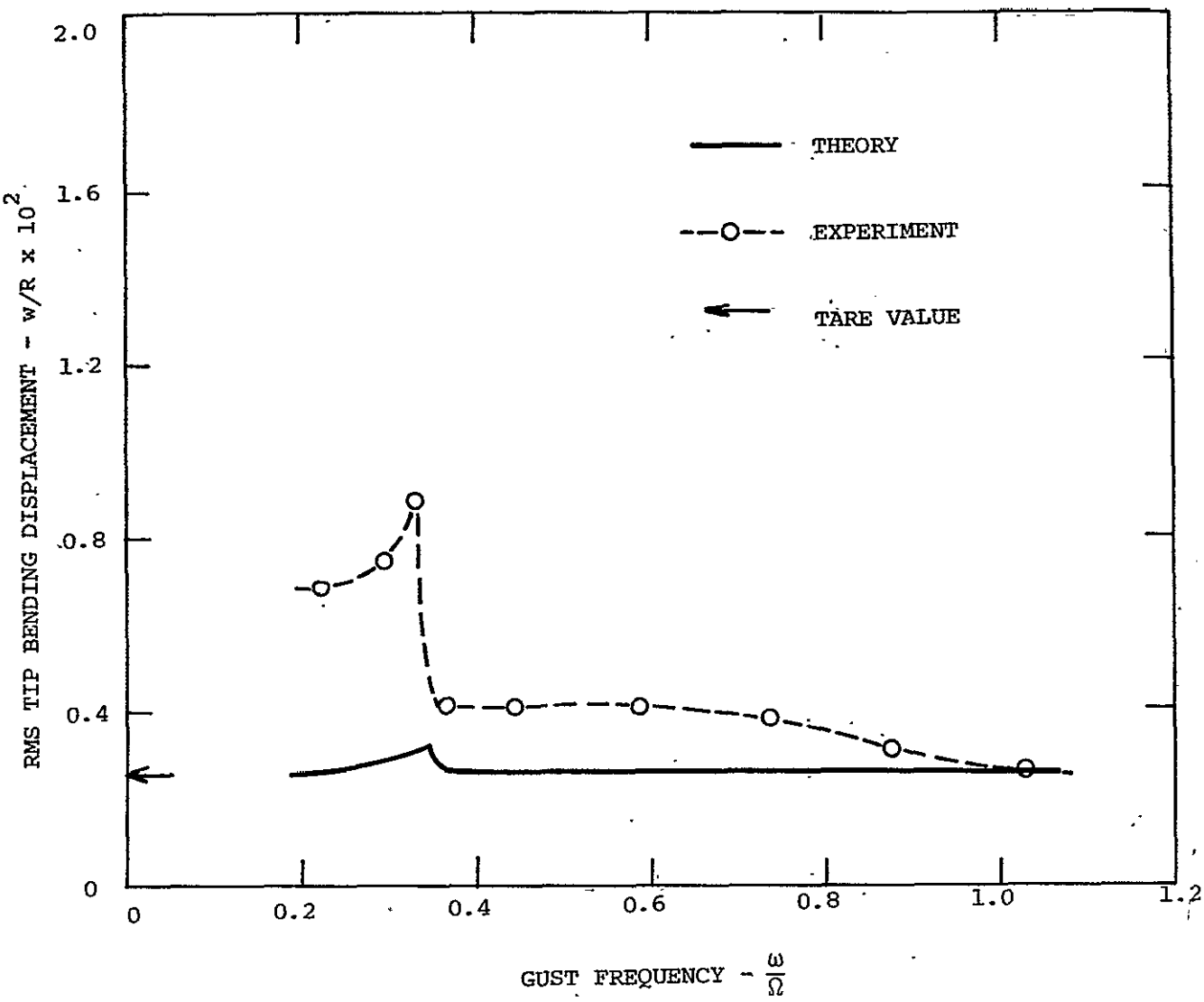

FIG. 16(b) VERTICAL GUST RESPONSE OF GIMBALLED ROTOR BLADE OUT-OF-PLANE BENDING

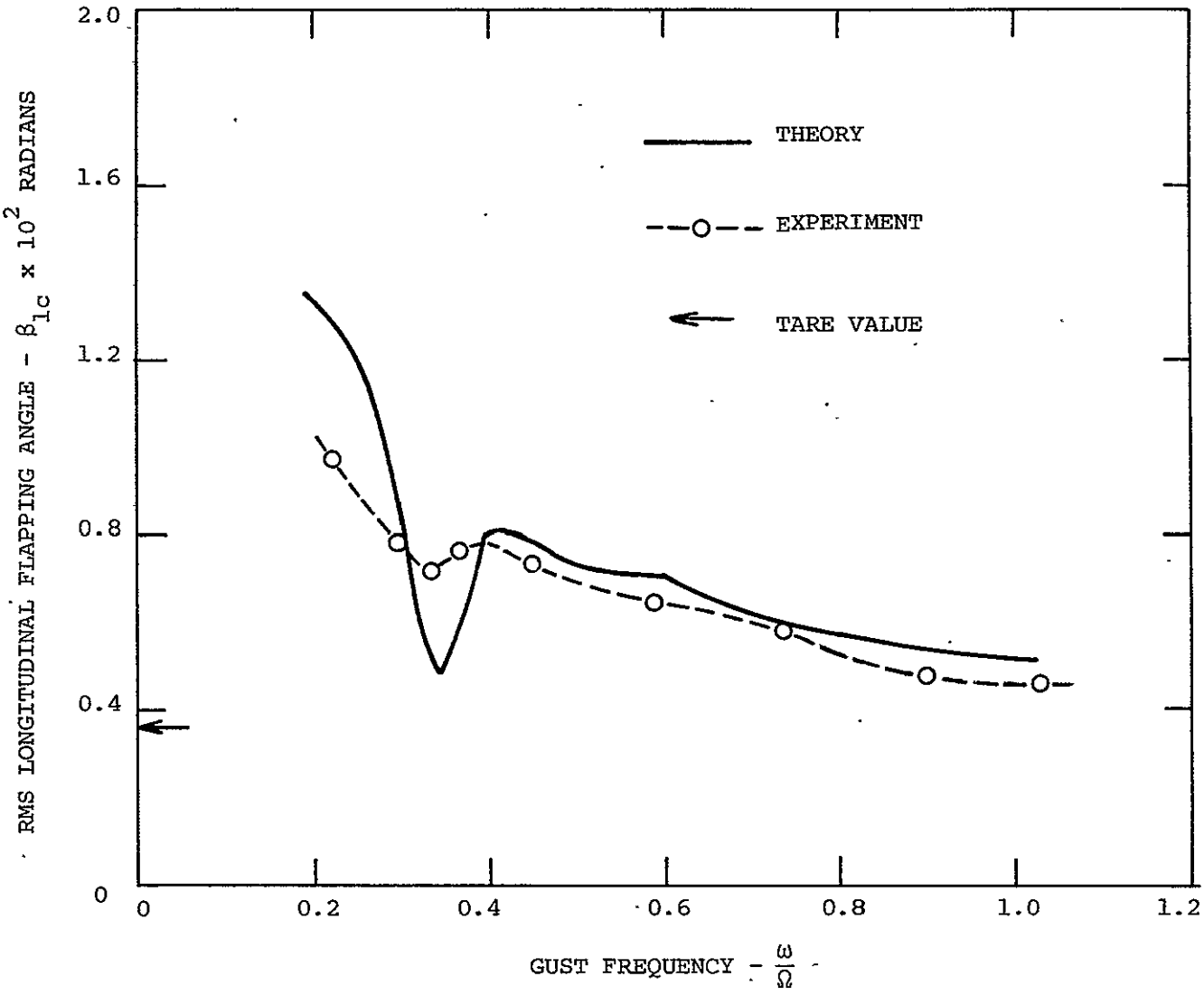

FIG. 16(c) VERTICAL GUST RESPONSE OF GIMBALLED ROTOR LONGITUDINAL FLAPPING

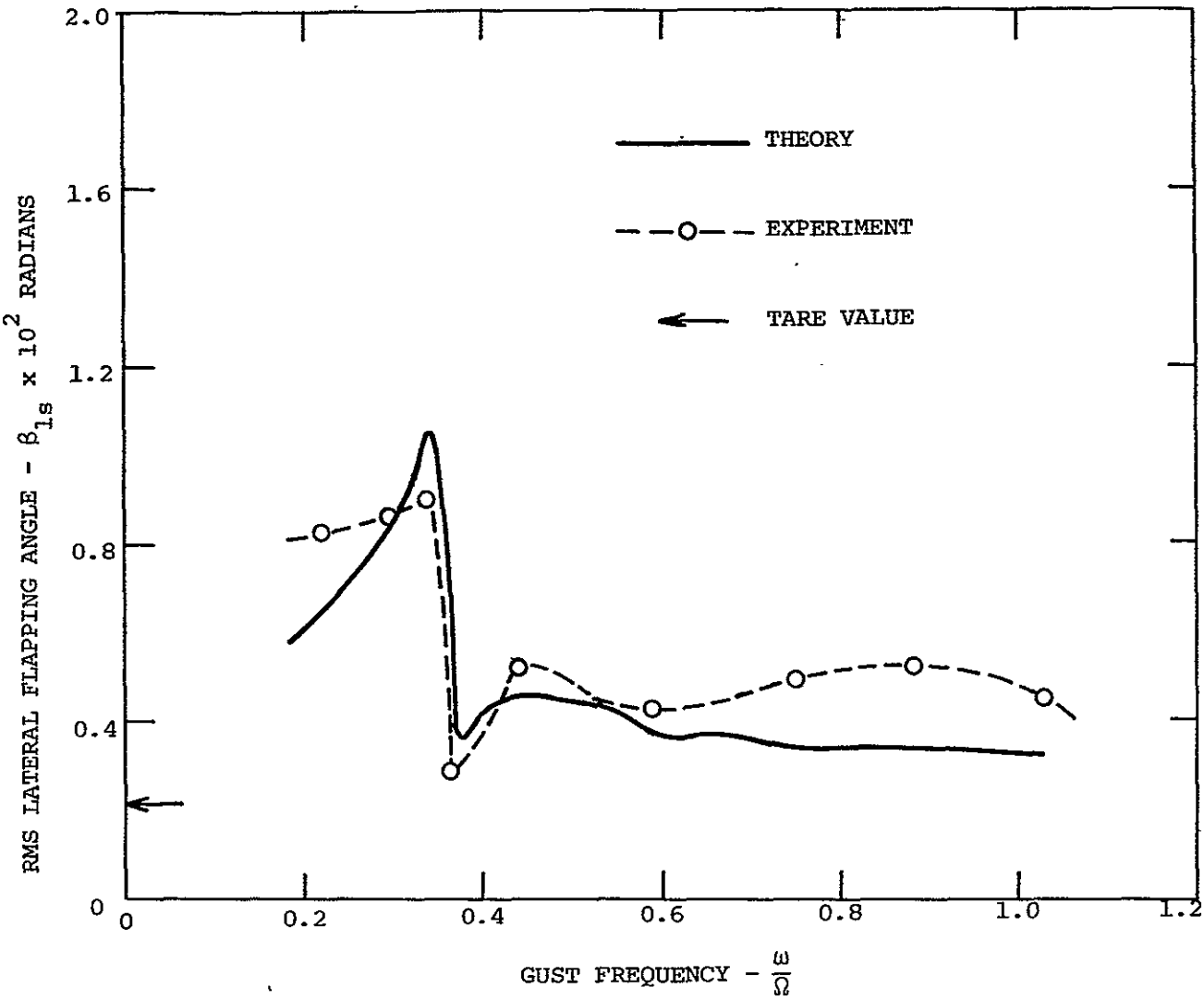

FIG. 16(d) VERTICAL GUST RESPONSE OF GIMBALLED ROTOR LATERAL FLAPPING

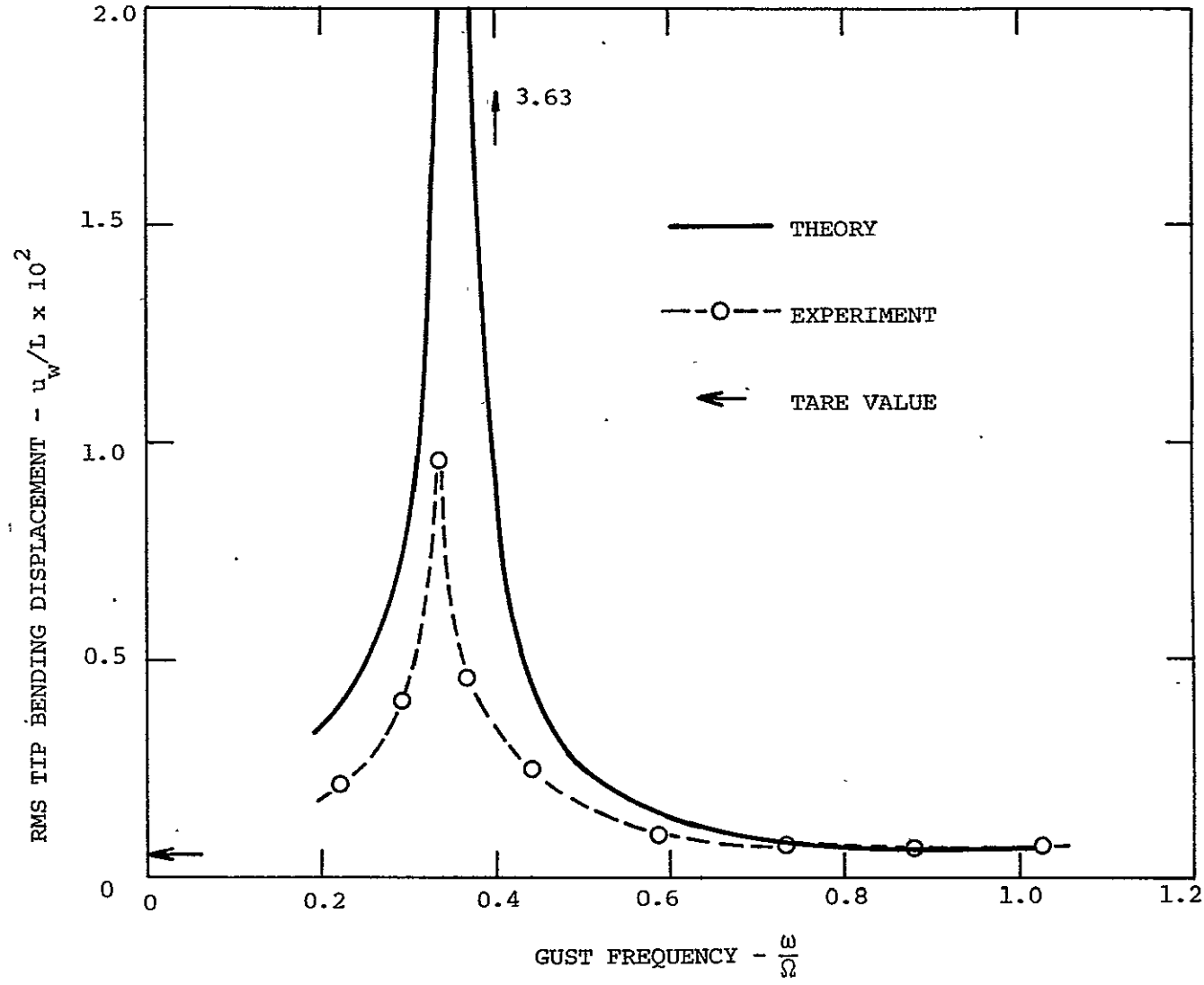

FIG. 16(e) VERTICAL GUST RESPONSE OF GIMBALLED ROTOR WING VERTICAL BENDING

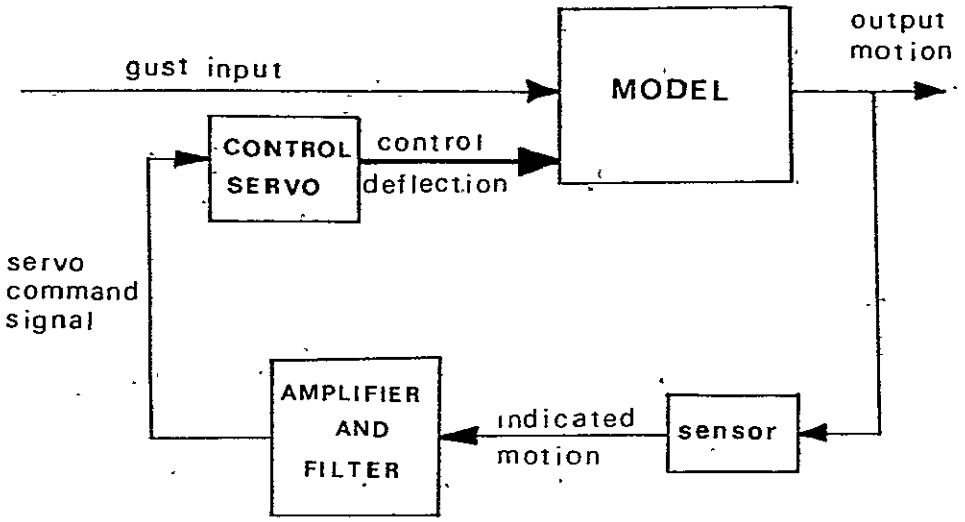

FIGURE 17 GENERAL ARRANGEMENT OF THE ACTIVE CONTROL SYSTEMS

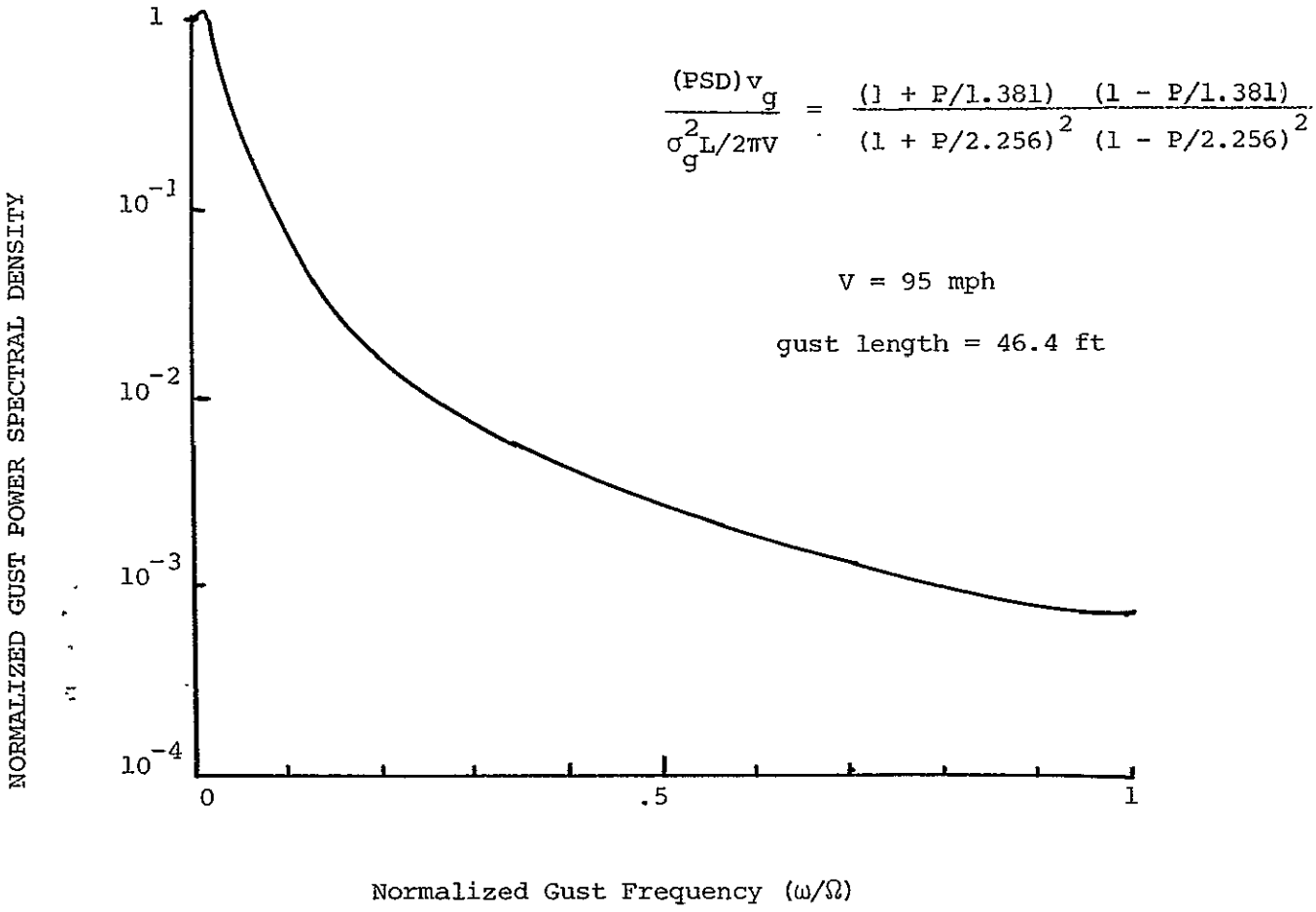

FIGURE 18 VON KARMAN GUST POWER SPECTRAL DENSITY

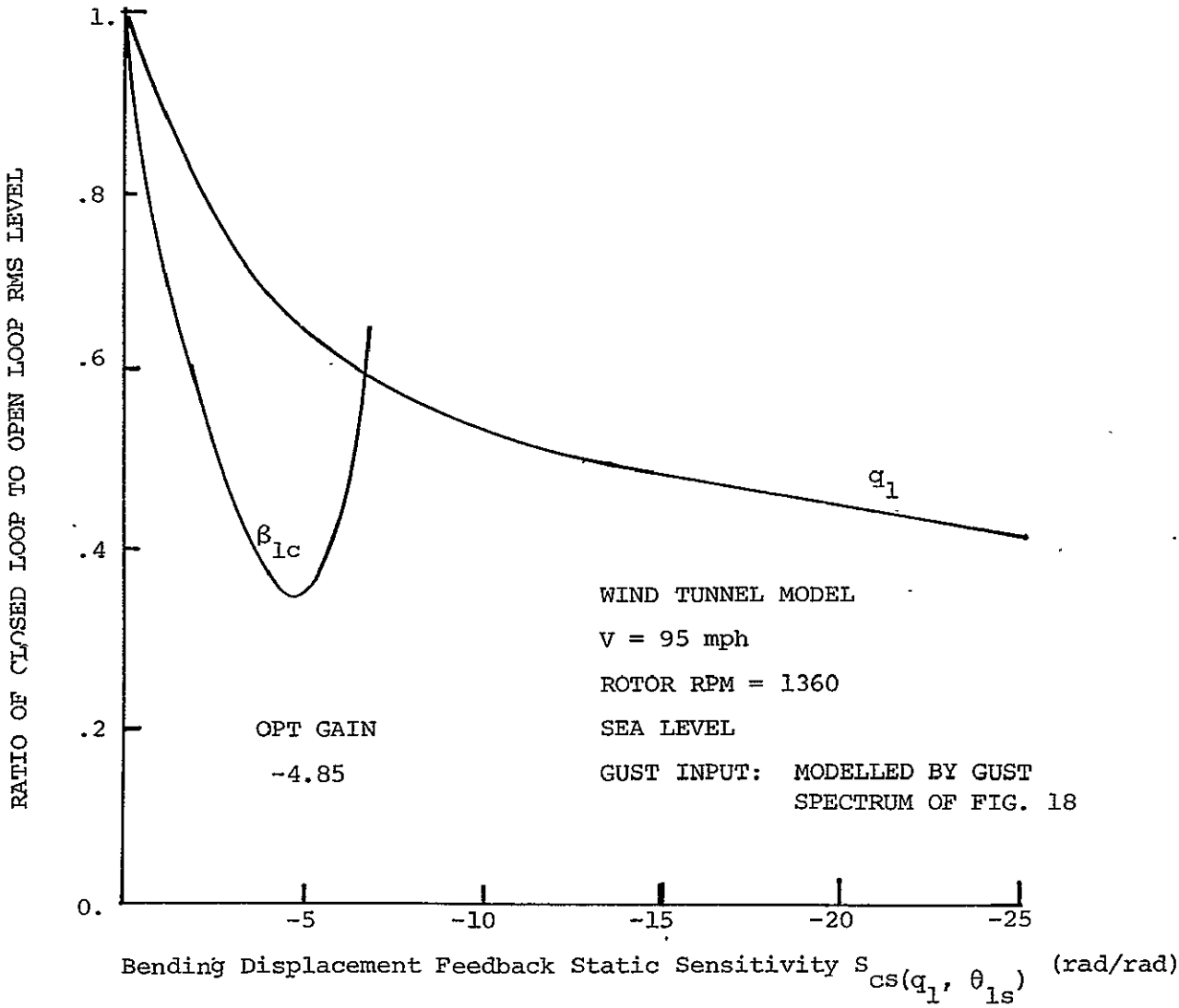

FIGURE 19 SYSTEM 1-1. VARIATION WITH CONTROL SYSTEM FEEDBACK STATIC SENSITIVITY OF THE RATIO OF THE (RMS) LEVELS OF CLOSED LOOP CONTROL SYSTEM RESPONSE TO UNCONTROLLED AIRPLANE RESPONSE

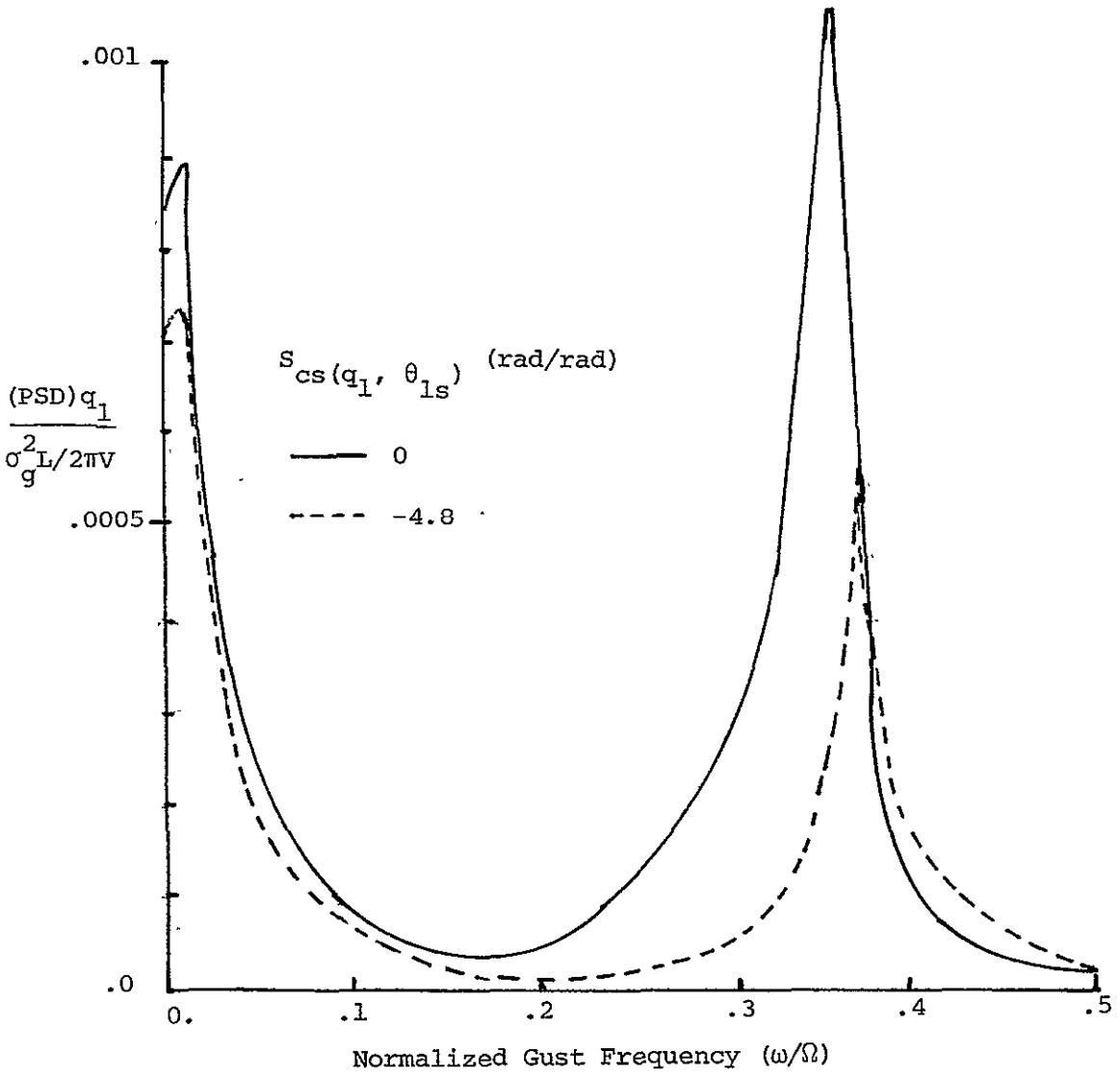

FIGURE 20 POWER SPECTRAL DENSITY OF WING VERTICAL BENDING FOR SYSTEM 1-1

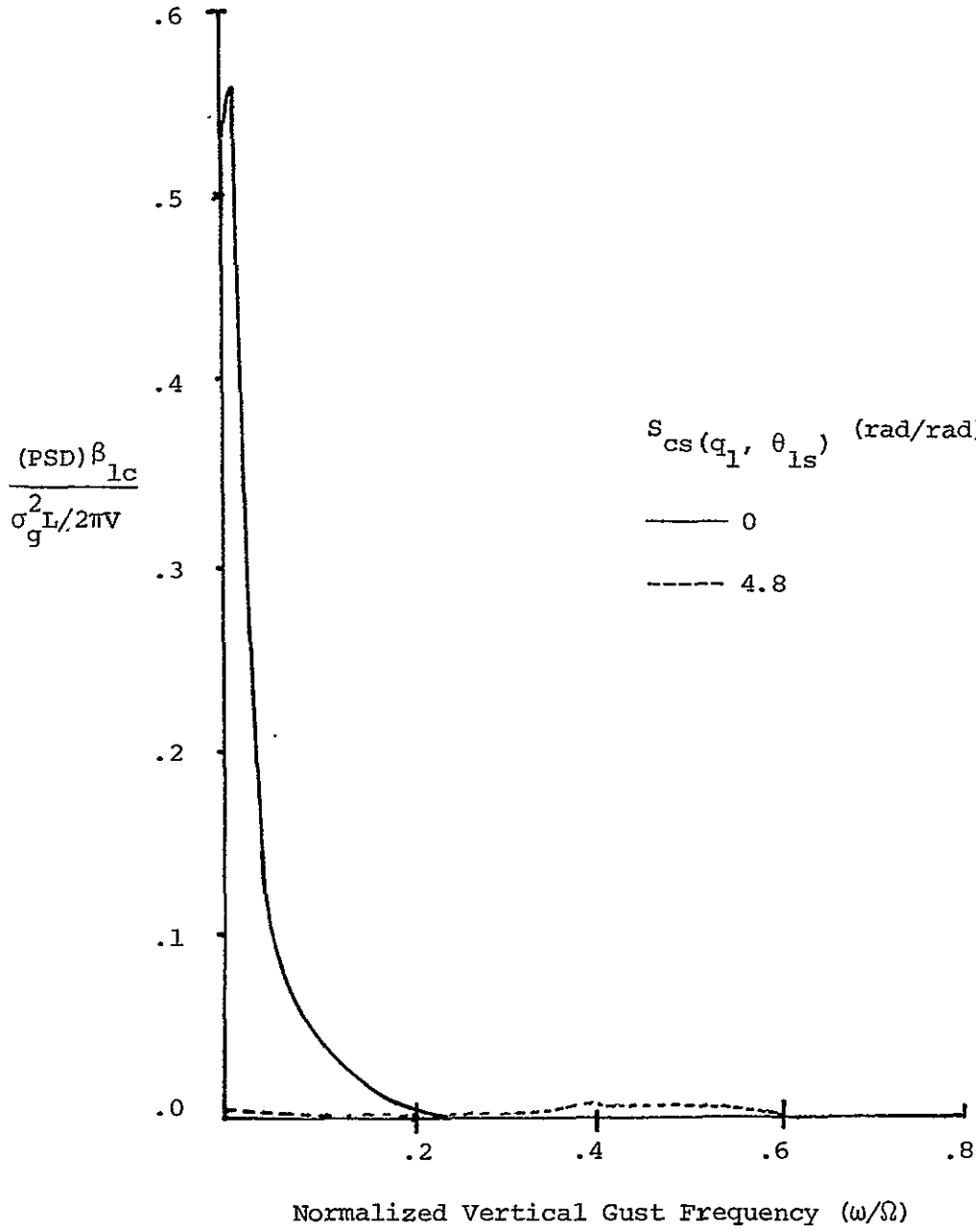

FIGURE 21 POWER SPECTRAL DENSITY OF ROTOR LONGITUDINAL CYCLIC FLAPPING FOR SYSTEM 1-1

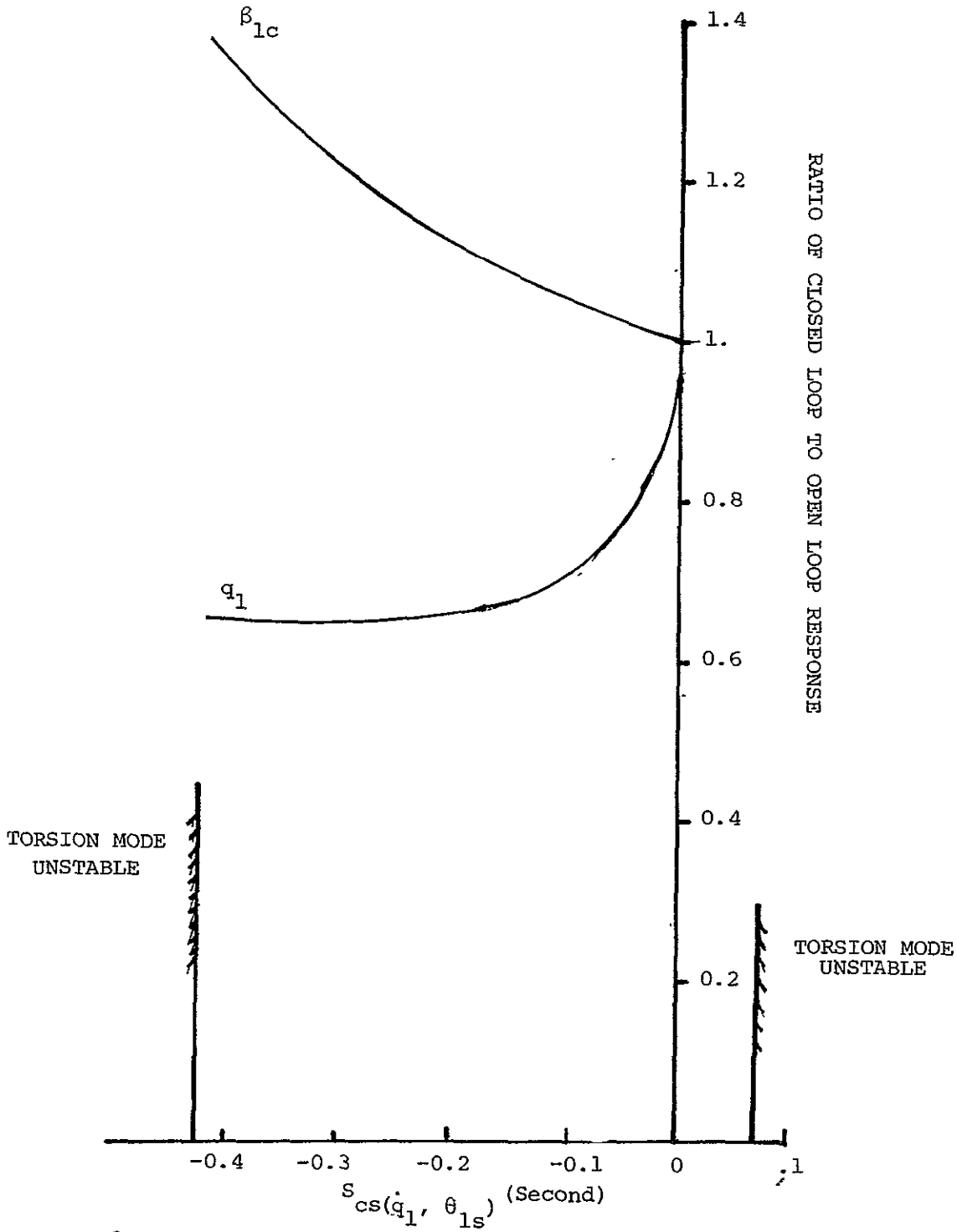

FIGURE 22 SYSTEM 1-2. VARIATION OF THE RATIO OF (RMS) LEVELS OF CLOSED LOOP CONTROL SYSTEM RESPONSE TO UNCONTROLLED AIRPLANE RESPONSE WITH CONTROL SYSTEM FEEDBACK STATIC SENSITIVITY

C-2

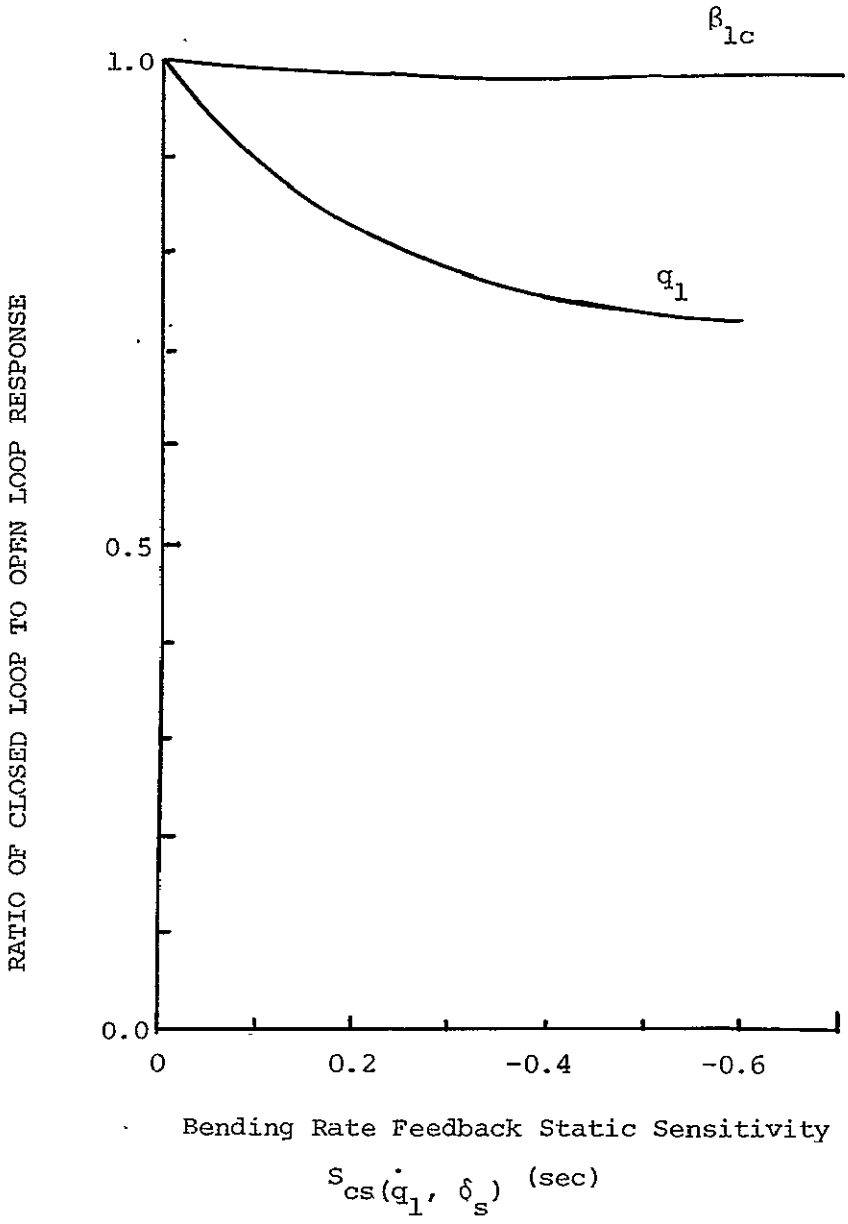

FIGURE 23 SYSTEM 2-2. VARIATION WITH CONTROL SYSTEM FEEDBACK STATIC SENSITIVITY OF THE RATIO OF THE (RMS) LEVELS OF CLOSED LOOP CONTROL SYSTEM RESPONSE TO UNCONTROLLED AIRPLANE RESPONSE

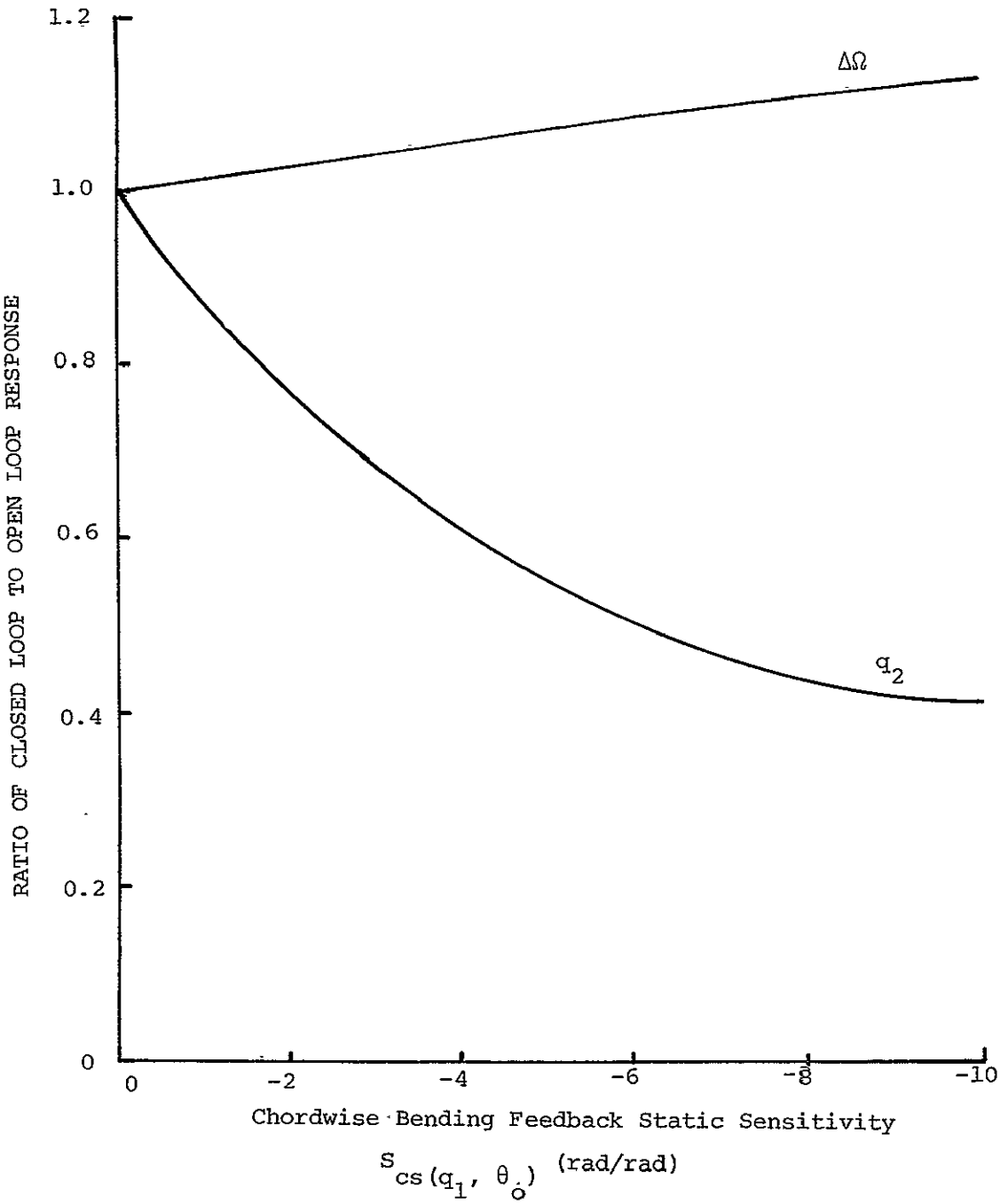

FIGURE 24 SYSTEM 3-1. VARIATION WITH CONTROL SYSTEM FEEDBACK STATIC SENSITIVITY OF THE RATIO OF THE (RMS) LEVELS OF CLOSED LOOP CONTROL SYSTEM RESPONSE TO UNCONTROLLED AIRPLANE RESPONSE

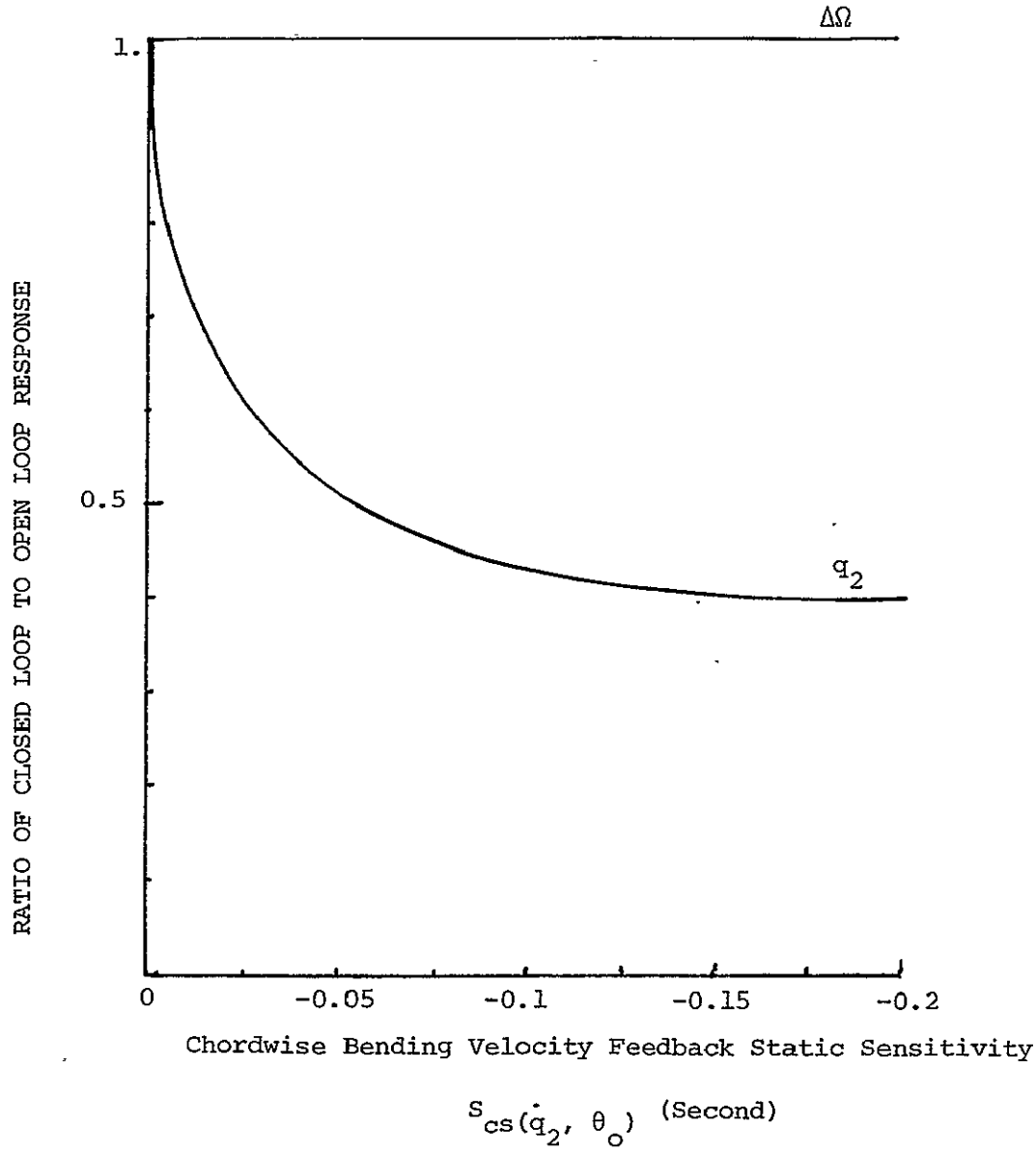

FIGURE 25 SYSTEM 3-2. VARIATION OF THE RATIO OF RMS LEVELS OF CLOSED LOOP TO OPEN LOOP RESPONSE WITH THE CONTROL SYSTEM FEEDBACK STATIC SENSITIVITY

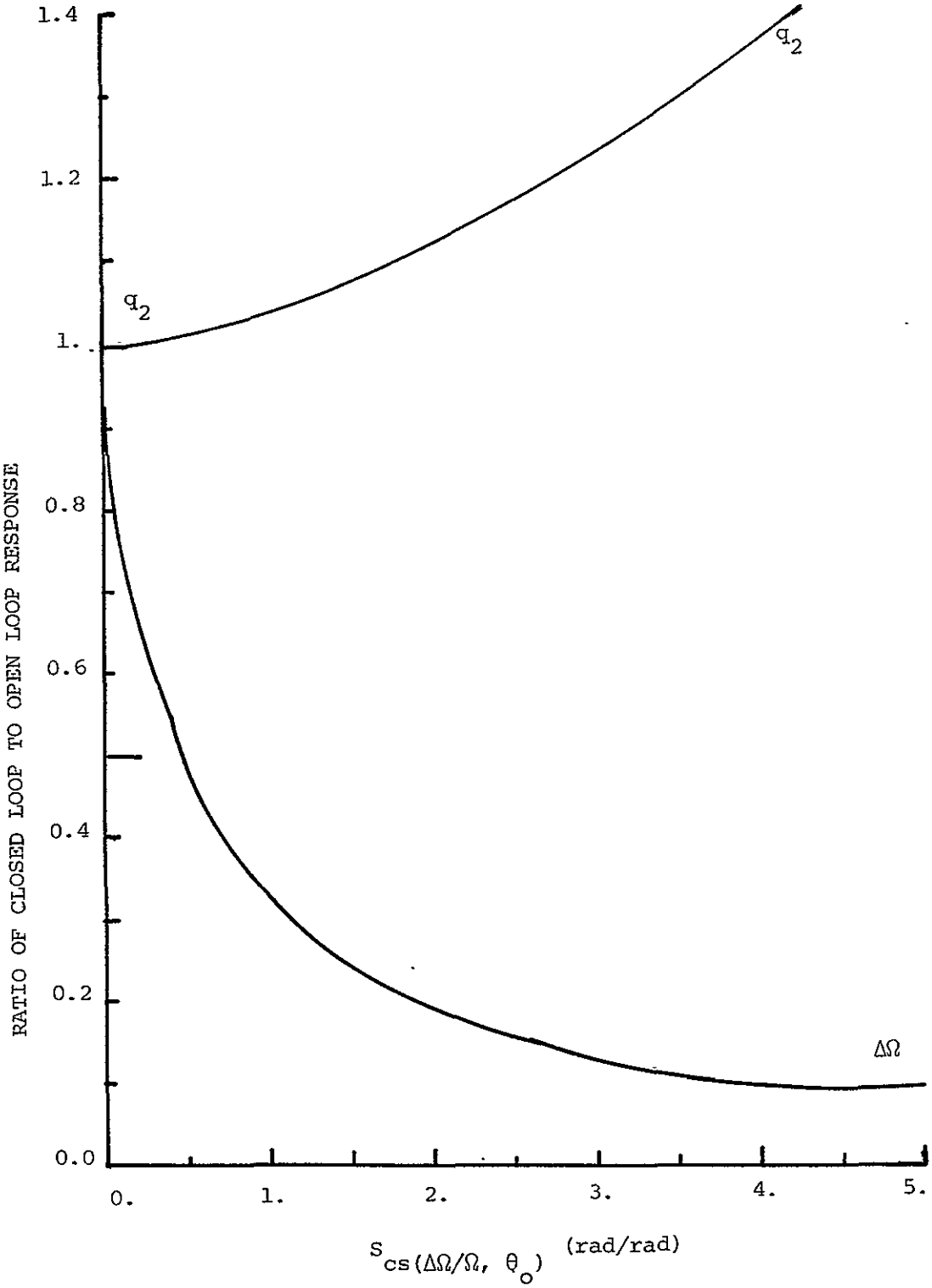

FIGURE 26 SYSTEM 4-1. VARIATION WITH CONTROL SYSTEM FEEDBACK STATIC SENSITIVITY OF THE RATIO OF THE (RMS) LEVELS OF CLOSED LOOP CONTROL SYSTEM RESPONSE TO UNCONTROLLED AIRPLANE RESPONSE

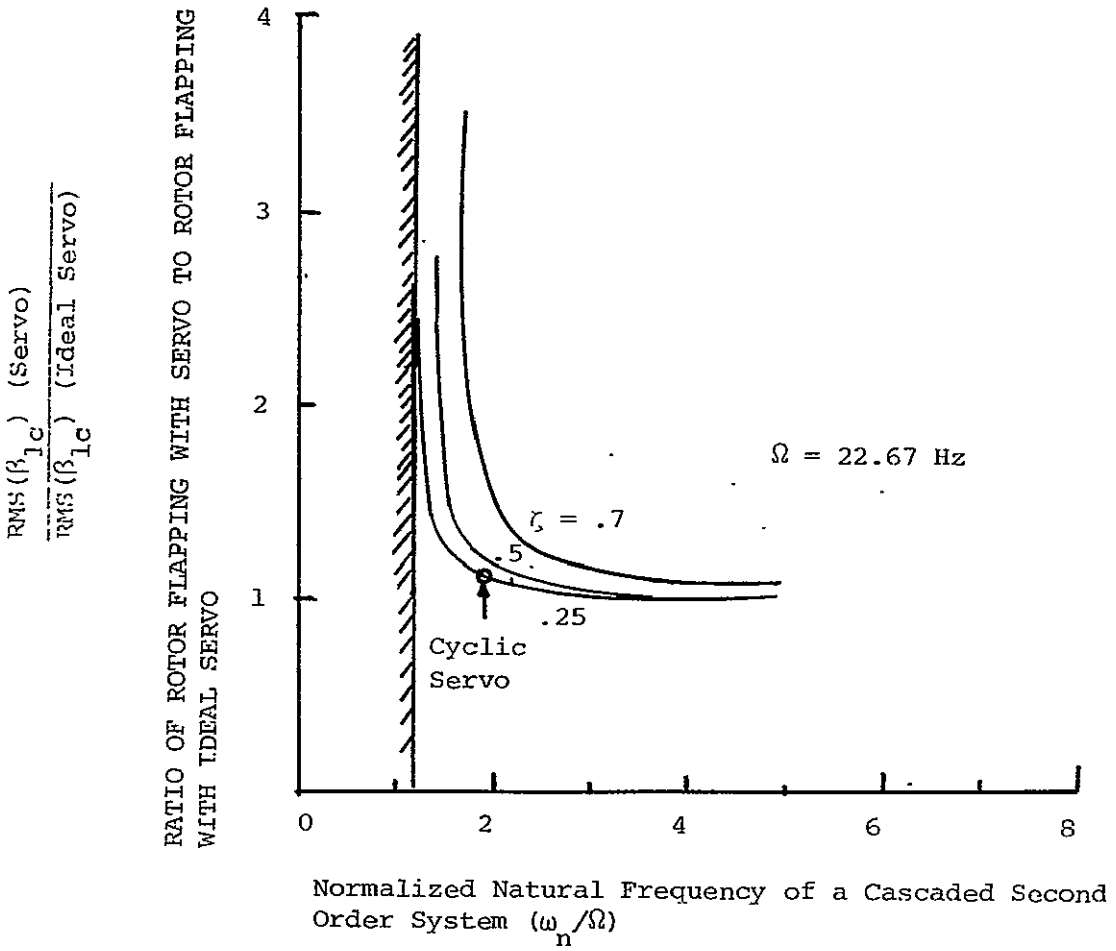

FIGURE 27 SYSTEM 1-1. VARIATION OF RMS(β_{1c}) WITH DAMPING RATIO AND NATURAL FREQUENCY OF A SECOND ORDER SERVO SYSTEM WHEN $S_{cs(q_1, \theta_{1s})}$ = 4.8 rad/rad

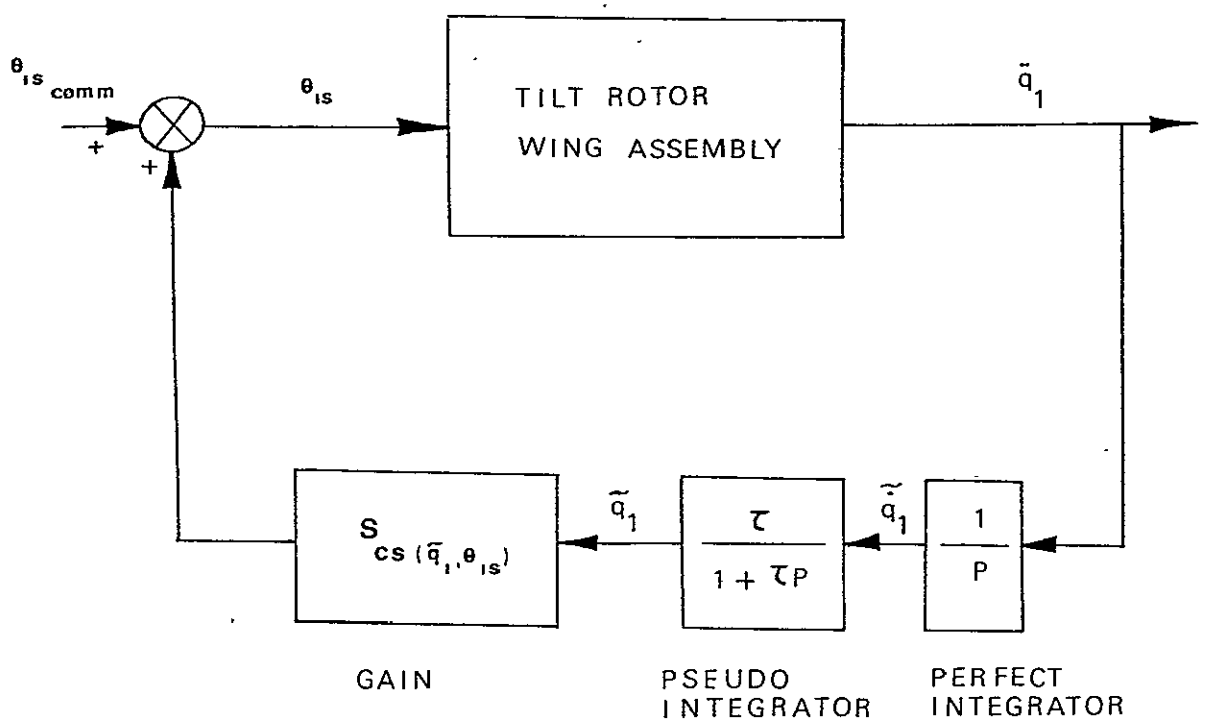

FIGURE 28 MATHEMATICAL BLOCK DIAGRAM OF SYSTEM 1-1 WITH ONE PSEUDO INTEGRATOR

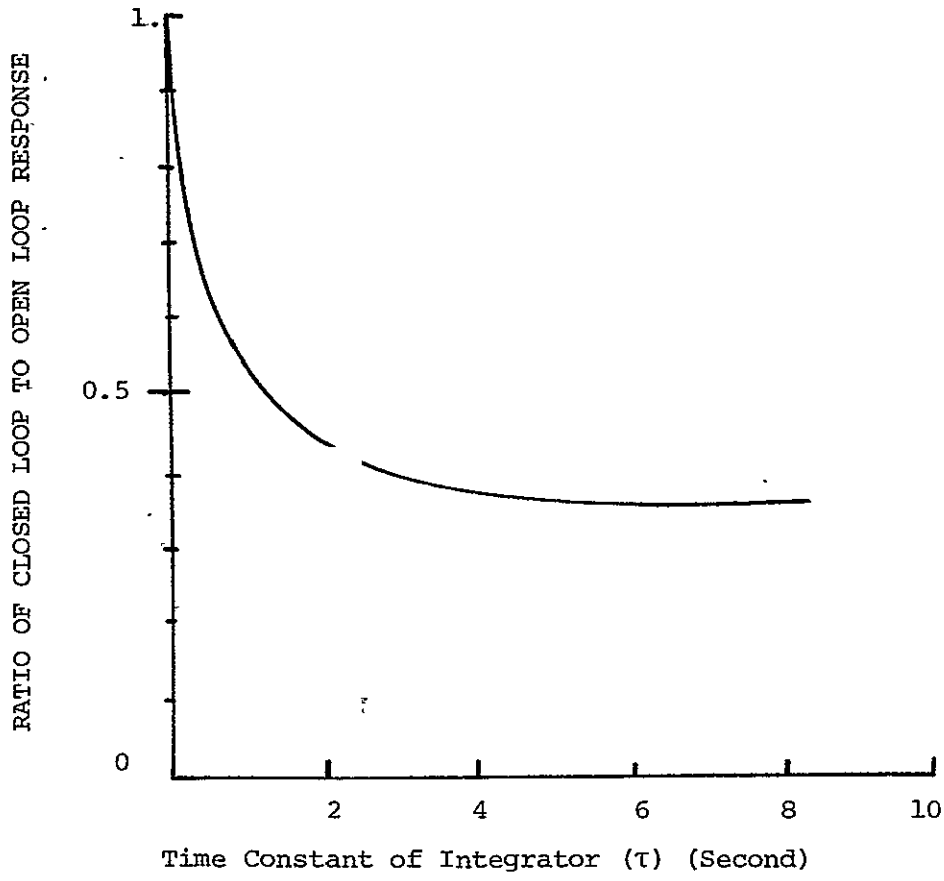

FIGURE 29 SYSTEM 1-1 VARIATION OF RMS(β_{1c}) WITH TIME CONSTANT OF INTEGRATOR WITH $S_{cs(q_1,\ \theta_{1s})} \equiv -4.84$

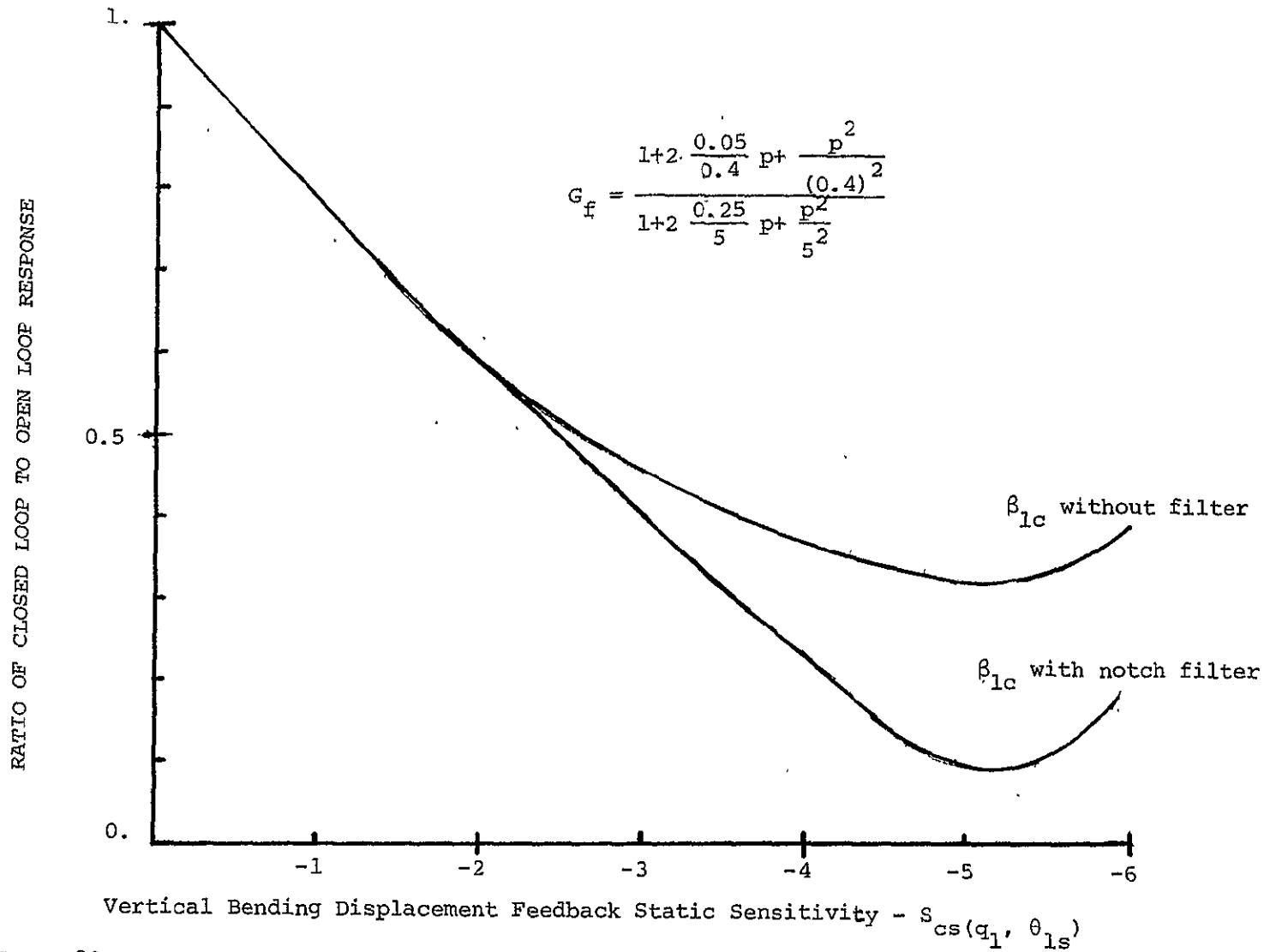

FIGURE 30 SYSTEM 1-1. VARIATION WITH CONTROL SYSTEM FEEDBACK STATIC SENSITIVITY OF THE RATIO OF (RMS)β_{1c} OF CLOSED LOOP CONTROL SYSTEM RESPONSE WITH AND WITHOUT A NOTCH FILTER TO UNCONTROLLED AIRPLANE RESPONSE

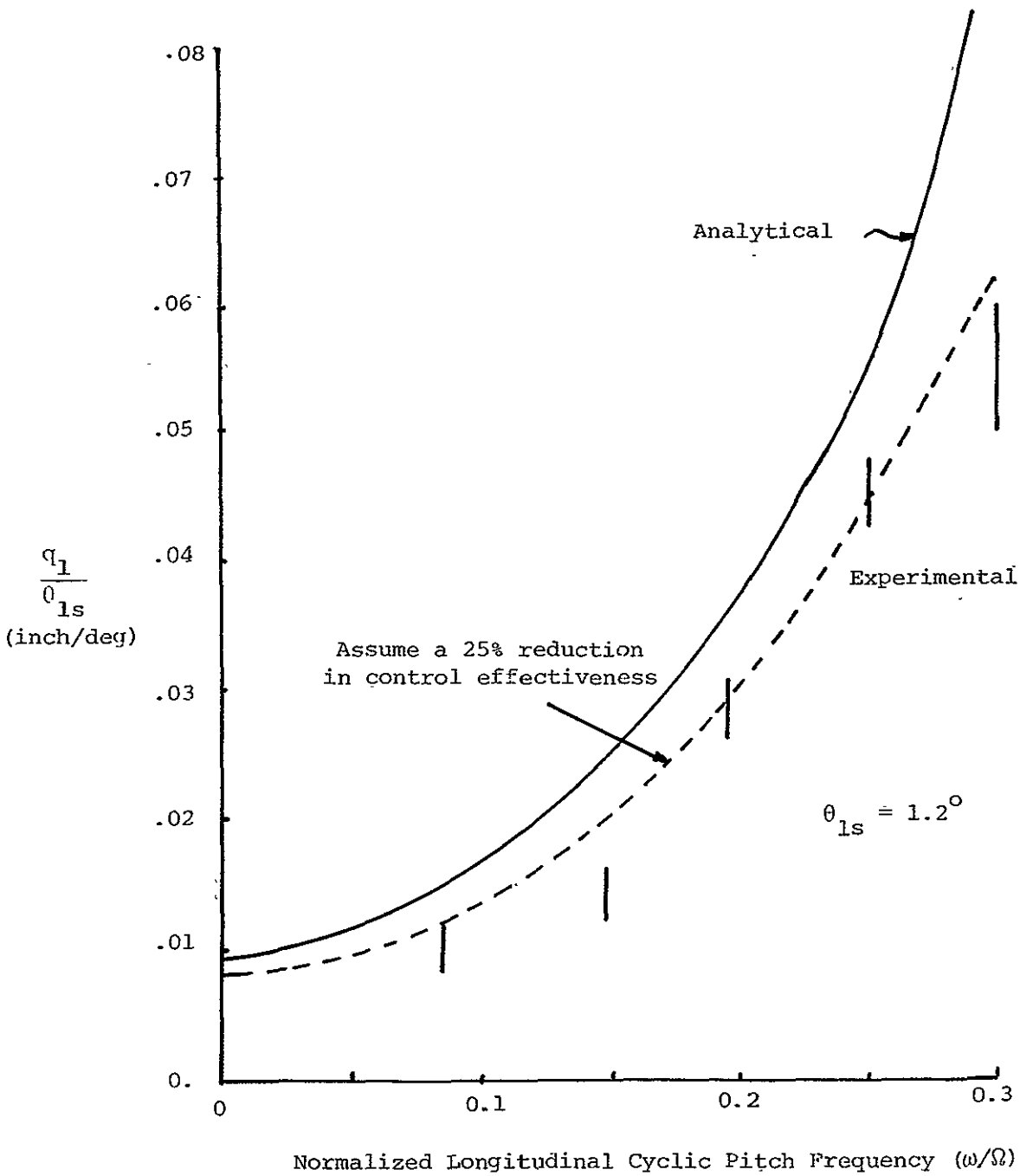

FIGURE 31 WING VERTICAL BENDING RESPONSE TO LONGITUDINAL CYCLIC PITCH

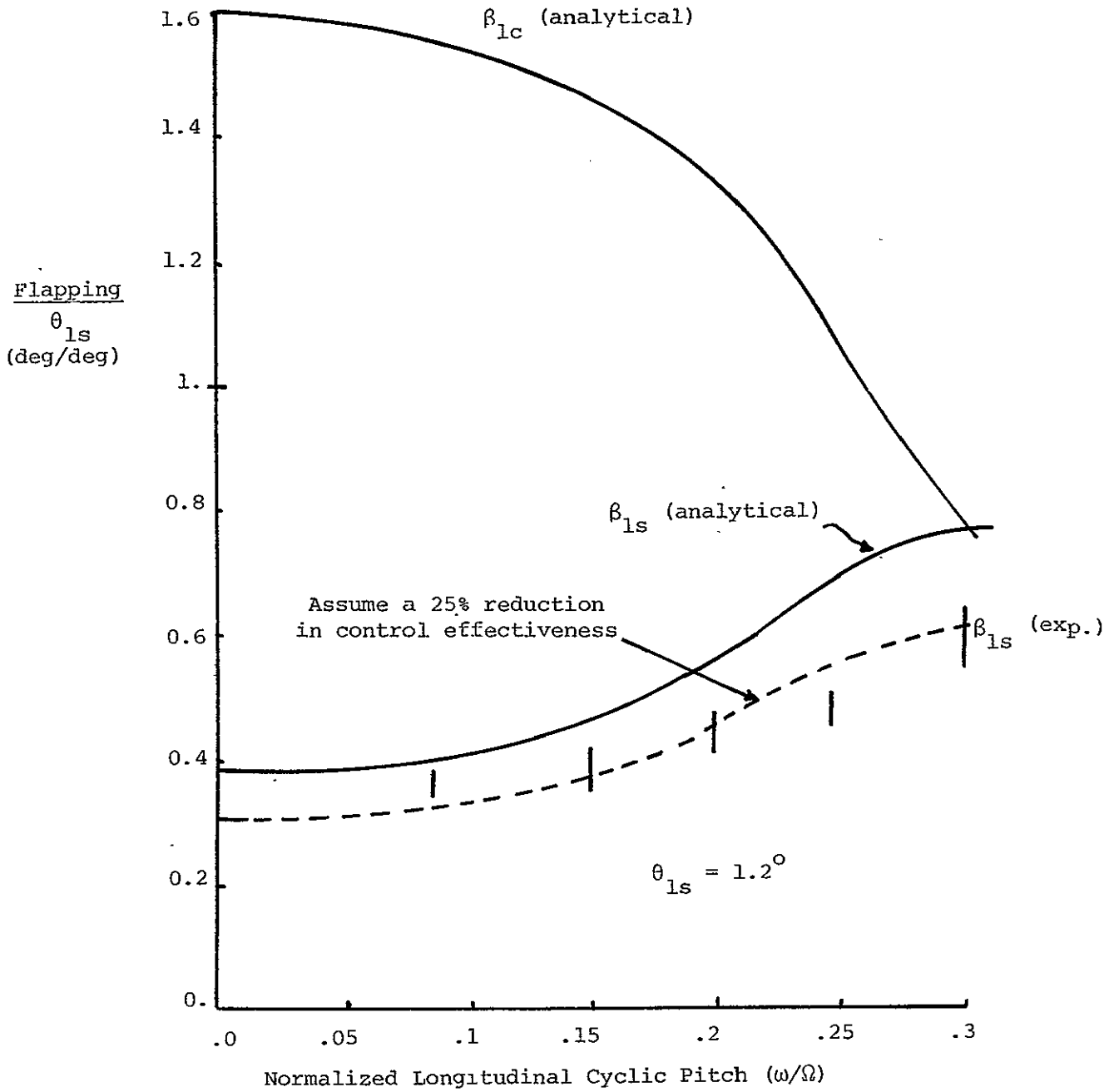

FIGURE 32 ROTOR CYCLIC FLAPPING RESPONSE TO LONGITUDINAL CYCLIC PITCH

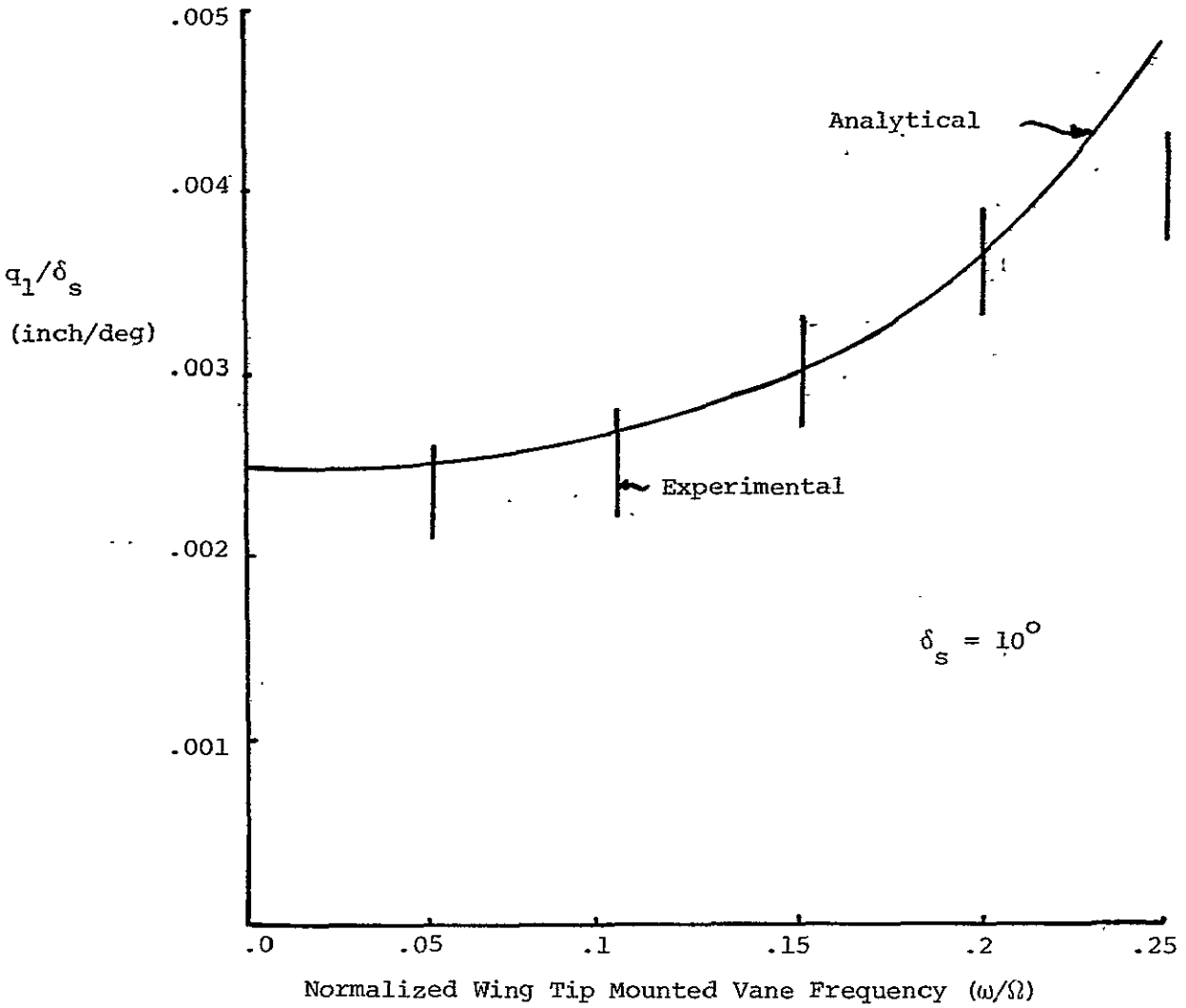

FIGURE 33 : WING VERTICAL BENDING RESPONSE TO WING TIP MOUNTED VANE

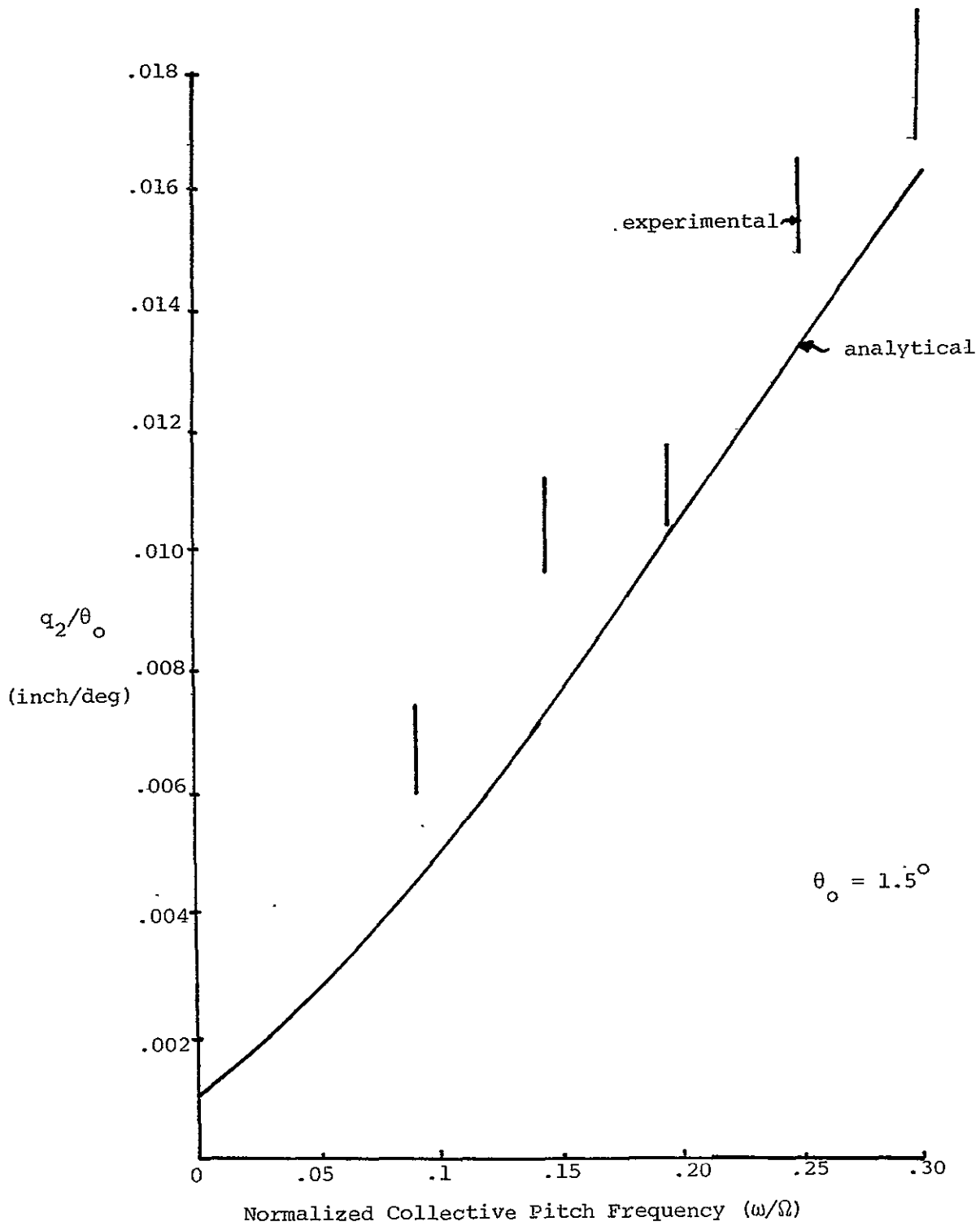

FIGURE 34 WING CHORDWISE BENDING RESPONSE TO COLLECTIVE PITCH

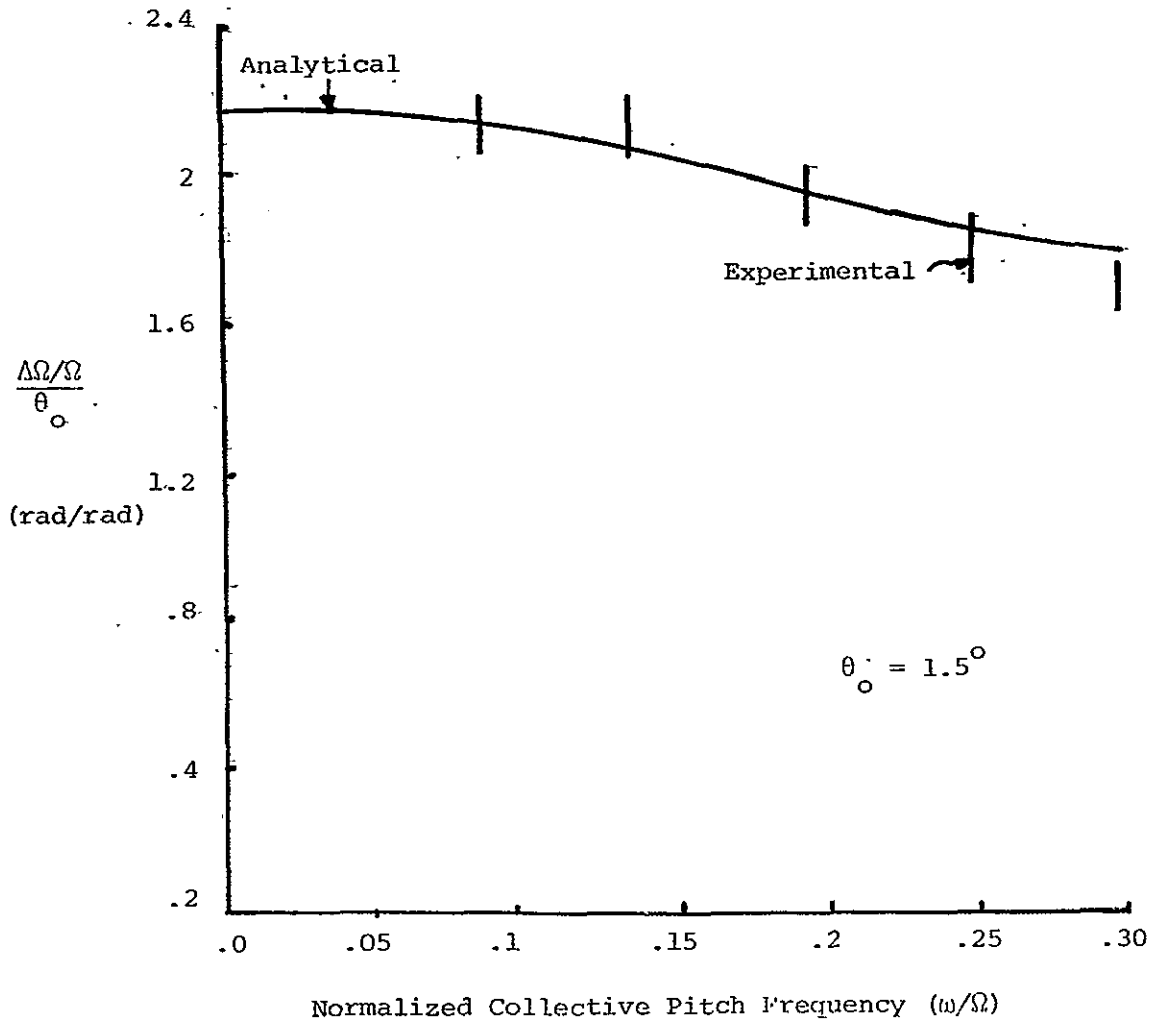

FIGURE 35 ROTOR ROTATIONAL SPEED CHANGE RESPONSE TO COLLECTIVE PITCH

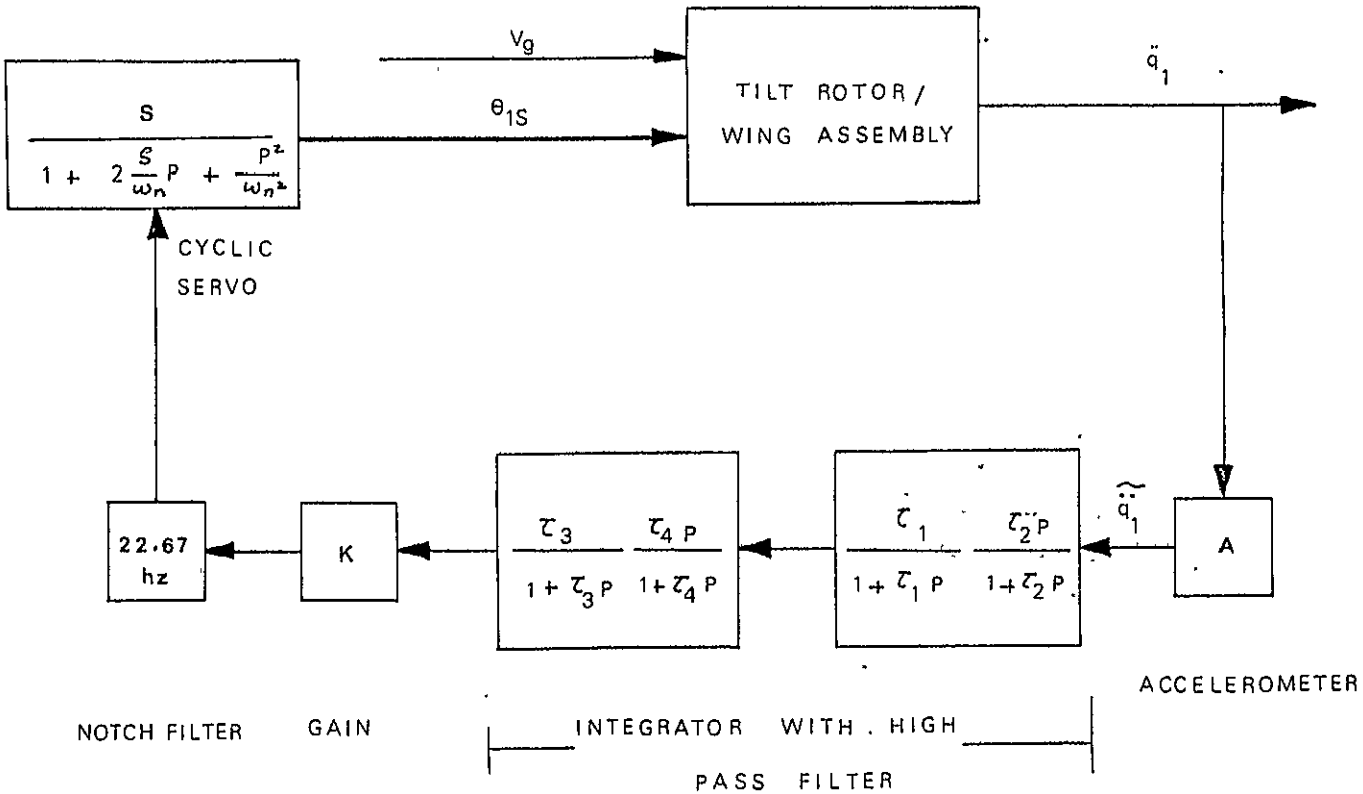

FIGURE 36 SYSTEM 1-1 MATHEMATICAL BLOCK DIAGRAM

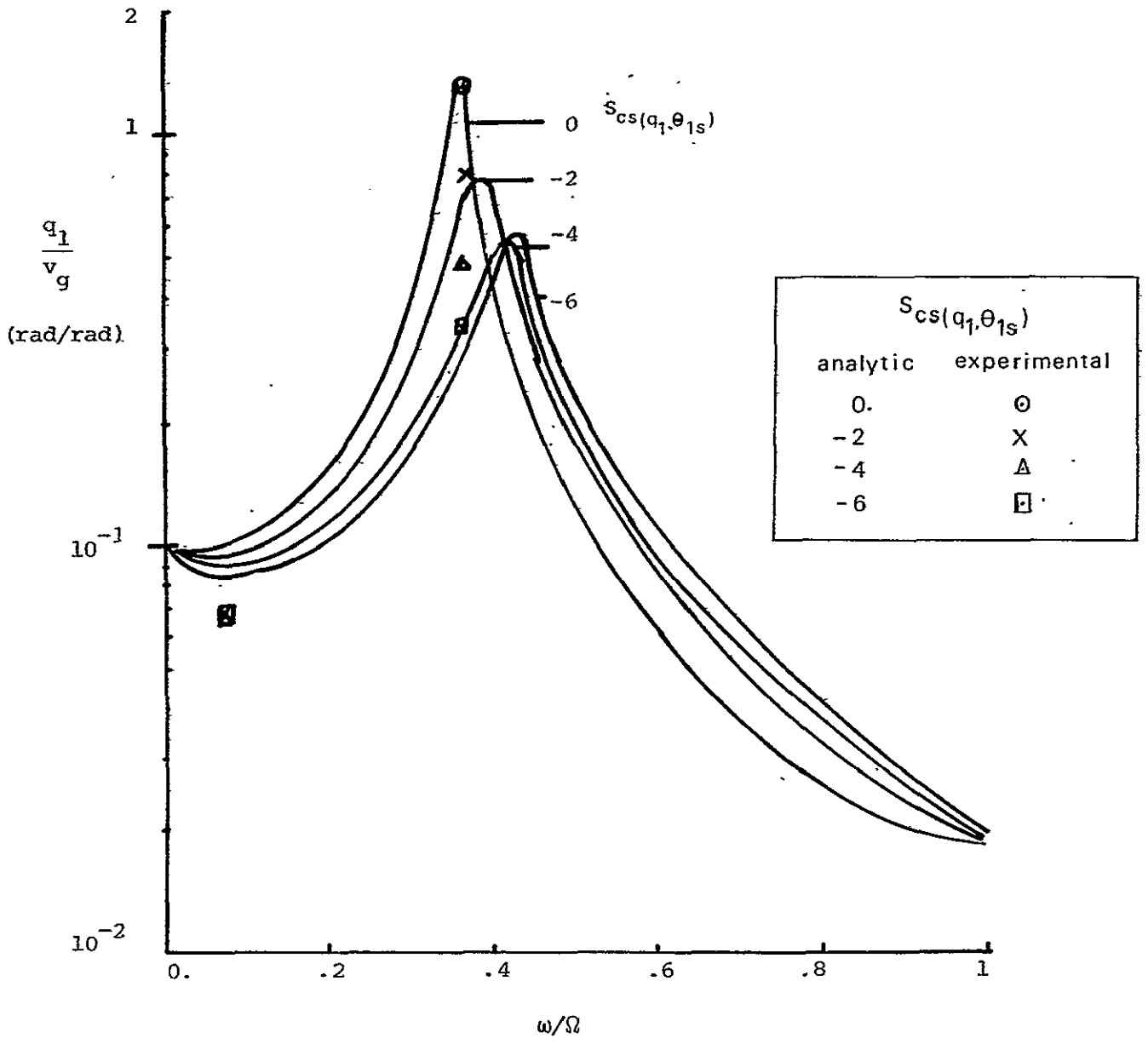

FIGURE 37 ANALYTICAL AND EXPERIMENTAL VALUES OF WING VERTICAL BENDING RESPONSE TO SINUSOIDAL GUST INPUTS FOR SYSTEM 1-1

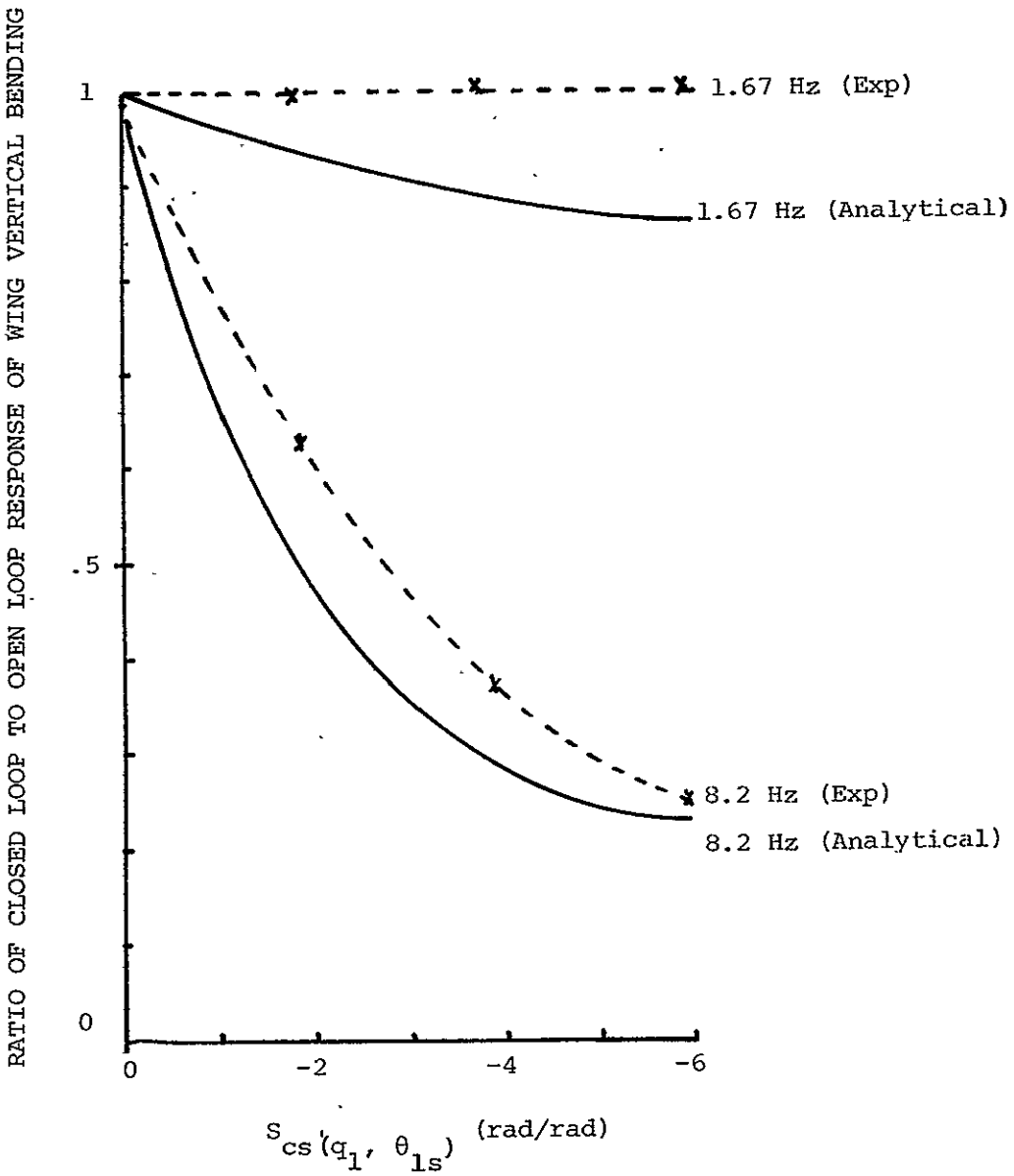

FIGURE 38 ANALYTICAL AND EXPERIMENTAL RATIOS OF CLOSED LOOP TO TO OPEN LOOP RESPONSE OF WING VERTICAL BENDING AT 1.67 Hz and 8.2 Hz FOR SYSTEM 1-1

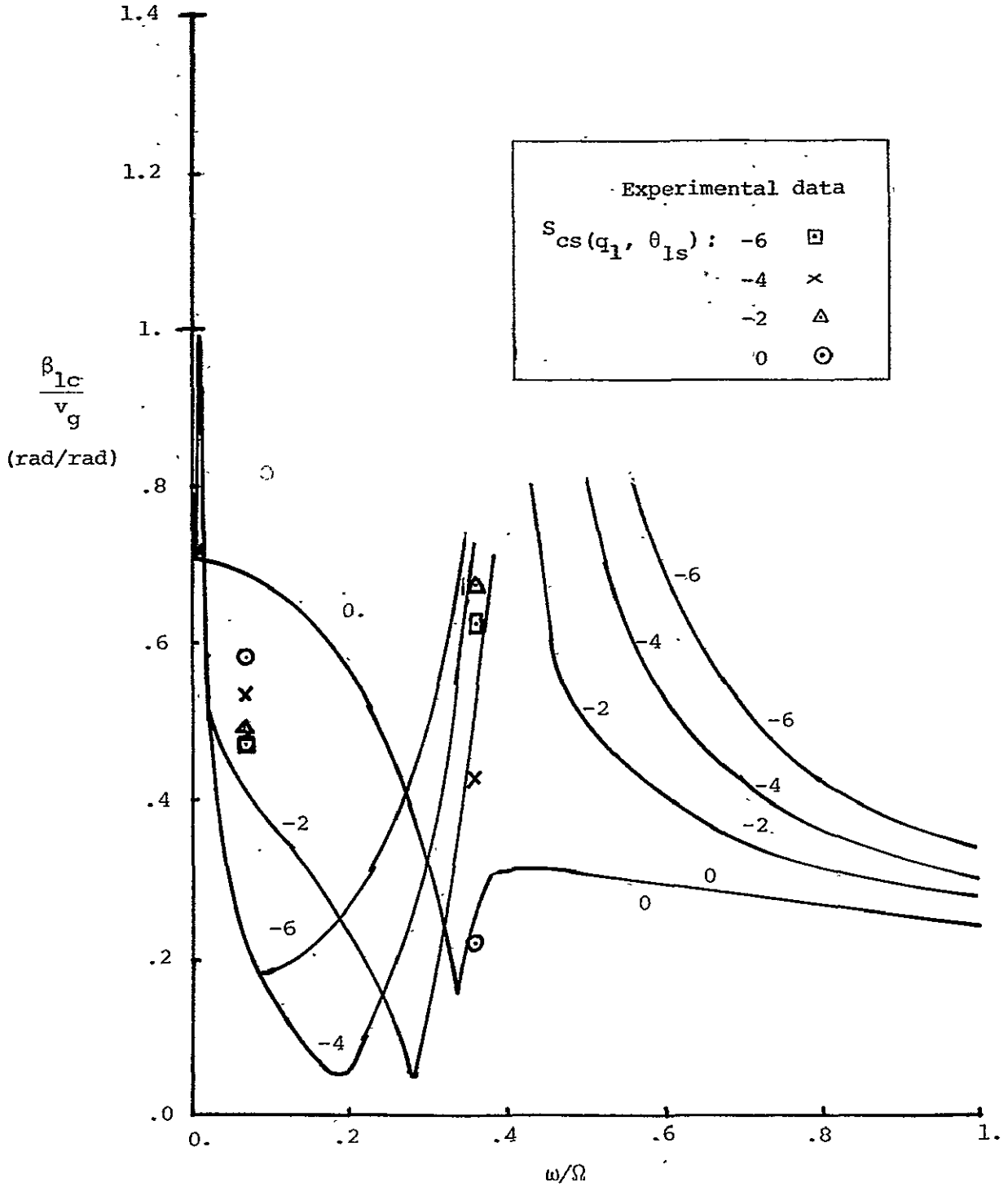

FIGURE 39 ANALYTICAL AND EXPERIMENTAL VALUES OF ROTOR LONGITUDINAL CYCLIC FLAPPING FOR SYSTEM 1-1

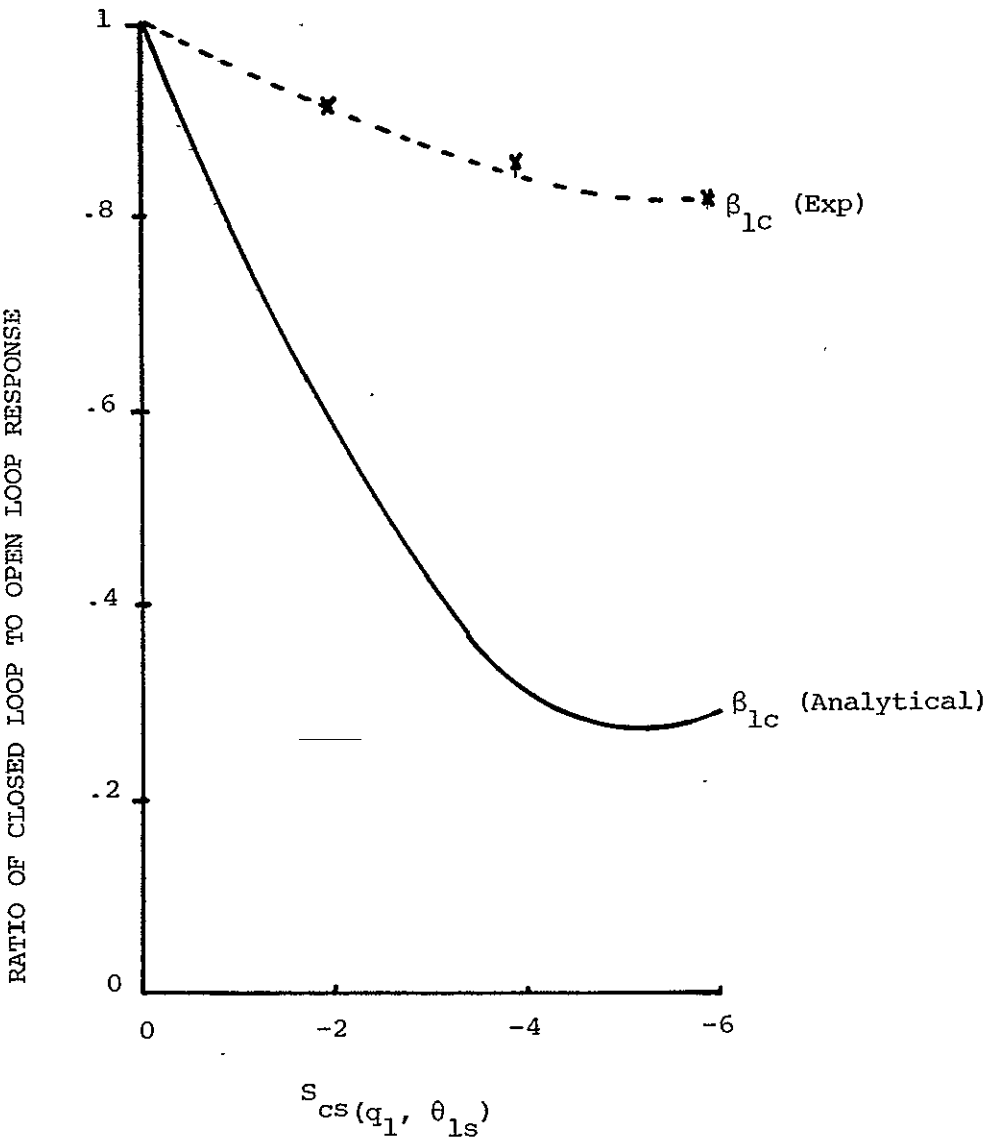

FIGURE 40 ANALYTICAL AND EXPERIMENTAL RATIOS OF CLOSED LOOP RESPONSE OF ROTOR LONGITUDINAL CYCLIC FLAPPING AT 1.67 Hz TO UNCONTROLLED RESPONSE FOR SYSTEM 1-1

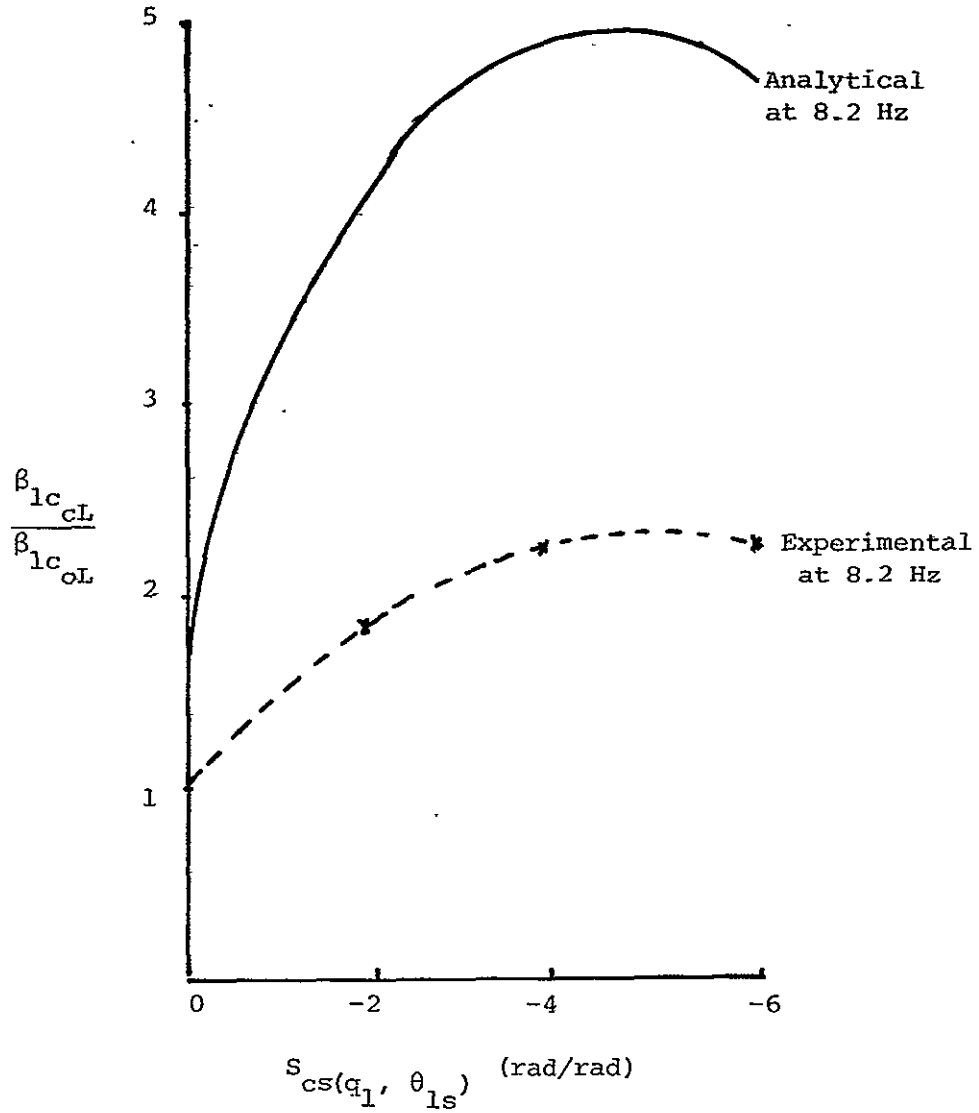

FIGURE 41 ANALYTICAL AND EXPERIMENTAL RATIOS OF CLOSED LOOP TO OPEN LOOP RESPONSE OF ROTOR LONGITUDINAL CYCLIC FLAPPING AT 8.2 HZ FOR SYSTEM 1-1

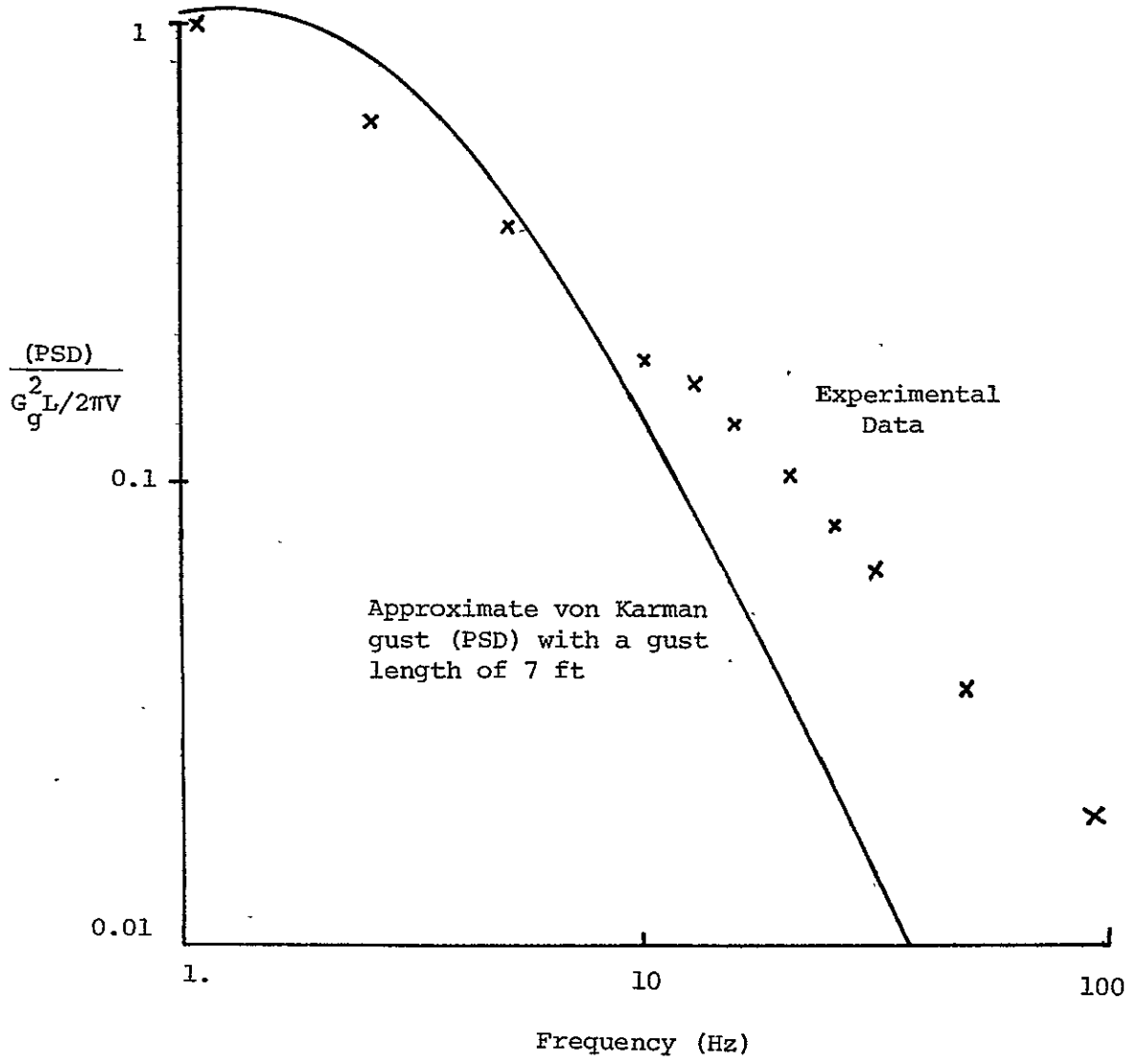

FIGURE 42 POWER SPECTRAL DENSITY OF THE TUNNEL TURBULENCE

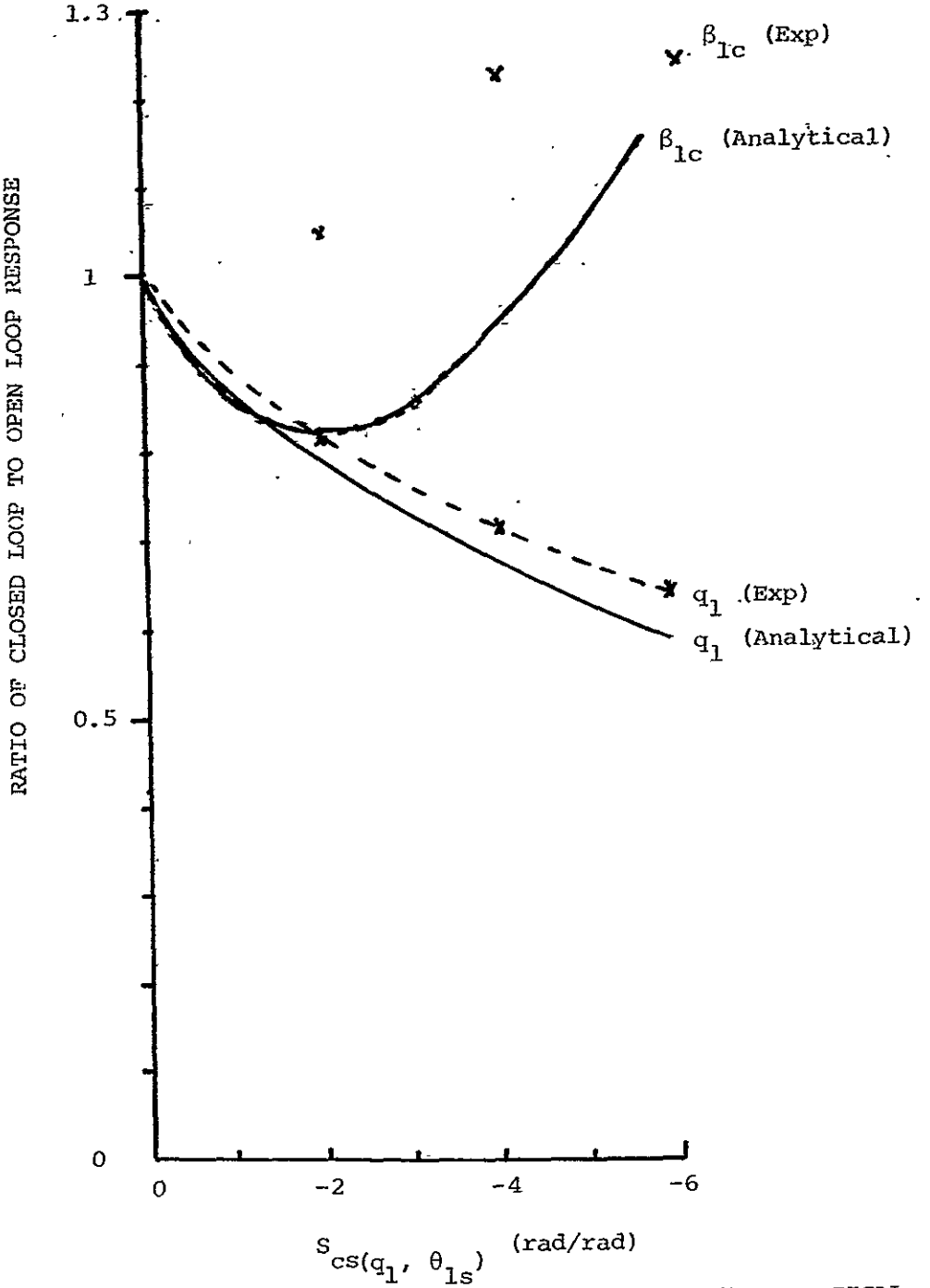

FIGURE 43 ANALYTICAL AND EXPERIMENTAL RMS LEVELS OF WING VERTICAL BENDING AND ROTOR LONGITUDINAL CYCLIC FLAPPING TO WIND TUNNEL TURBULENCE FOR SYSTEM 1-1

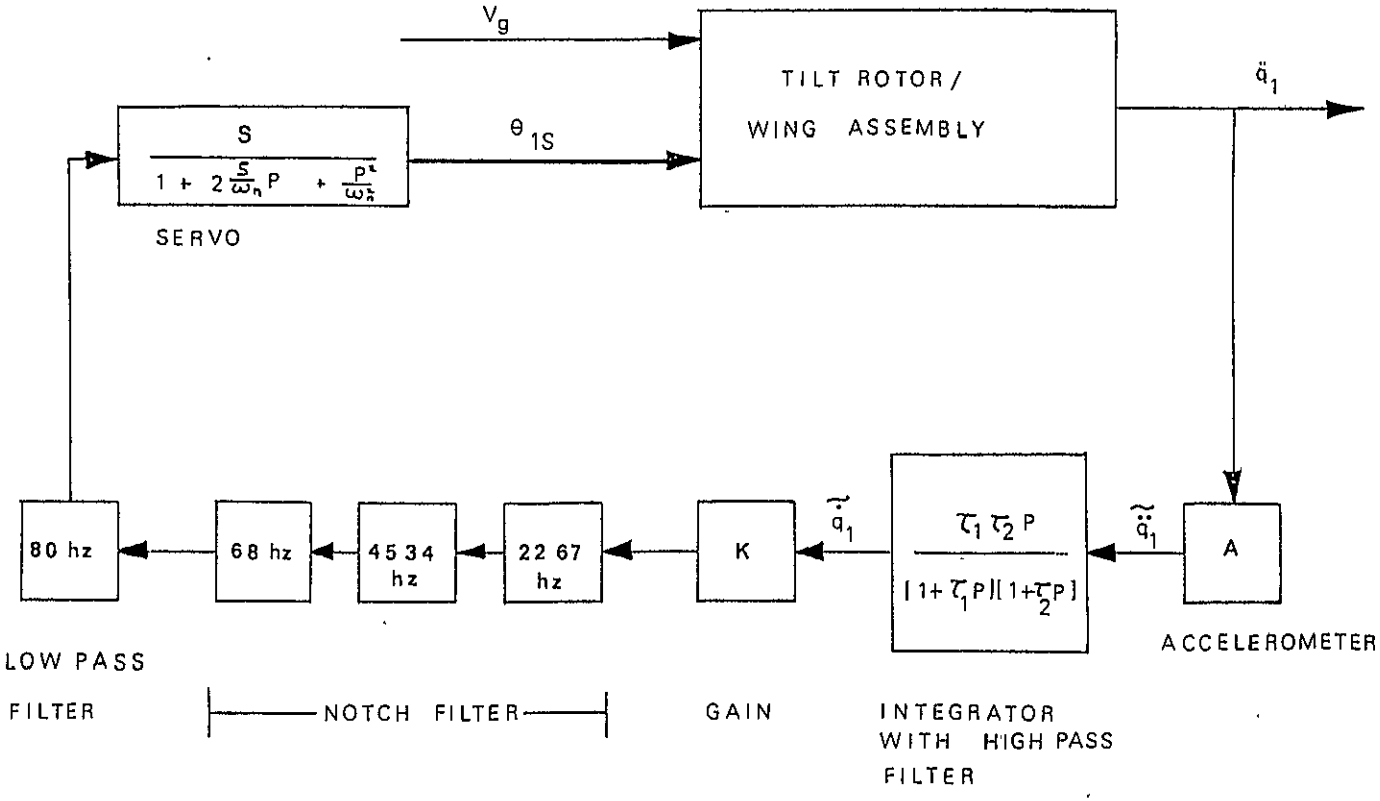

FIGURE 44 SYSTEM 1-2 MATHEMATICAL BLOCK DIAGRAM

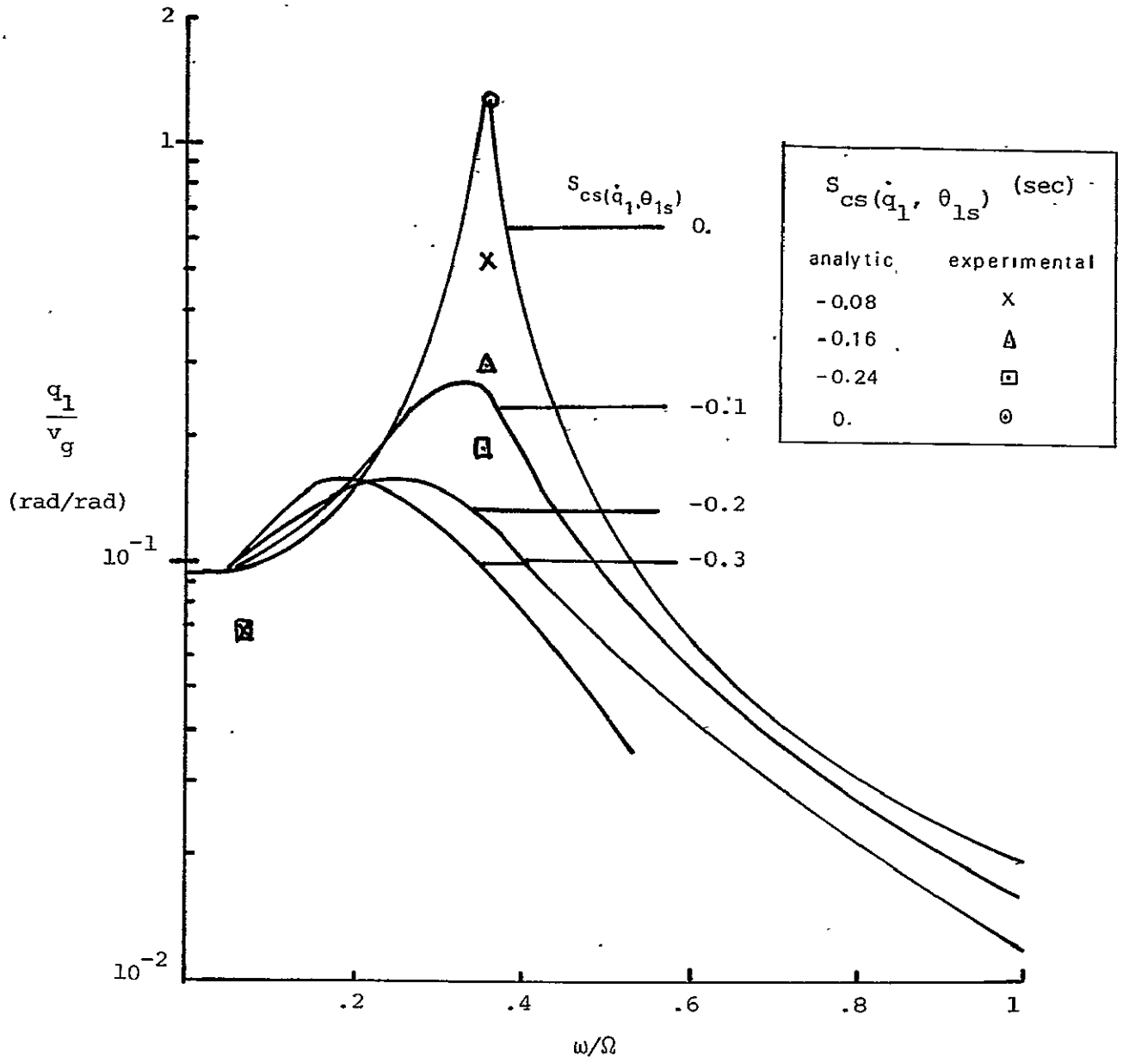

FIGURE 45 ANALYTICAL AND EXPERIMENTAL VALUES OF WING VERTICAL BENDING FOR SYSTEM 1-2

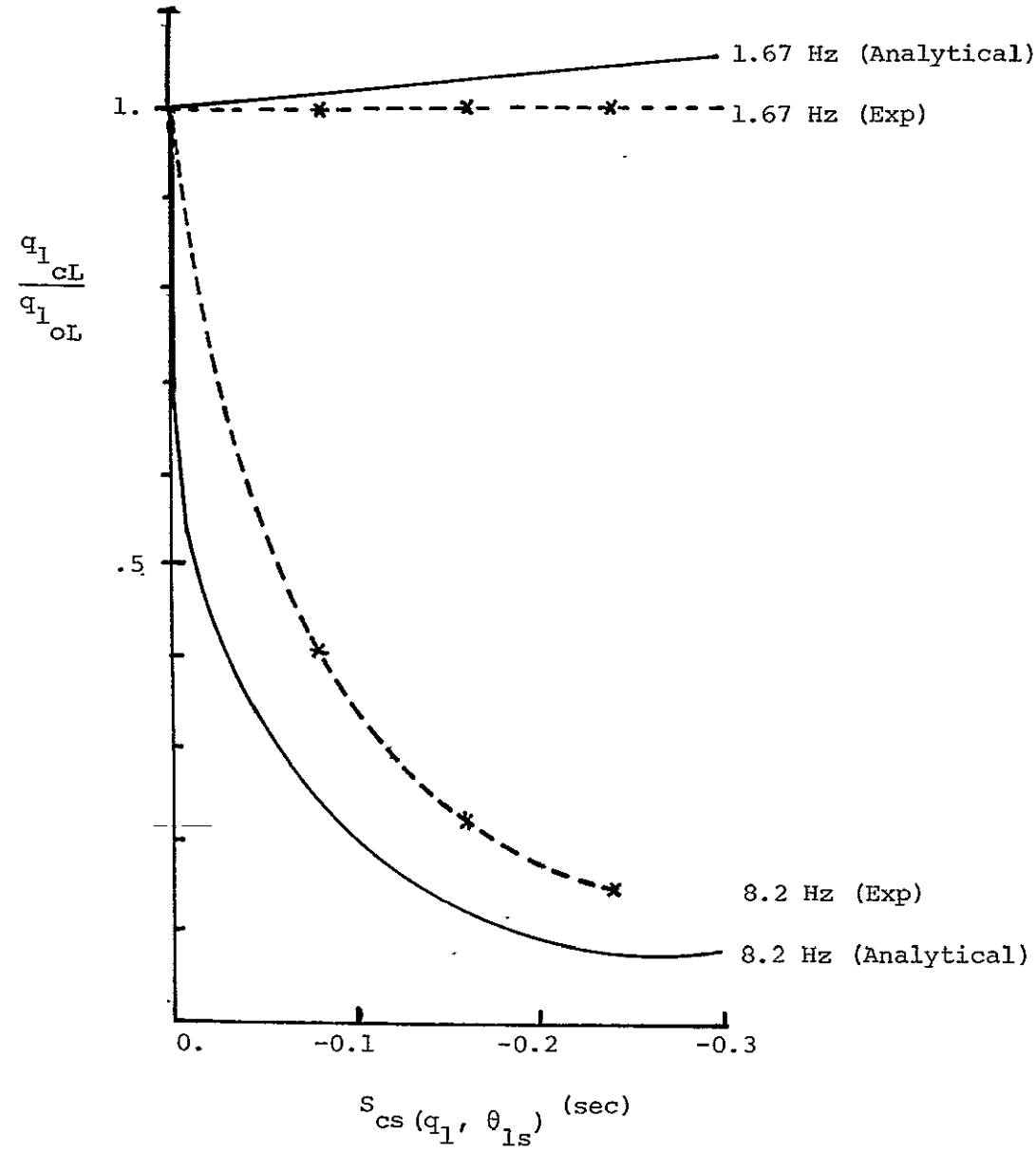

FIGURE 46 ANALYTICAL AND EXPERIMENTAL VALUES OF RATIOS OF CLOSED LOOP TO OPEN LOOP RESPONSE OF WING VERTICAL BENDING FOR SYSTEM 1-2 TO 1.67 AND 8.2 Hz GUSTS

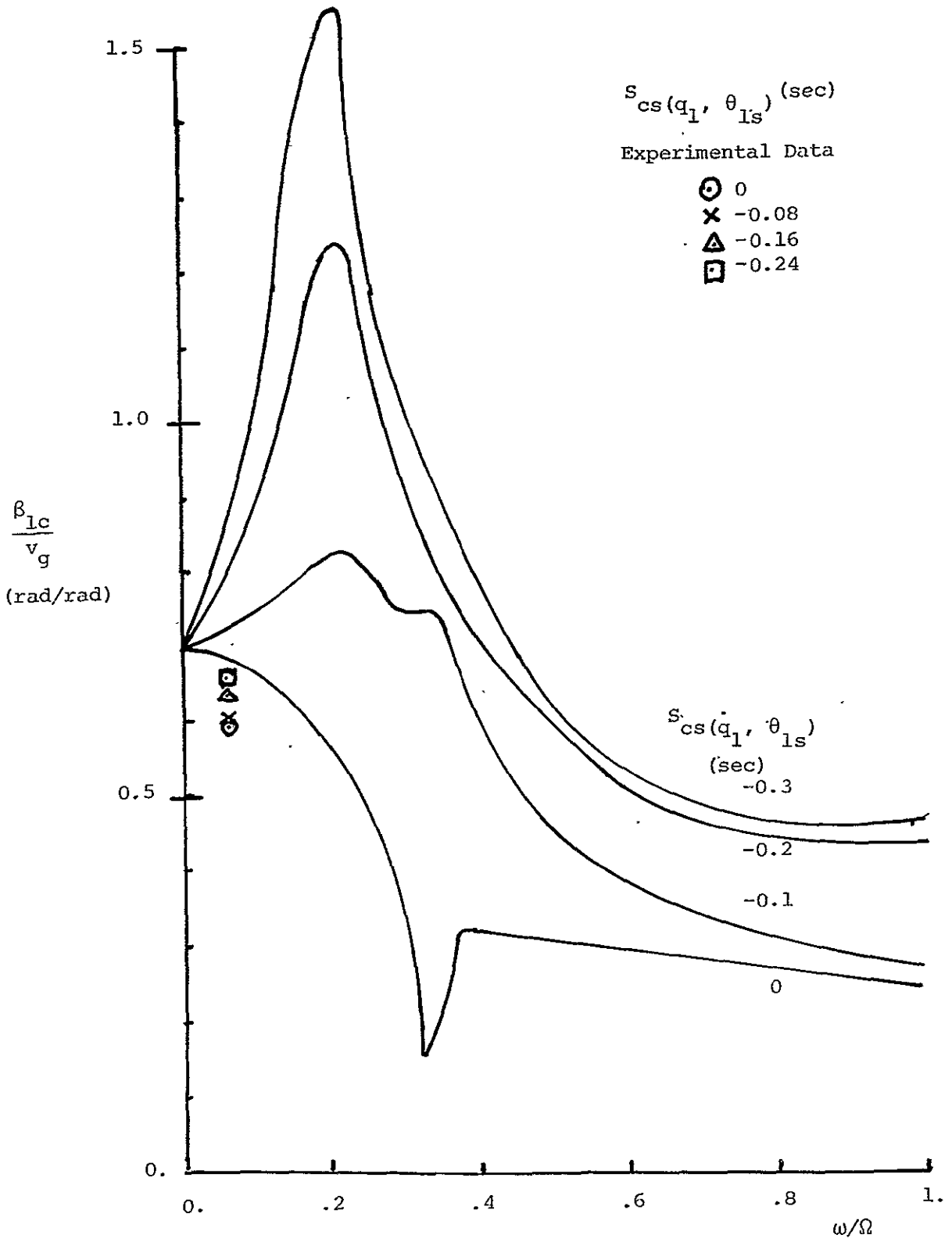

FIGURE 47 ANALYTICAL AND EXPERIMENTAL VALUES OF ROTOR LONGITUDINAL CYCLIC FLAPPING FOR SYSTEM 1-2

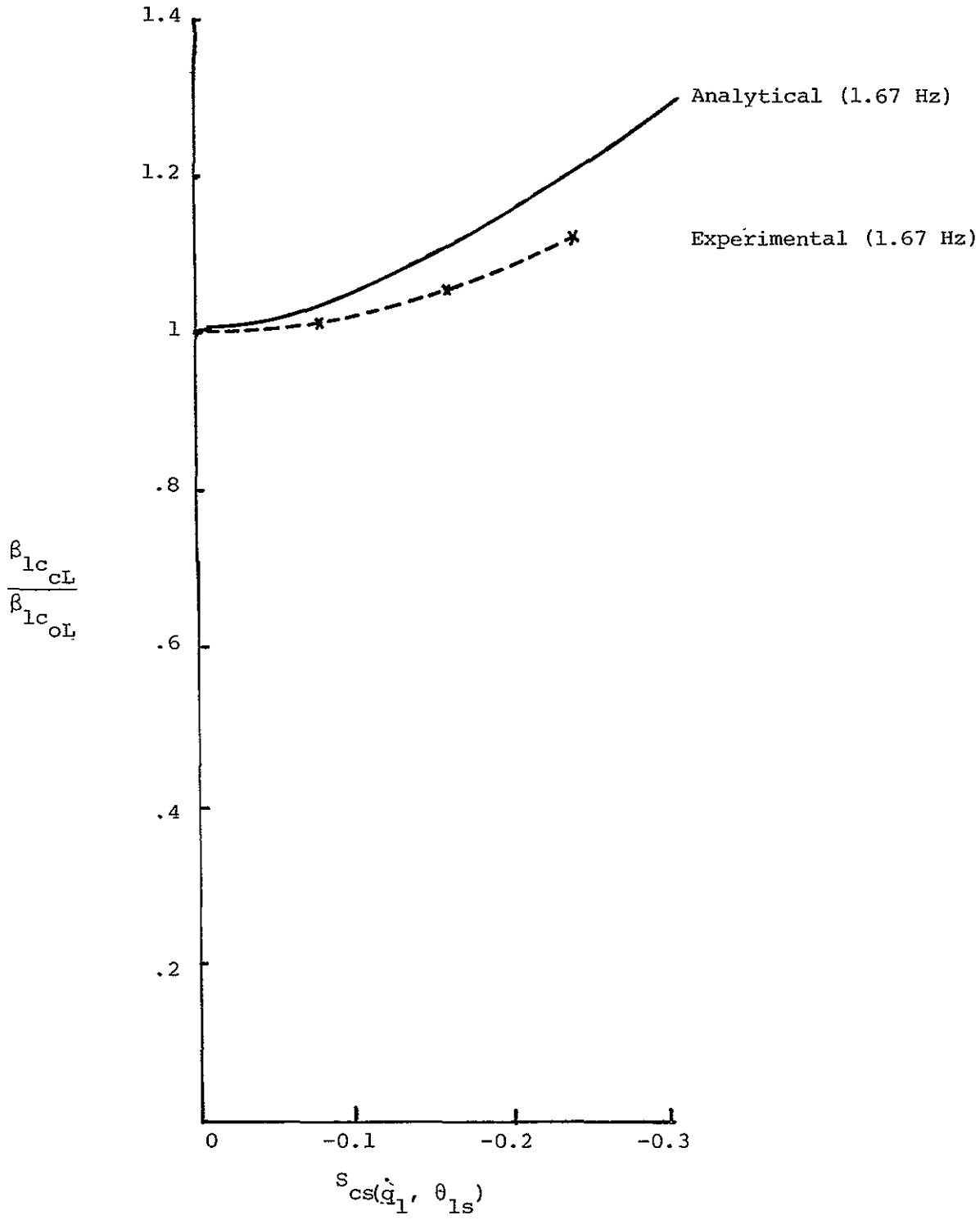

FIGURE 48 ANALYTICAL AND EXPERIMENTAL VALUES OF RATIOS OF CLOSED LOOP TO OPEN LOOP RESPONSE OF ROTOR LONGITUDINAL CYCLIC FLAPPING FOR SYSTEM 1-2 TO 1.67 Hz GUSTS

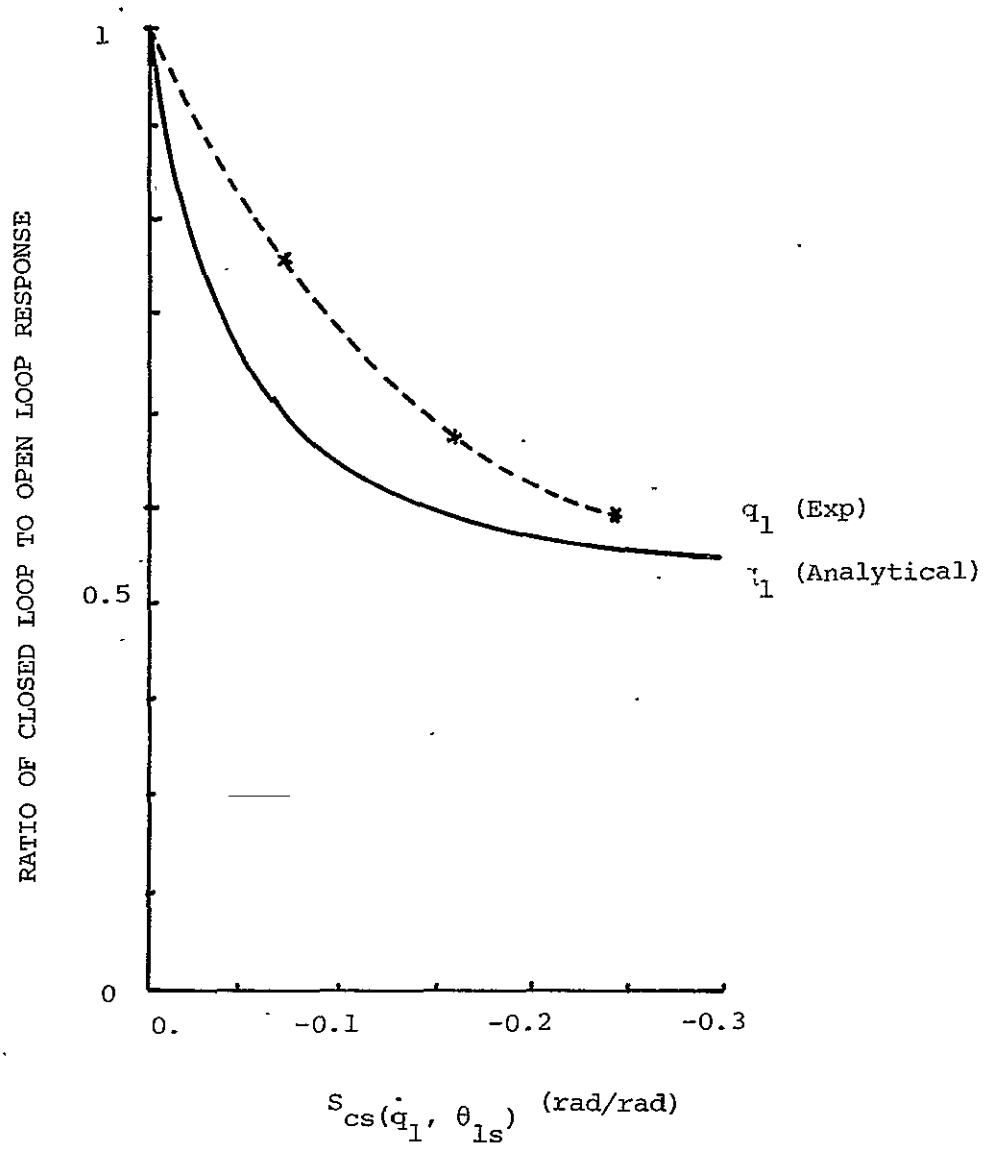

FIGURE 49 ANALYTICAL AND EXPERIMENTAL RMS LEVEL OF WING VERTICAL BENDING TO WIND TUNNEL TURBULENCE. FOR SYSTEM 1-2

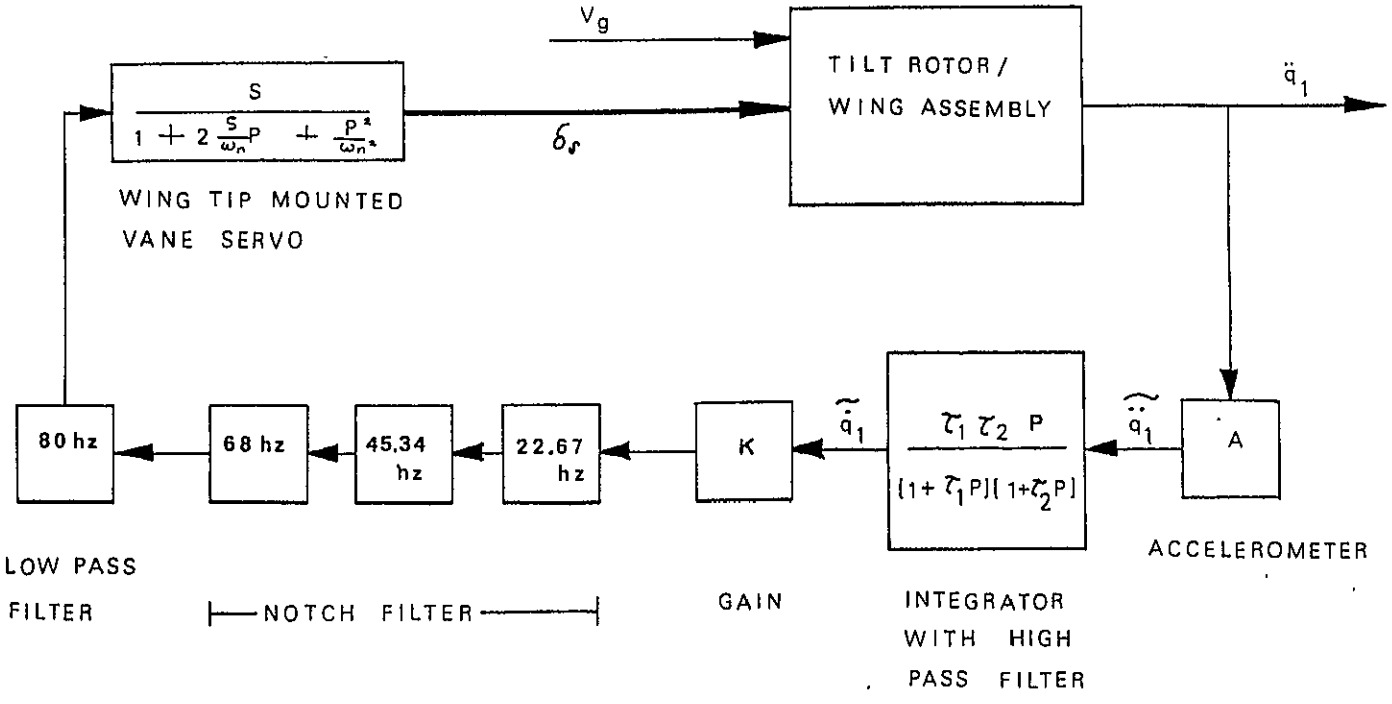

FIGURE 50 SYSTEM 2-2 MATHEMATICAL BLOCK DIAGRAM

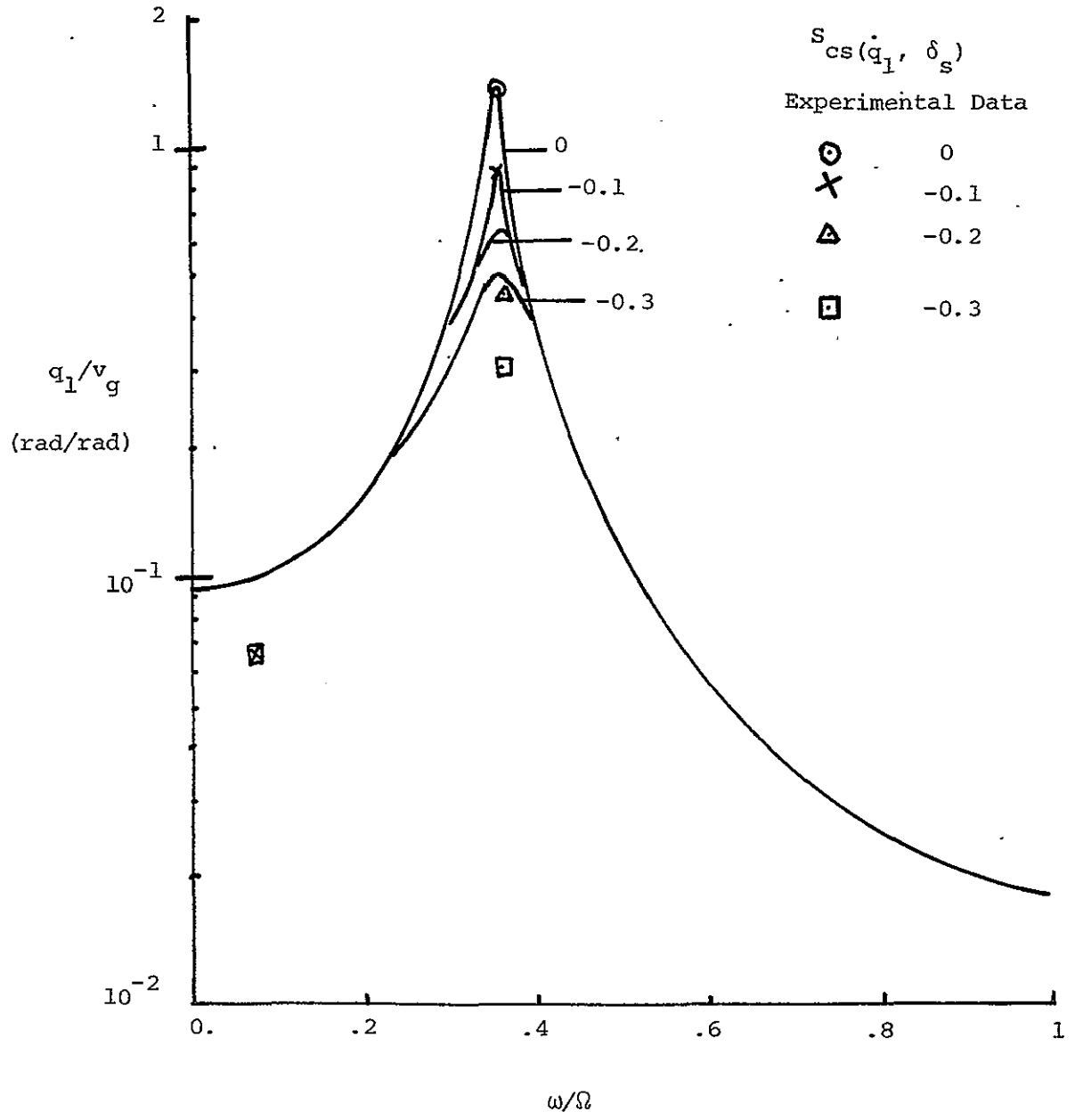

FIGURE 51 ANALYTICAL AND EXPERIMENTAL VALUES OF WING VERTICAL BENDING WITH WING VERTICAL BENDING VELOCITY FED TO THE WING TIP MOUNTED VANE

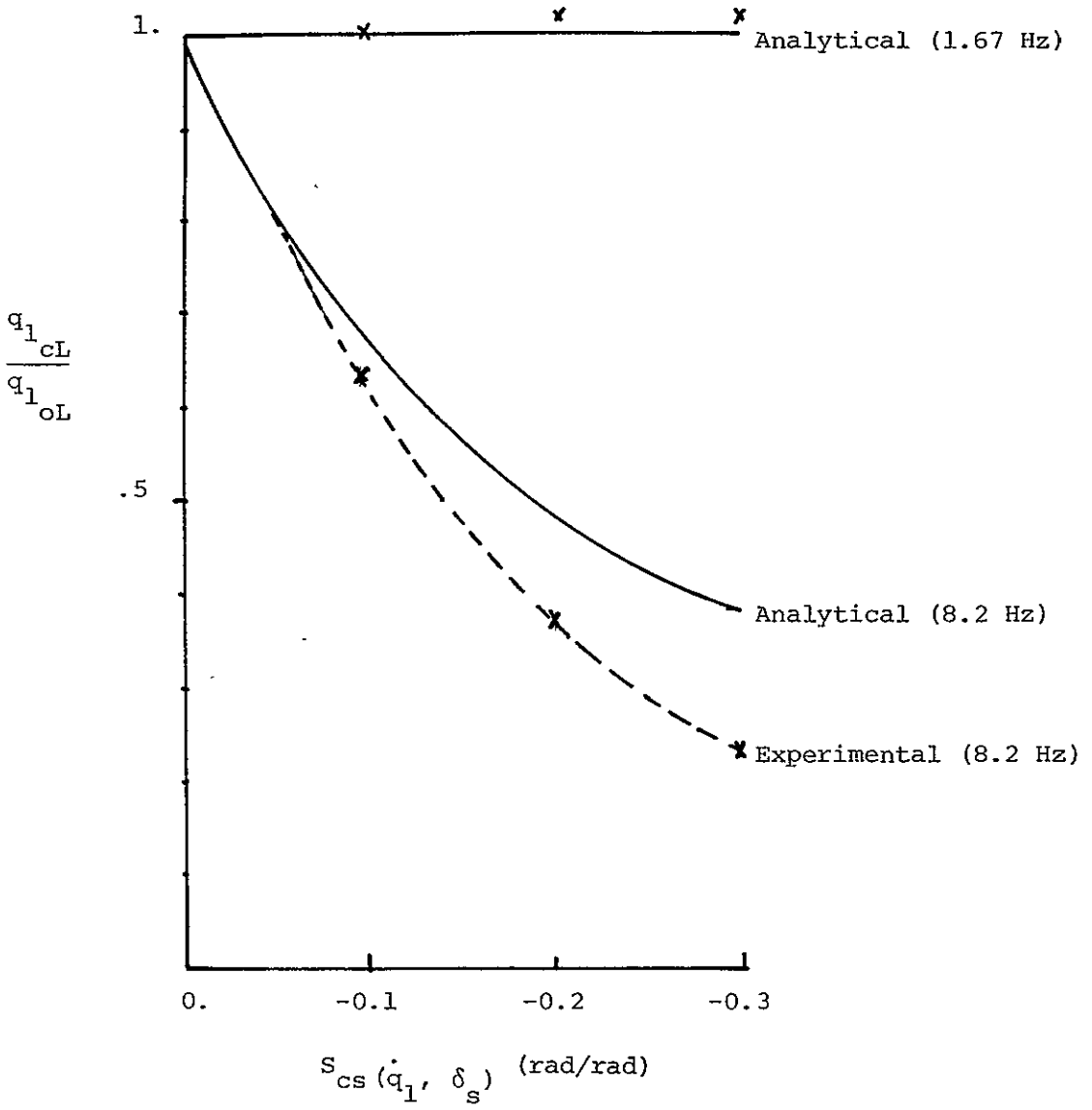

FIGURE 52 ANALYTICAL AND EXPERIMENTAL VALUES OF RATIOS OF CLOSED LOOP TO OPEN LOOP RESPONSE OF WING VERTICAL BENDING FOR SYSTEM 2-2 TO 1.67 AND 8.2 Hz GUSTS

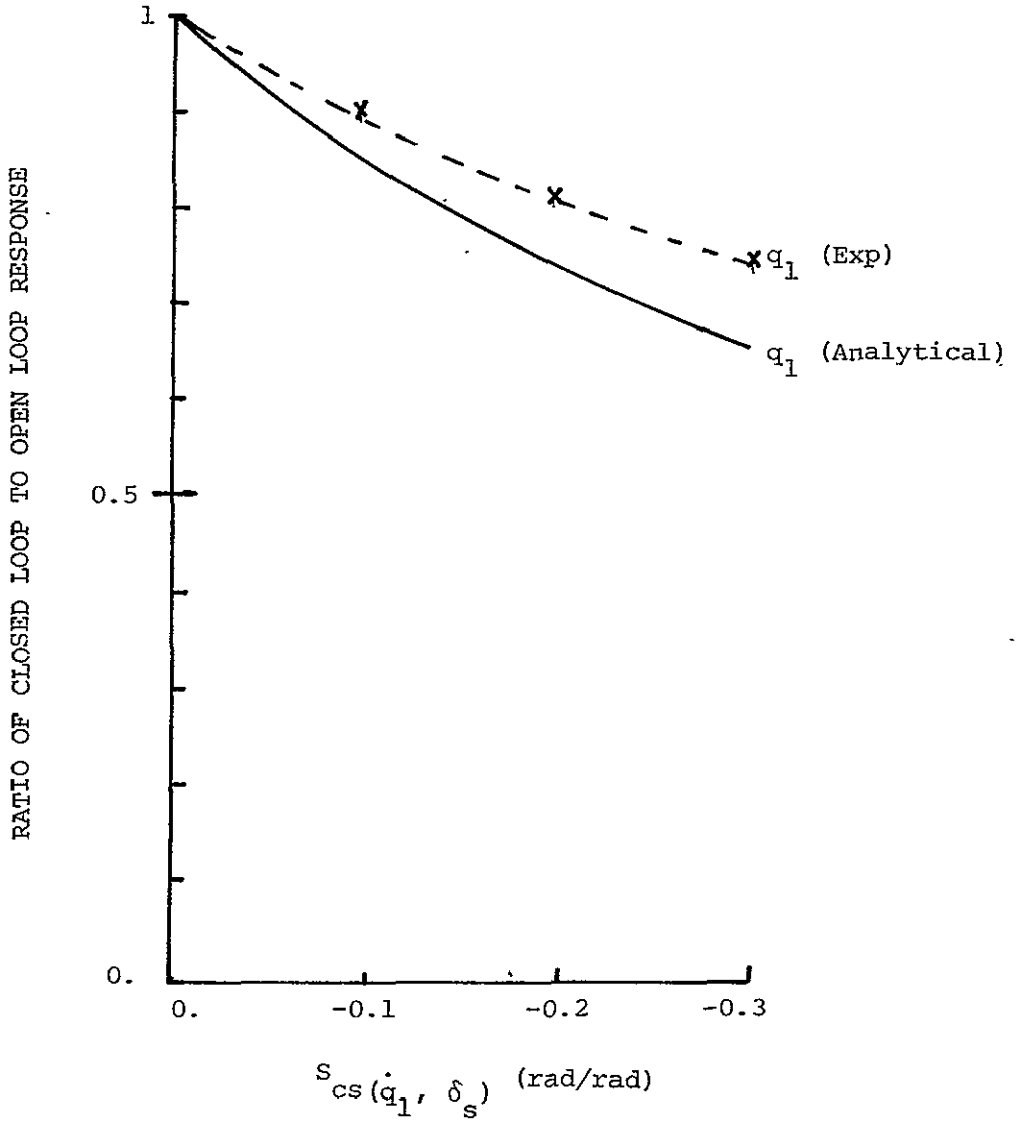

FIGURE 53 ANALYTICAL AND EXPERIMENTAL RMS LEVEL OF WING VERTICAL BENDING IN WIND TUNNEL TURBULENCE FOR SYSTEM 2-2

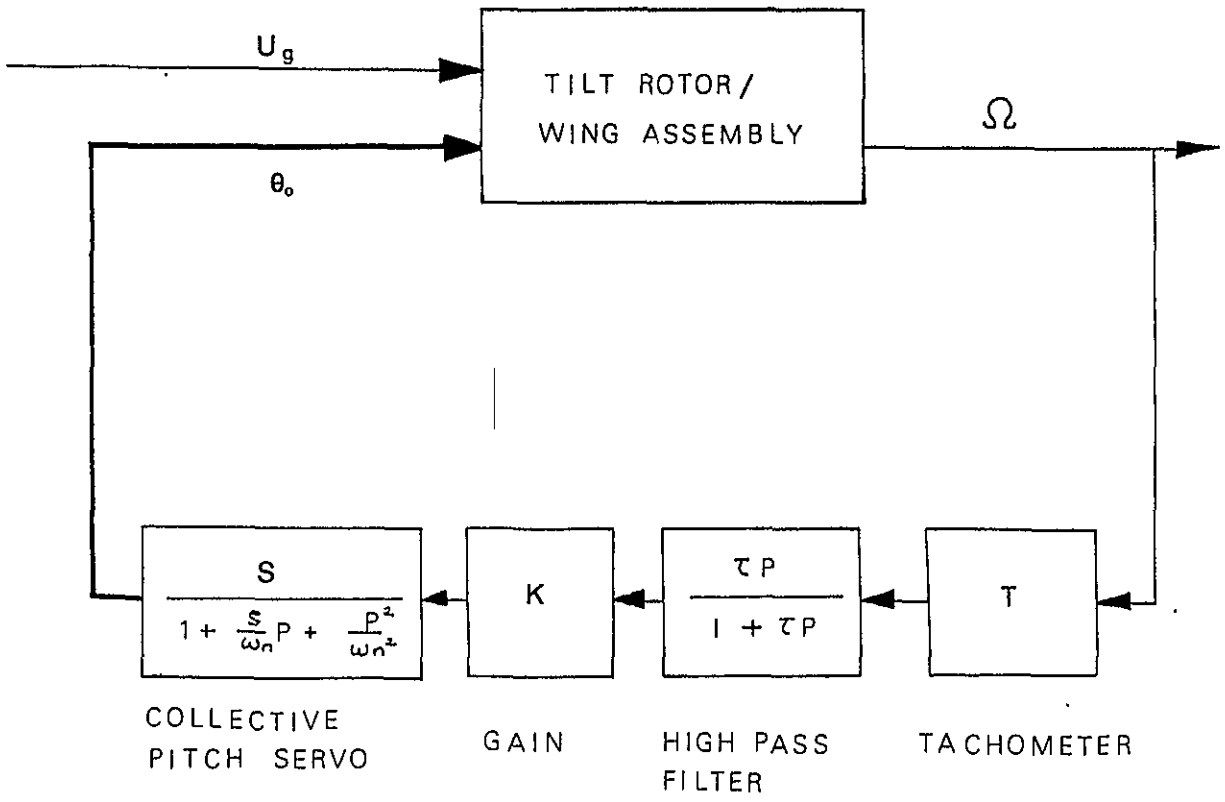

FIGURE 54 SYSTEM 4-1 MATHEMATICAL BLOCK DIAGRAM

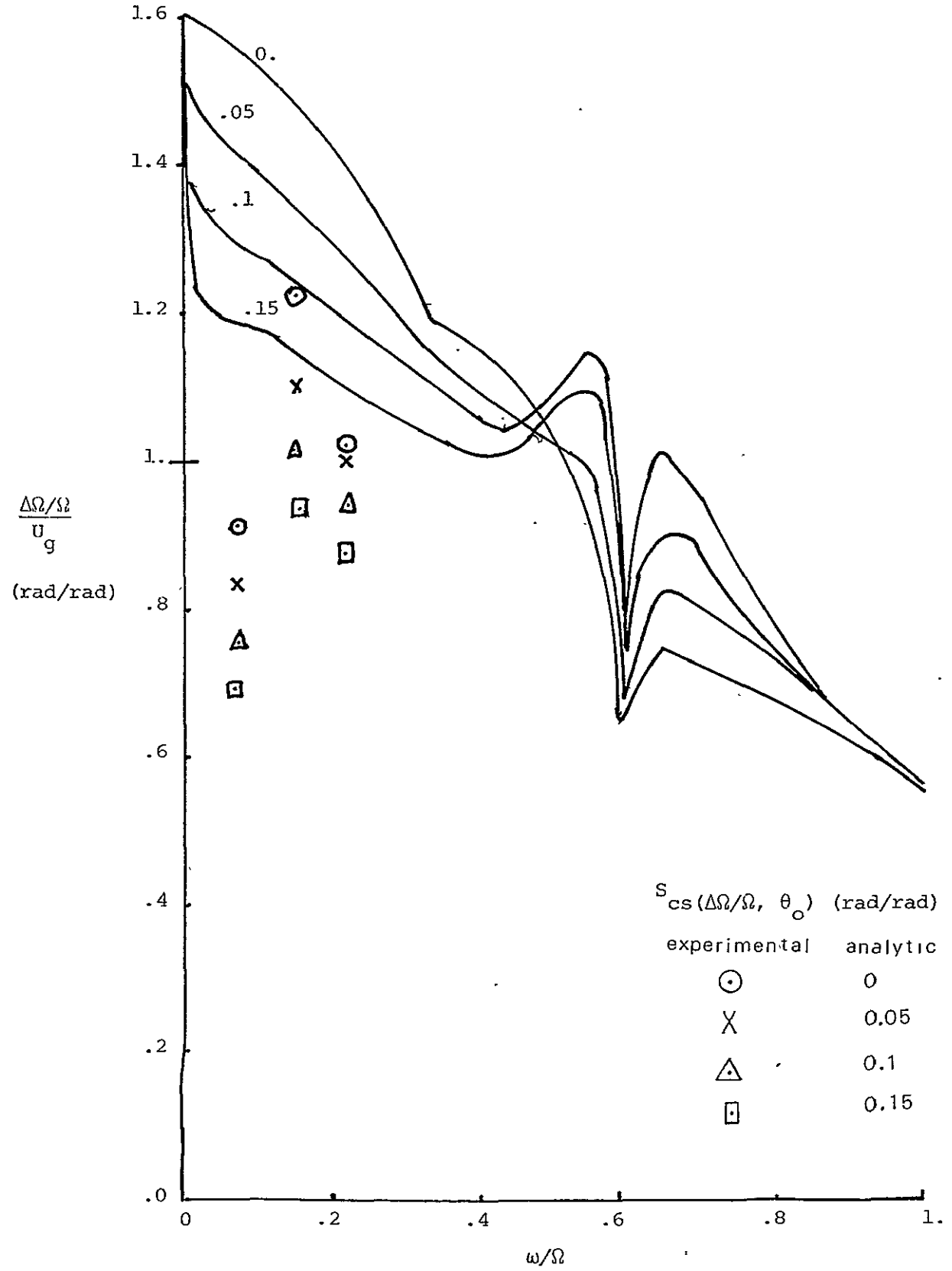

FIGURE 55 ANALYTICAL AND EXPERIMENTAL VALUES OF ROTOR ROTATIONAL SPEED CHANGE RESPONSE TO 1.67, 3.33, 5.0 Hz GUSTS FOR SYSTEM 4-1

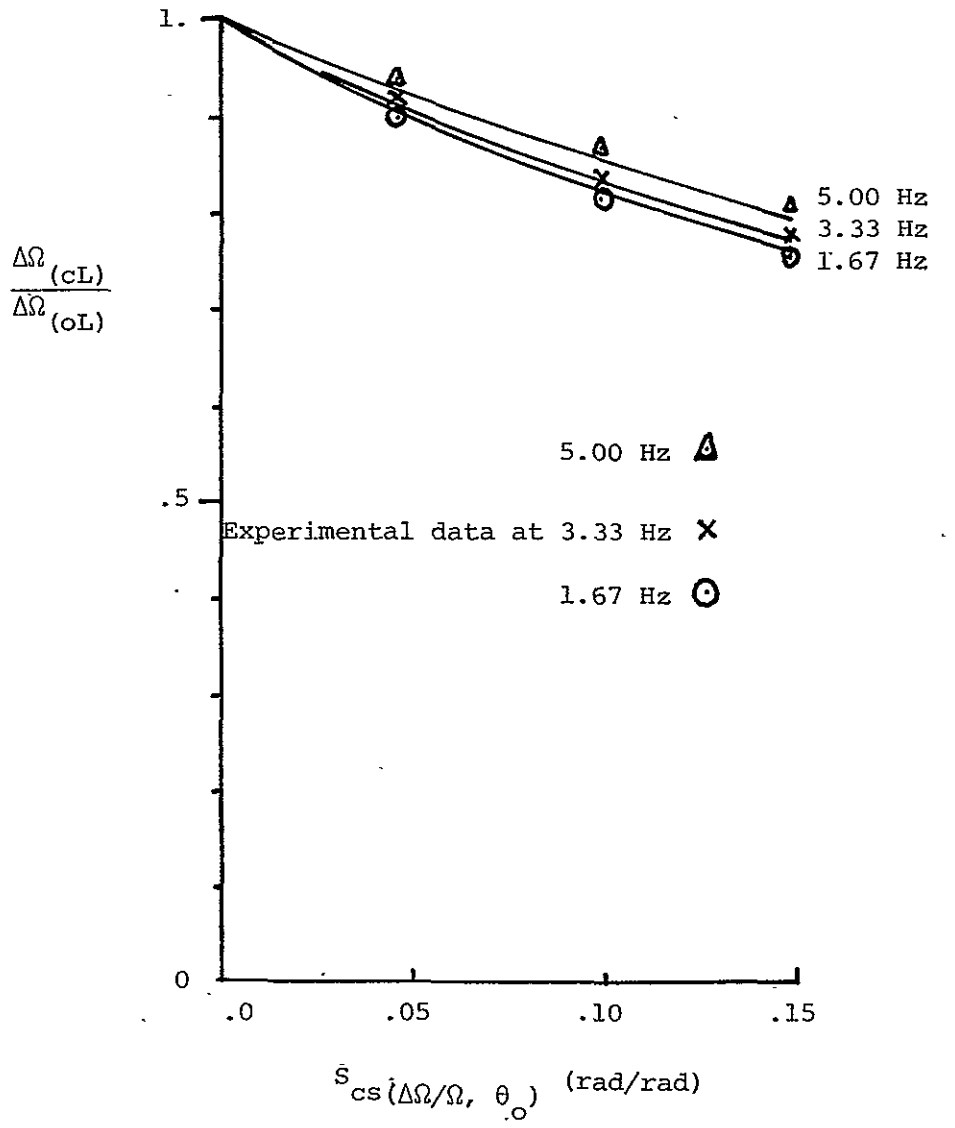

FIGURE 56 ANALYTICAL AND EXPERIMENTAL VALUES OF RATIOS OF CLOSED LOOP TO OPEN LOOP RESPONSE OF ROTOR ROTATIONAL SPEED CHANGE RESPONSE TO 3.33 AND 5.00 Hz GUSTS FOR SYSTEM 4-1

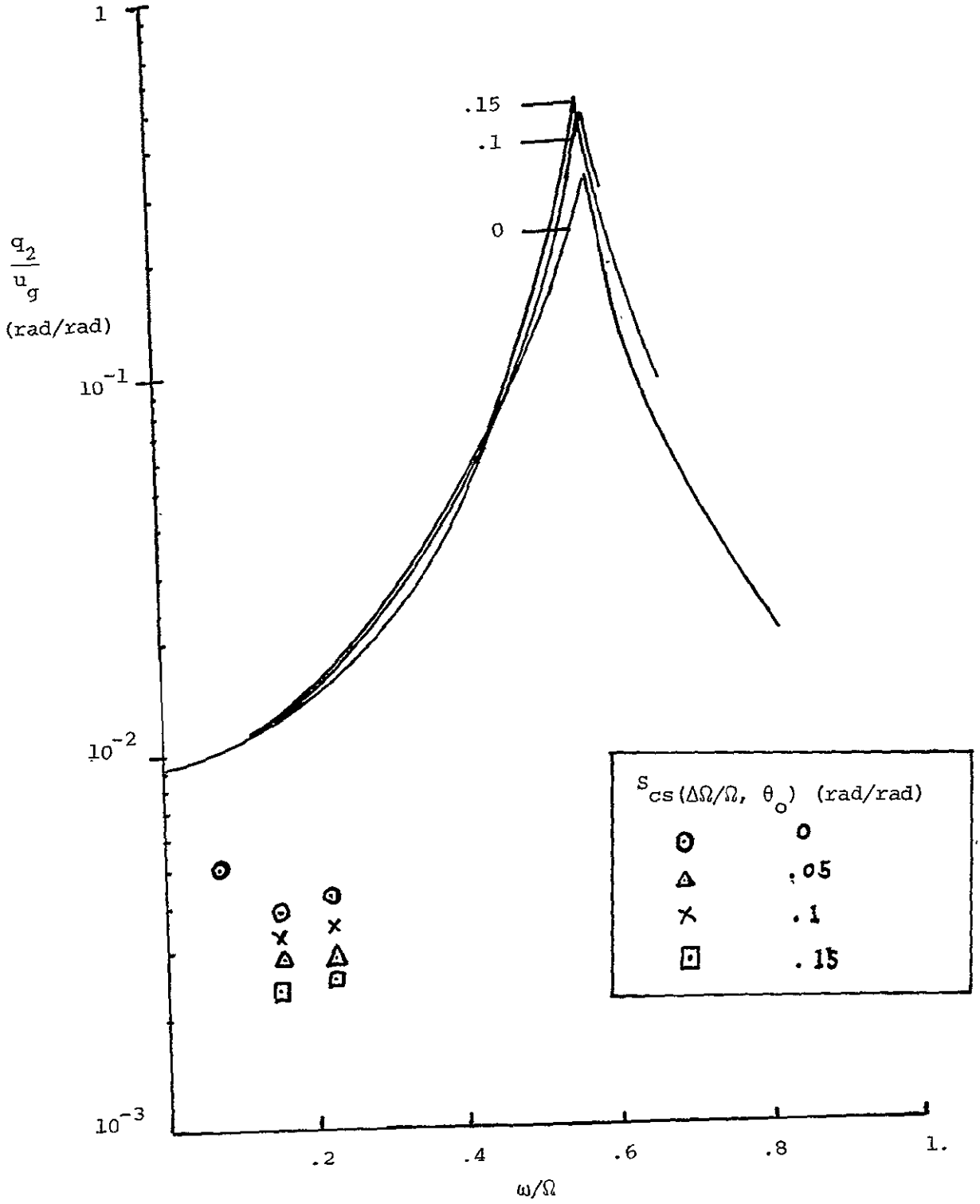

FIGURE 57 ANALYTICAL AND EXPERIMENTAL VALUES OF WING CHORDWISE BENDING RESPONSE TO 1.67, 3.33, AND 5.00 Hz GUSTS FOR SYSTEM 4-1

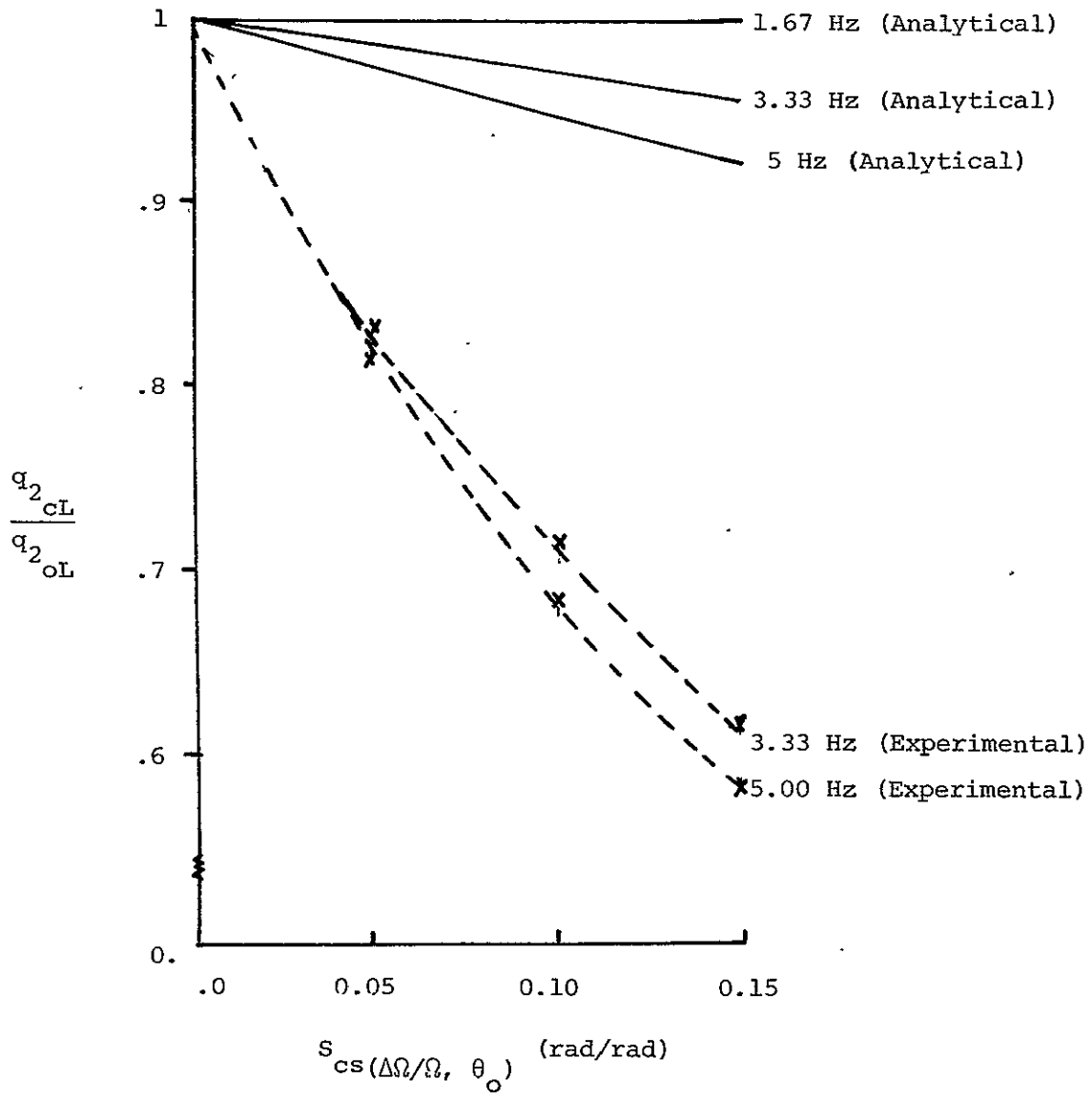

FIGURE 58 ANALYTICAL AND EXPERIMENTAL VALUES OF RATIOS OF CLOSED LOOP TO OPEN LOOP RESPONSE OF WING CHORDWISE BENDING RESPONSE TO 3.33 AND 5.00 Hz GUSTS FOR SYSTEM 4-1

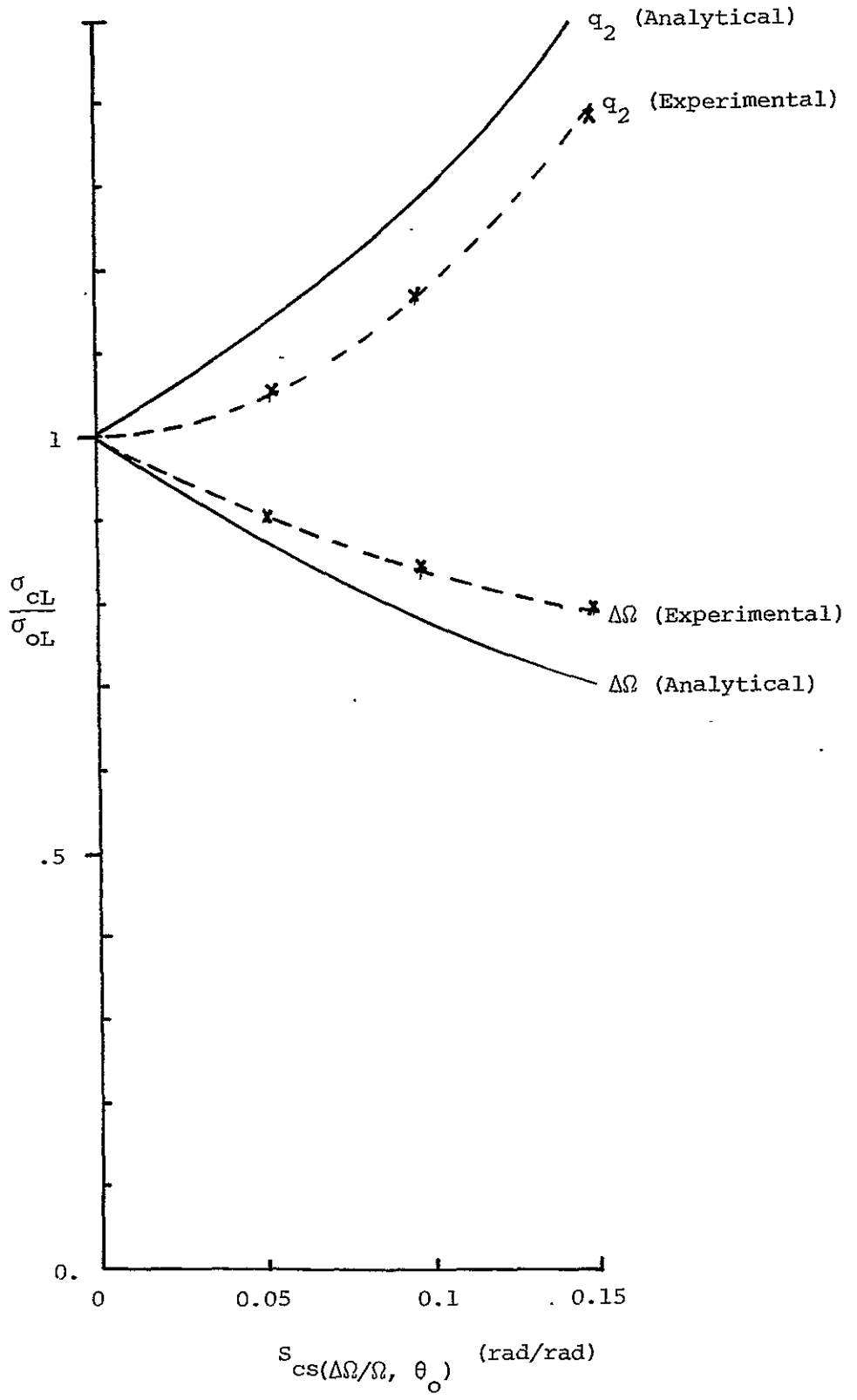

FIGURE 59 . ANALYTICAL AND EXPERIMENTAL RMS LEVEL OF WING CHORDWISE BENDING AND ROTOR ROTATIONAL SPEED CHANGE IN WIND TUNNEL TURBULENCE FOR SYSTEM 4-1

APPENDIX

Reference A.1 describes the design and testing of an active-control gust-alleviation system for tilt-rotor aircraft with hingeless rotors. This appendix summarizes the results.

Table A.1 gives a comparison of the RMS reductions due to gust-alleviation systems of the blade longitudinal cyclic flapping and wing vertical bending for the hingeless rotor and the gimballed rotor considered previously. There are no significant differences in performance between these two systems. For the gimballed rotor the maximum RMS reduction of the blade longitudinal cyclic flapping was 18.0 percent at control system static sensitivity of -2.0 rad/rad, while for the hingeless rotor, this reduction was about 12 percent at a control system static sensitivity of -1.48 rad/rad. The wing vertical bending RMS reduction was 30 percent for the gimballed rotor and was about 28 percent for the hingeless rotor.

The reduction in the RMS level of the rotor rotational speed change are almost the same between these two rotors. For the gimballed rotor the reduction was about 30 percent at $S_{cs}(\Delta\Omega,\theta_o)$ equal to 0.18 rad/rad, while for the hingeless rotor this reduction was 25 percent $S_{cs}(\Delta\Omega,\theta_o)$ equal to 0.225 rad/rad. For both rotors the wing chordwise bending increased for the value of control system static sensitivity that minimized rotor rotational speed change RMS level.

It was concluded that the performance of the System 1-1 to reduce blade-longitudinal cyclic flapping and wing vertical bending RMS levels gave no significant difference in performance for the gimballed and hingeless rotors. System 4-1 also gave the same result for the $\Delta\Omega$ RMS reduction for the

gimballed and the gimballed and the hingeless rotors. The results of the investigation of the various control systems can be summarized as follows.

Using both cyclic pitch controllers, namely longitudinal and lateral cyclic pitch and bending displacement feedback, q_1, the reduction of the RMS value of both wing vertical bending and blade longitudinal cyclic flapping showed a negligible improvement over that utilizing longitudinal cyclic pitch only.

The reduction in the q_1 RMS level can be significantly improved if the bending rate feedback, $\dot{q}_1$, is incorporated with the displacement feedback. Using only longitudinal cyclic pitch as controller, the reduction of the q_1 RMS level is increased to 34 percent. However, no improvement can be achieved in the β_{1c} RMS level. If both cyclic pitch controls are used in this configuration, the reduction of the RMS level of the wing vertical bending increased to 47 percent and for the blade longitudinal cyclic flapping this reduction increased to 20 percent, i.e., only a slight improvement of the β_{1c} RMS level can be obtained.

It can be concluded generally that a control system using vertical bending feedback -- displacement and velocity -- can reduce the wing vertical bending RMS level significantly. Using this system the reduction of the RMS level of the blade longitudinal cyclic flapping cannot achieve more than a 20 percent reduction.

The following section gives a discussion of the use of blade flapping feedback to improve the RMS reduction of the blade longitudinal cyclic flapping. This system measures directly the blade longitudinal cyclic flapping and feeds this signal into both cyclic pitch controllers.

The RMS level reduction of the blade longitudinal cyclic flapping when this system is used is about 68.0 percent. The corresponding control system static sensitivities $S_{cs}(\beta_{1c},\theta_{1s})$ and $S_{cs}(\beta_{1c},\theta_{1c})$ are 1.13 and -3.08 rad/rad respectively. However, the RMS level of the wing vertical bending is slightly increased by 0.08 percent. To obtain simultaneous significant reduction of the wing vertical bending and blade cyclic flapping, a control system which feeds both of these quantities to the cyclic pitch controllers is suggested.

Using the above optimum values of $S_{cs}(\beta_{1c},\theta_{1s})$ and $S_{cs}(\beta_{1c},\theta_{1c})$ and using the optimum $S_{cs}(q_1,\theta_{1s})$ of System 1-1 the RMS level reductions of the wing vertical bending and the blade longitudinal cyclic flapping are very promising. The reduction of the wing vertical bending is 27 percent while the reduction of the blade longitudinal cyclic flapping is 58 percent.

Reference

A.1 Jenie, S.D., "The Application of Active Control Technology to a Gust Alleviation System for Tilt-Rotor Aircraft with Hingeless Rotors", NASA CR-152173, February 1978.

TABLE A.1

COMPARISON BETWEEN GIMBALLED AND HINGELESS ROTORS

System	Gimballed		Hingeless	
	$S_{cs}(\frac{rad}{rad})$	RMS Reduction	$S_{cs}(\frac{rad}{rad})$	RMS Reduction
1-1	-2.0	q_1: 30% β_{1c}: 18%	-1.48	q_1: 28% β_{1c}: 11%
4-1	-0.18	$\Delta\Omega$: 30%	-0.25	$\Delta\Omega$: 25%